Title

Identification and characterization of Pref-1 receptor and a lipid droplet associated protein supporting glycolysis during thermogenesis

Author

Nguyen, Hai

Publication Date

2020

Peer reviewed|Thesis/dissertation

Identification and characterization of Pref-1 receptor and a lipid droplet associated protein supporting glycolysis during thermogenesis

By

Hai Nguyen

A dissertation submitted in partial satisfaction of the

requirement for the degree of

Doctor of Philosophy

in

Endocrinology

in the

Graduate Division

of the

University of California, Berkeley

Committee in charge:

Professor Hei Sook Sul, Chair
Professor Jen-Chywan Wang
Professor Kaoru Saijo
Professor Russell Vance

Abstract

Identification and characterization of Pref-1 receptor and
a lipid droplet associated protein supporting glycolysis during thermogenesis

by
Hai Phi Nguyen
Doctor of Philosophy in Endocrinology
University of California, Berkeley
Professor Hei Sook Sul, Chair

Obesity, an excess accumulation of white adipose tissue, has become a global epidemic. White adipose tissue (WAT) plays a critical role by serving as the major energy storage site and by secreting adipokines that control various biological processes such as appetite, metabolism and insulin sensitivity. In contrast, brown adipose tissue (BAT) or BAT-like tissue dissipate energy via non-shivering thermogenesis to maintain body temperature and is known to inversely correlate with adiposity. BAT not only has high capacity of glucose and fatty acid (FA) uptake, but also secretes adipokines, all potentially contributing to insulin sensitivity. Understanding how adipocyte differentiation (adipogenesis) and thermogenesis is regulated and supported can further effort of developing therapeutic strategies against obesity/lipodystrophy. The aims of this dissertation work were to identify the receptor of Pref-1, an adipose tissue-specific secreted factor that inhibits adipogenesis and to characterize Aifm2 function during thermogenesis in BAT.

Chapter 1 reviews the developmental of various adipose depots. While subcutaneous WAT develops perinatally, visceral WAT develops after birth. They are derived from adipose progenitors expressing distinctive markers depending on the anatomical location. Adipogenesis is controlled by transcription factors which is tightly regulated by secreted factors such as Wnt, and Pref-1. In contrast, BAT forms in early embryogenesis from Myf5+, Pax7+ precursors. Brown fat-like cells can be found in WAT upon cold exposure or β-adrenergic stimulation. In this chapter, transcriptional and epigenetic control of brown and beige adipocyte differentiation and thermogenic program is discussed. Finally, how metabolites can regulate this transcriptional machinery and support thermogenesis in BAT and BAT-like tissues is also highlighted.

Chapter 2 profiles my effort to identify the receptor of Pref-1 by employing a new improved and more sensitive method of crosslinking in live cells. I found a high level of plasma membrane ST2 in 3T3-L1 preadipocytes and in preadipocytes of SVF from WAT. Like Pref-1, ST2 is downregulated during adipocyte differentiation. In contrast, IL-33, the ST2 known ligands, is upregulated during adipocyte differentiation. I also found that Pref-1 binds tightly to ST2 at the plasma membrane of adipose precursor cells to inhibit adipogenesis. ST2 KO prevented Pref-1 activation of phospho-ERK and its inhibitory effect on adipogenesis. Moreover, our ST2 loss-of function approaches in mice showed *in vivo* evidence of ST2 requirement for Pref-1 to exert its effects on adipogenesis.

Chapter 3 profiles my discovery of Aifm2 as a lipid droplet (LD) associated NADH oxidase that is expressed at a high level only in BAT, but not in other tissues, and is cold

inducible. I found Aifm2 to increase cytosolic NAD/NADH, correlating with higher glycolytic rate leading to higher oxygen consumption/uncoupled respiration and heat production in BAT cells. The Aifm2 BAT specific knockout mice were cold-sensitive due to impaired thermogenesis and, with decreased energy expenditure, they exhibited a higher adiposity. Conversely, our transgenic mice overexpressing Aifm2 in $UCP1^{+}$ cells had a higher thermogenic capacity to better maintain body temperature upon cold exposure, increasing energy expenditure with decreasing adiposity.

To my dad, my biggest cheerleader whose endless support, encouragement, and example have made me who I am today. (Cam on, ba, cho moi dieu ba da lam cho con)

Table of Contents

List of Figures

List of Tables

Acknowledgement

Graduate school truly has been one of the most exciting and liberating experience of my life. It has been an incredible journey, made worthwhile by my mentors, friends and family all of whom I humbly thank for their role in this journey.

Foremost, I would like to begin my acknowledgements by thanking my boss and mentor, Dr. Hei Sook Sul, for her tireless support and encouragement for me and my projects throughout my graduate career. Not only has she been a fantastic mentor to me, but she has taught me how to mentor other people. I will always be grateful to her for your support and kindness.

I would also like to thank the members of my dissertation committee, Jen-Chywan Wang, Kaoru Saijo, and Russell Vance, for lending me their guidance and insight, both indirectly and directly, over the years.

I would not have been able to accomplish nearly as much as I have without the help and friendship of my amazing friend, lab mate, and collaborator, Danielle Yi. Also, a special thanks to all my amazing undergraduate assistants, Frances Lin, Katina Ngo, and Gawon Shin, who have been greatly contributing to all the projects. It has been a great experience to mentor them and see them achieving their goals after graduation. I also want to thank all my great collaborators Olga Gylyaeva. and Jose Viscarra for teaching and assisting me all these years. I also want to acknowledge Yuhui Wang, whose years of experience and wisdom have assisted immeasurably in advancing my research. To my friends, Christina Cheung and Amanda Luu, thank you for your support and willingness to grab a dinner with me anytime I need a break.

Chapter 1:

Adipose tissue development and metabolic regulation

Adipose Tissue Development and Metabolic Regulation

Abstract

White adipose tissue (WAT) is the primary energy storage organ and its excess contributes to obesity, while brown adipose tissue (BAT) and inducible thermogenic (beige/brite) adipocytes in WAT dissipate energy via UCP1 to maintain body temperature. Adipose tissues can develop during embryogenesis and after birth depending on anatomical origin. In adipose tissue, differentiation of adipose precursors to adipocytes is governed by transcription factors such as PPARγ, C/EBPβ, Zfp423 and Sox9 and this process is tightly regulated by secreted factors including Pref-1 and Wnt. Additionally, thermogenic gene activation in brown and beige adipocytes relies on common transcriptional machinery that includes PRDM16, Zfp516, Zc3h10, and LSD1, play an important role in regulating the thermogenic gene program. These transcription factors actions are also regulated by metabolites that acts as agonists or cofactor. With the presence of BAT-like tissues in human adults, increasing thermogenic activity these tissues may help to combat obesity.

Introduction

In modern society, excess WAT leading to obesity has become an epidemic and is closely associated with metabolic diseases. However, WAT deficiency, such as lipodystrophy, also manifests as insulin resistance (IR) with ectopic lipid accumulation in other tissues, such as muscle and liver, underscoring the importance of maintaining the proper WAT mass [1, 2]. The main function of white adipocytes is to store excess calories in the form of triglycerides, while secreting adipokines. The ability to store lipid effectively prevents lipotoxicity in other tissues including muscle, liver and heart in which ectopic lipids deposits results in insulin resistance, non-alcoholic liver disease (NAFLD), and cardiovascular disease [1]. Additionally, WAT provides insulation in cold conditions. WAT also "wrap" around and protect critical internal organs such as the heart, adrenal glands, kidneys, and ovaries. Moreover, WAT provides cushioning in regions with high mechanical stress including palm, heel, and buttocks. Thus, white adipose tissue (WAT) is categorized anatomically into subcutaneous adipose depots and visceral adipose depots which are mainly for energy storage [2]. Subcutaneous WAT is found in interscapular and inguinal regions, while visceral WAT is found in perigonadal (epididymal), perirenal, epicardial, retroperitoneal and mesenteric regions. These WAT depots are distinct and heterogeneous [3-6].

An additional class of adipose tissue referred as brown adipose tissue (BAT) found in many mammals has function distinct from WAT by burning energy for heat generation to maintain body temperature [7]. The major function of BAT is mediating adaptive thermogenesis or non-shivering thermogenesis [8]. BAT is enriched with a high number of mitochondria that possess a specialized inner mitochondrial H^+/ fatty acid symporter, Uncoupling Protein 1 (UCP1) for thermogenesis, heat production. Since brown adipocytes are surrounded with many capillaries, heat generated by BAT can be immediately distributed by vascular system to maintain body temperature]. In mice, expression of UCP1 is restricted to only BAT in unstimulated condition. However, upon cold exposure, $UCP1^+$ thermogenic adipocytes, termed "beige" or "brite" cells can arise in WAT depots, especially subcutaneous WAT, although whether this is from recruitment and/or transdifferentiation of white adipocytes is currently not well understood [9]. The presence of BAT or BAT-like tissues in human adults has now been established. BAT is detected mainly in the supraclavicular, paravertebral, and cervical regions in

adult humans. Theses tissues have been shown to increase in adults upon cold exposure and is known to inversely correlate with adiposity. Although the underlying mechanism is not clear, BAT affects insulin sensitivity also [10]. BAT, not only has high capacity of glucose and fatty acid (FA) uptake, but also secretes adipokines, all potentially contributing to insulin sensitivity [11].

Bone marrow adipose tissue (BMAT) is an adipose depot with unique features [12]. Unlike other WATs, BMAT are more rigid due to structural composition of cortical bone. BMAT was demonstrated to support critical cell differentiation in bone marrow. There is evidence that BMAT is derived from distinct progenitors from both BAT and iWAT. BMAT is composed of two different populations including regulating BMAT (rMAT) that affect hematopoiesis and constitutive BMAT (cMAT) that is important for early vertebrate development. BMAT also participate in local and systematic metabolic processes.

These various adipose tissues critical not only for energy metabolism but also secrete adipokines that regulate various biological processes including appetite, metabolism and insulin sensitivity. Origin, development and function of these adipose tissues have been studied extensively in recent years. A better understanding of development and function of adipose tissues may provide future therapeutic targets for obesity and related diseases, such as type 2 diabetes, hepatosteatosis, and cardiovascular diseases.

Developmental origin of WAT

Adipose tissue is composed of adipocytes and a so-called stromal vascular fraction which includes preadipocytes, macrophages, endothelial cells and immune cells. Preadipocytes are thought to arise from mesenchymal cells which undergo a process called adipogenesis to commit and differentiate into mature adipocytes. Due to the heterogeneity of the stromal vascular fraction in adipose tissue, fluorescence activated cell sorting (FACS) using stem cell markers to selectively enrich SVF for the progenitor/precursor populations by sorting for Lin- ($Cd31^-$, $Cd45^-$, $Ter119^-$) eliminated the majority of endothelial, hematopoietic cells and erythrocytes [13]. However, the selected progenitor/precursor population may be at different stages of differentiation, such as stem cells, committed preadipocytes, or those cells at early stage of differentiation. In order to select pure adipose precursors, Rodeheffer et al. isolated a Lin^-: $CD29^+$, $CD34^+$: $Sca1^+$: $CD24^+$ population of proliferating adipose precursors that gave rise to $Cd24^-$ cells *in vivo* during adipogenesis [13]. Additionally, $Cd24^-$ cells of the precursor population were shown to represent preadipocytes that express PPARγ and C/EBPα, key adipogenic transcription factors. Since PGFFRα$^+$ labeled both $Cd24^+$ and $Cd24^-$ precursor populations in WAT, isolation of Lin^-: PGFFRα$^+$ cells may represent a strategy to enrich for adipocyte precursors in adipose tissue. Using inducible Pref-1 promoter coupled with two fluorescent reporters - H2BGFP for transient labeling and Rosa26-flox-stop-flox-tdTomato for permanent labeling, Pref-1+ precursor cells was shown to first appear at E10.5 in mouse embryogenesis in the dorsal mesenteric region at the presumptive inguinal or dorsal subcutaneous depots. At E17.5, these precursor cells differentiated into lipid-containing adipocytes forming subcutaneous WAT. By E19.5, the number of lipid-filled cells more than doubled in this region, indicating hyperplasia as a mechanism for WAT expansion during embryogenesis. Interestingly, no Pref-1+ cells were detected in the visceral WAT development. These cells only appeared in visceral WAT postnatally. This is an evidence of that subcutaneous WAT starts its development perinatally, while visceral fat development takes place after birth. In humans, light microscope examination showed the WAT first appear at the 14^{th} and 16^{th} weeks

of prenatal life. In the context of the adipogenic lineage, Pref-1^+ cells and showed their mesenchymal origin ($Sox9^+$, $Cd29^+$, $Sca1^+$, $Cd105^+$ and $Cd34^+$). The transiently labeled Pref-1^+ cells did not yet express the adipogenic transcription factor PPARγ or adipose commitment factor Zfp423, but were proliferative precursors based on expression of Cd24 and Ki-67 and incorporation of BrdU [14]. Some of the permanently labeled Pref-1 cells had lipid laden morphology and expressed Zfp423, PPARγ and C/EBPα indicating that Pref-1 cells indeed are adipose precursors. Additionally, using Pref-1-reverse tetracycline *trans*-activator (rtTA)/Tet-responsive element (TRE)-Cre, Sox9 ablation from WAT precursors in mice in an inducible manner diminishes the pool of proliferating Pref-1^+ cells by progressing these cells to become $PGFFRa^+$ cells that do not proliferate but express early adipogenic genes. Pref-1^+: $Sox9^+$ cells are shown to appear prior to $PGFFRa^+$ cells in the adipogenic pathway. To maintain early adipose precursors, Sox9 also activates Meis1, which in turn inhibits adipocyte differentiation [15]. There is clear evidence that adipose SVF contains a hierarchy of progenitor populations with different degree of progression from adipose commitment to differentiation. However, FACS using cell surface markers results in a biased sampling of known cell types. Recently, single-cell RNA sequencing allows to explore heterogeneity if cellular population in a completely unbiased and detailed manner. Using this method, it has recently been reported that myofibrobalst arising from diet-induced obesity came from highly proliferative $Cd9^{high}$, PDGFRα$^+$ cells with high Pref-1 expression. In contract, $Cd9^{low}$, PDGFRα$^+$ population was enriched for PPARγ and C/EBPα, with low Pref-1 expression, having low proliferative capacity but high adipogenic potential [16]. Overall, the relationship between cell populations identified based on the expression of various markers needs further investigation. Identification and characterization of stage specific markers may help to isolate and define various precursor populations and their relationship during WAT development.

Given the difference in the formation and function of subcutaneous WAT *versus* visceral fat, it is still unclear whether distinct progenitor populations give rise to subcutaneous WAT and visceral WAT. However, there are several studies supporting such hypothesis. It was reported that unlike subcutaneous WAT or BAT, there were six different visceral WAT depots occurred from cell expressing Wilms Tumor 1 (Wt1) in late gestation [17]. It also suggested that WAT depots associated with visceral organs have a mesothelial layer to supply adipocyte progenitors. Subcutaneous adipocytes were derived from cells expressing Prx1, a homeobox transcription factor expressed in embryonic limb and bud [18]. Interestingly, linage tracing using mT/mG with Myf5-Cre that was assumed to labeled only muscle and BAT, also labeled most cells of anterior subcutaneous WAT [19]. When neural crest cells were marked using Sox10-Cre and R26-YFP, Billon et al. found that only cephalic WAT around salivary glands was labeled, but not other WAT [20]. This study shows that craniofacial adipocytes arise from neural crest cells. Utilizing recent advantageous scRNA-seq, Min et al. showed that there were four subtypes of human adipocytes that derived from distinct progenitors. They were shown to have different gene-expression profiles associated with different adipocyte metabolic functions including lipogenesis specialized adipocytes, thermogenic/"brite" cells, and extracellular matrix and regulatory signaling sensitive adipocytes. Similarly, Gupta lab showed that there are two a distinct pro-inflammatory/pro-fibrogenic and thermogenic/brite progenitors within the visceral fat [21]. These studies, overall, highlight that a simplistic division of WAT into visceral and subcutaneous may need to be reconsidered. It is probable that different WAT depots may have different origins and even cells within the same adipose tissue may be heterogeneous in origin.

Regulation of WAT development

In studying adipocyte differentiation in vitro, preadipocyte cell lines, such as 3T3-L1 and F442A or primary SVF cells from adipose tissue, are treated with a differentiation cocktail containing DEX, MIX, insulin and/or TZD. A cascade of transcription factors is involved in adipose differentiation. Notably, PPARγ and C/EBPα are the key drivers of adipogenesis, while C/EBPβ and C/EBP expressed early in differentiation induce C/EBPα and PPARγ [22, 23]. Forced expression of PPARγ is sufficient to induce adipocyte differentiation in fibroblast. There has been no factor found to induce differentiation without PPARγ. The C/EBP family and Kruppel-like factors (KLFs) have been shown to induce PPARγ promoters. In contrast, GATA factors were shown to repress PPARγ expression [24]. Some C/EBP family members, including C/EBPα, C/EBPβ, and C/EBP are expressed highly in adipocytes [25]. Early induction of C/EBPβ and C/EBP results in increased C/EBPα expression. The KLFs family is composed of C2H2 zinc-finger transcription factors that regulate apoptosis, proliferation and differentiation. KLF proteins were shown to involve in various steps during adipocyte differentiation. For instance, KLF15 can promote adipocyte differentiation and even induce glucose transporter 4 (GLUT4) while KLF5 is induced by C/EBPβ and C/EBP and in turn increase PPARγ2 [26, 27]. In contrast, KLF2 and KLF7 both inhibit adipogenesis. KLF2 directly binds to PPARγ2 promoter and inhibits transcriptional activity in early development and KLF5 then binds to PPARγ promoter and replace KLF2 to activate PPARγ transcription [28]. There are other factors are involved in different stage of adipocyte differentiation including KRX20 (early growth response protein-2), LXRα and LXRβ (Liver X receptors), and SREBP1c [29].

Numerous soluble factors and growth factors regulate adipose differentiation also. For example, by binding to their cognate plasma membrane receptors, Insulin/IGF1 enhances, whereas Wnt and TGFβ inhibit differentiation [27, 30]. We originally cloned and identified Preadipocyte factor-1 (Pref-1) as an adipose tissue-specific gene, expressed in preadipocytes, but not in mature adipocytes. Pref-1 is detected in several tissues during embryogenesis but extinguished postnatally and is restricted mainly to preadipocytes of adipose tissue, with an exception of certain neuroendocrine cells. Pref-1 is highly expressed before adipose conversion but is downregulated during adipogenesis, Pref-1 level inversely correlating with the degree of differentiation [13, 31-34] and thus Pref-1 is used as a preadipocyte marker. By lineage tracing showed that Pref-1 marks very early adipose progenitors during embryogenesis and that they are required for adipose development and expansion in mice in adult stage. Pref-1 level increases greatly in murine models of lipodystrophies, while it is significantly lower in obesity models. Pref-1 is detected also in human preadipocytes and its level is higher in lipodystrophy-like syndrome, while lower in human obesity. In this regard, adipocytes have been reported to be derived from distinct cells [3, 33-35]. In fact, recent studies characterizing SVF cells of WAT showed presence of early adipose progenitors with high level Pref-1 expression, which progress into preadipocytes/adipose precursors having a low Pref-1 level. In addition, studies also found profibrogenic precursors that contain high Pref-1 level mainly in visceral WAT when mice were on high fat diet (HFD), which, depending on environmental cues, inhibit preadipocyte differentiation or are converted into adipocytes.

In cultured 3T3-L1 cells, constitutively expressing Pref-1 prevents differentiation [35, 36], and knockdown (KD) of Pref-1 enhances adipocyte differentiation. DEX, a component of adipogenic cocktail, downregulates Pref-1, allowing cells to undergo adipocyte differentiation [37]. Moreover, inhibitory function of Pref-1 in adipogenesis was unequivocally demonstrated in Pref-1-KO mice that showed increased adiposity [38]. Conversely, ectopic Pref-1 overexpression

protected mice from diet-induced obesity, causing partial lipodystrophy [39, 40]. In this regard, Pref-1 is synthesized as a transmembrane protein, having a N-terminal signal sequence and a single transmembrane-spanning domain [35]. The transmembrane form of Pref-1 is cleaved at the juxtamembrane region by TNFα converting enzyme (TACE/ADAM17) [41], releasing the ectodomain to become biologically active soluble Pref-1. Thus, treatment with soluble Pref-1 inhibits 3T3-L1 or primary preadipocyte differentiation, whereas the expression of the uncleavable membrane mutant is ineffective [41, 42]. It has been shown that Pref-1 activates MEK/ERK in a time and dose dependent manner [43]. By activating MEK/ERK, Pref-1 upregulates Sox9, which in turn suppresses C/EBPβ and C/EBP, to inhibit adipocyte differentiation [44]. In understanding mechanism underlying Pref-1 function in adipogenesis, the most critical component missing at this time is the plasma membrane receptor.

Transcriptional regulation of the thermogenic adipose program

Brown adipose tissue uniquely harbors UCP1, to dissipate chemical energy as heat. Upon cold exposure, sympathetic nervous system (SNS) releases norepinephrine via B3 adrenergic receptor-cAMP-PKA-p38 pathway to stimulate lipolysis to increase fatty acids to fuel mitochondria for oxidation. Early work describing regulation of the UCP1 promoter centered on the norepinephrine-β3AR -cAMP-cyclic AMP response element binding protein (CREB)/p38 MAP kinase axis central to the response to cold. Thus, several target genes of this signaling pathway have been described such as PPARγ-coactivator 1α (PGC1α), CCAAT-enhancer binding protein β(C/EBPβ), diodinase 2 (Dio2) as well as UCP1 itself [45].

In the work of identifying cell autonomous transcriptional effectors of thermogenesis, the coregulatory PR domain containing 16 (PRDM16) is the first identified, BAT-enriched coregulator of the BAT gene program by RT-qPCR analysis of WAT and BAT [46]. Harms et al. showed that PRDM16 determines cell fate as PRDM16 overexpression in skeletal myotubules results in brown adipocyte differentiation [47]. Interestingly, PRDM16 is not regulated by cold and must rely on interacting factors to facilitate PRDM16-mediated BAT gene induction. Since the BAT program is induced upon cold exposure, DNA binding transcription factors that are enriched in BAT and also cold inducible may act by interacting with PRDM16. One such factor is Zfp516 which was found by screening known and putative transcription factors at a global level for activation of the UCP1 promoter. Zfp516 is BAT enriched, cold-induced, and Zfp516 binds and activates the proximal UCP1 promoter and other BAT enriched genes such as PGC1α. Furthermore, Zfp516 also interacts and recruits LSD1, a H3K9 demethylase, to UCP1 and other BAT enriched genes to promote thermogenesis. Furthermore, PRDM16 interacts with a wide variety of transcription factors and cofactors including C/EBPβ, C-terminal binding protein 1 and 2 (CTBP1, CTBP2), histone deacetylase 1 and 2 (HDAC1/2), mediator complex subunit 1 (MED1), PGC1α, PPARγ, and Zfp516 as well as epigenetic regulators-euchromatic histone lysine methyltransferase 1 (Ehmt1) and lysine specific demethylase 1 (LSD1) [48, 49]. Most PRDM16 interacting transcription factors bind at the -2.5kb region of the UCP1 promoter, and Med1 interacts with PRDM16 to facilitate the ability of enhancer-bound transcription factors to recruit RNA pol II or writers of activation marks at BAT specific genes bringing distal enhancers to proximity to the transcription start site facilitating transcriptional activation.

PPARγ agonists have also been reported to increase mitochondrial biogenesis in white adipocytes and to induce brown adipose-selective markers including UCP1, PGC1α, and Cidea. A BAT specific transcription factor, early B cell factor 2 (EBF2) has been shown to bind at PPARγ sites of BAT-enriched genes to recruit PPARγ to promote PRDM16 transcription [50]. PPARγ coactivator-1α (PGC1α) is a transcriptional coactivator of PPARs and of many other

transcription factors that are abundantly expressed in BAT and is further increased during cold exposure. Ectopic expression of PGC1α in mouse white adipocytes stimulates mitochondrial biogenesis and induces the expression of several genes involved in thermogenesis, such as UCP1 and Dio2 [51]. However, PGC1α-deficient adipose tissue shows reduced thermogenic defect. Another cold inducible factor, Interferon regulatory factor 4 (IRF4) has been reported to interact with PGC1α to upregulate thermogenesis, and Irf4-deficient mice have a thermogenic deficiency [52]. Recently, Zc3h10, a member of CCCH-type zinc finger proteins, has recently been a DNA-binding transcription factor that activates UCP1 and thermogenic gene program. Zc3h10 is brown fat enriched, cold inducible and overexpression of Zc3h10 increases thermogenic gene expressions in BAT and iWAT in vivo. Upon sympathetic signaling, Zc3h10 is phosphorylated by p38 MAPK to increase its binding to its target genes including Tfam and Nrf1, resulting in an increase in mitochondria number in BAT. Interestingly, while the majority of known transcription factors, such as ATF2, TR and PPARγ, all act through the -2.5 kb enhancer region of the UCP1, Zc3h10 binds to -4.6 kb UCP1 promoter [53](**Fig.1**).

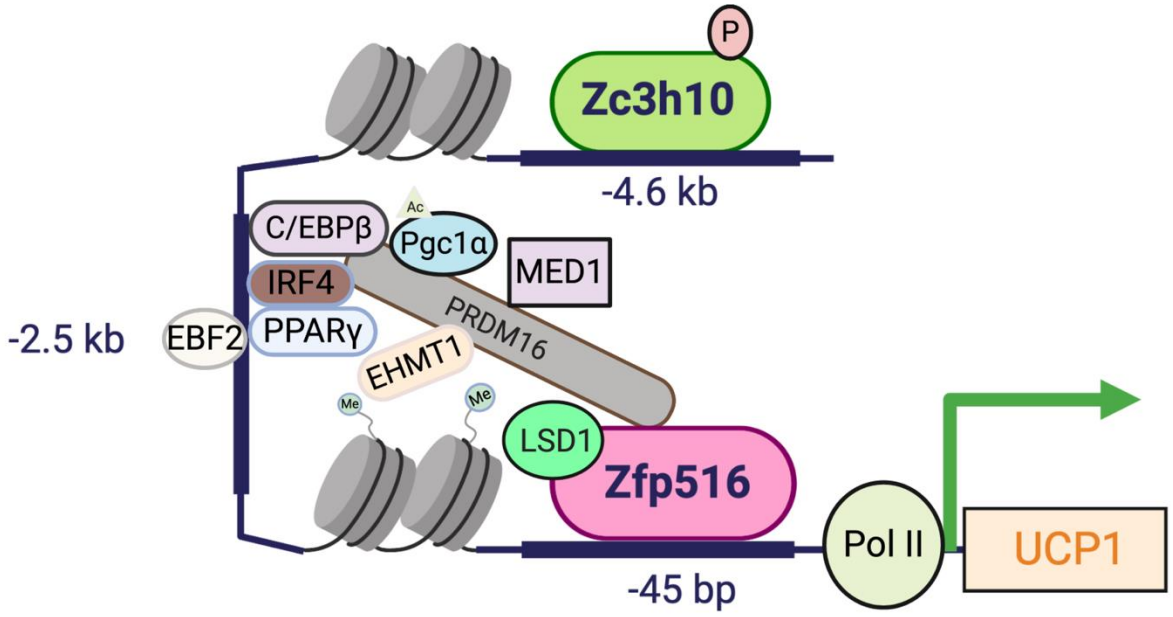

Figure 1. Transcriptional regulation of thermogenic program of BAT

Fat Metabolism in WAT and BAT

Adipose tissue stores as triglycerides in a unilocular lipid droplet (LD), which encompasses most of the cell volume. While the LDs are unilocular in WAT, numerous smaller LDs are found in BAT. LD is composed of core neutral lipids mainly TAG and sterol esters, surrounded by a phospholipid monolayer. The surface of lipid droplets is decorated by a number of proteins which are involved in the regulation of lipid metabolism. During excessive energy or fed state, TAG is synthesized in the ER and immediately incorporated into LDs which then exit the ER membrane and reside in the cytosol. In contrast, during energy deprivation or fasted state, TAG is hydrolyzed on the LD surface and fatty acids (FAs) are then released into circulation for other tissues to use as energy source. In fasted stated, by b-adrenergic stimulation, lipolysis in WAT increases and causes lipid droplets to be fragmented. Lipolysis proceeds in an orderly and

regulated manner, by converting TAG to DAG, MAG and then FAs. Each reaction is catalyzed by desnutrin/ATGL, hormone sensitive lipase (HSL), and monoglyceride lipase (MGL), respectively [54]. The enzymatic steps carried out by these lipases are under tight hormonal regulation. During fasting, glucocorticoid is elevated and increase desnutrin/ATGL transcription. In addition, catecholamines bind to Gαs0-coupled B adrenergic receptors to activate adenylate cyclase, which increases cAMP levels activating protein kinase A (PKA). PKA then phosphorylates HSL, which translocate from the cytosol to its site of action on the lipid droplet. PKA also phosphorylates the lipid droplet associated protein, perilipin, and causing it to dissociate from the lipid droplet, exposing a greater surface for Desnutrin/ATGL and MGL to access and function [55]. During fed state, lipolysis is inhibited by insulin binding to its receptor on adipocytes. Insulin signaling activates phosphodiesterase 3B by phosphorylation, which subsequently decreases cAMP and thus PKA activity. This causes reduced HSL/perilipin phosphorylation and eventually decreased lipolysis. Other cytokines, growth hormones, AMP-activated protein kinase (AMPK), and other molecules also affect lipolysis [56]. Thus, AMPK phosphorylates and activates Desnutrin/ATGL to stimulate lipolysis. Beside endocrine effect of molecules such insulin and catecholamines, lipolysis is regulated by autocrine/paracrine factors. TNF-a, secreted by adipocyte and macrophage, is showed to increase lipolysis. Prostaglandins have also been reported to affect lipolysis. Adipose-specific phospholipase A2 (AdPLA) has such an important role in adipocyte-derived PGE2 in the autocrine/paracrine regulation of lipolysis. AdPLA deficient mice exhibited resistance to high fat diet induced obesity and displayed an increase in lipolytic activity in white adipose tissue. In these mice, there was an increase in PEG2 production along with a lean phenotype even when on a high fat diet. This result indicates PGE2 is the predominant prostaglandin produced in WAT. In adipose tissue, PGE2 produced upon release of AA catalyzed by AdPLA acts through the Gi-alpha coupled EP3 to suppress lipolysis in a cAMP dependent manner. AdPLA-PGE2-EP3 is composed of an autocrine-paracrine regulation of lipolysis in the adipose tissue [57].

Since, lipolysis is a critical metabolic process in both WAT and BAT, adipose overexpression of ATGL/desnutrin in mice increases lipolysis and FA oxidation, resulting in resistance to diet-induced obesity. These mice also show enhanced thermogenesis upon cold exposure having higher energy expenditure. conversely, adipose-specific ablation of desnutrin/ATGL not only manifests in obesity but converts BAT to a WAT-like tissue. Thus, these mice also exhibited impaired thermogenesis with decreased expression of UCP1, with lower PPARα binding to its promoter, revealing the requirement of desnutrin/ATGL-catalyzed lipolysis in the maintenance of a BAT phenotype. In fact, due to decrease in lipolysis, intracellular fatty acid level was lower, resulting in lower ligand concentration of PPARα which is critical for BAT phenotype and is present at the highest level among PPAR family of transcription factors. Thus, PPARα binding and activation of UCP1 promoter was diminished upon desnutrin/ATGL KO BAT, and synthetic PPARα ligand, AICAR, could rescue the defective brown adipocyte morphology and thermogenesis from desnutrin/ ATGL ablation [58].

Fatty acid vs Glucose metabolism for thermogenesis

Thermogenesis is a highly energetic process requiring a readily available fuel supply of glucose and FAs. In addition, BAT also contributes to whole body energy substrate homeostasis. After a meal. FAs and glucose are stored as triglycerides (TGs) in adipose tissue. Even though these nutrients can also be stored in other organs such as liver, muscle and heart, white adipose is the major storage of these fuels. Upon fasting or energy depletion, TGs are hydrolyzed to release

FAs via lipolysis. FAs derived from lipolysis from the circulation are presumed to be used by active BAT [59-61]. Upon cold exposure, norepinephrine released from the sympathetic innervation in BAT stimulates β_3-adrenergic receptor increasing lipolysis via ATGL and HSL. FAs thus produced are presumed to be used for oxidation and also for direct binding to UCP1 for activation.

Recently, however, it has been reported that FAs are taken up from circulation to be used for thermogenesis, especially in fasted condition and that lipolysis within BAT is not essential for thermogenesis [62, 63]. Regardless, after cold exposure or β-adrenergic stimulation, glucose uptake increases in BAT, and BAT is the tissue with the highest glucose uptake [60, 64]. In revealing the importance of glucose metabolism in thermogenesis, many proteins involved in glucose uptake and metabolism, including glucose transporter and glycolytic enzymes, are induced in BAT upon cold exposure and restricting glycolysis has been shown to impair thermogenesis [65-67]. In fact, it has recently been shown that glycolysis is essential for optogenetically induced thermogenesis [65]. The contribution of glucose in fueling thermogenesis, however, has not been well-established. The major portion of glucose is converted into pyruvate and lactate through glycolysis as evidenced by the secretion of both metabolites from BAT following norepinephrine stimulation. Glycolysis in BAT may run close to maximum capacity upon β-adrenergic stimulation. Glucose metabolized to pyruvate via glycolysis can also be transported into mitochondria to be oxidized via TCA cycle and citrate from TCA cycle can also be transported out to cytoplasm to be used for de novo lipogenesis. This can explain how lipogenesis and lipolysis are increased in parallel during thermogenesis [68, 69]. Glucose utilization for BAT thermogenesis is particularly relevant in the fed state, when circulating glucose in high, with low NEFA released from WAT lipolysis due to insulin secretion [60].

In maintaining robust glycolysis, cytosolic NAD is critical for glyceraldehyde-3-phosphate dehydrogenase reaction in the glycolytic pathway. Inner mitochondrial membrane is impermeable to NADH or NAD. Thus, in most tissues, including liver and heart, malate-aspartate shuttle transfers NADH produced from glycolysis into mitochondria for ETC and return NAD to cytosol for glycolysis. Blocking malate-aspartate shuttle in many tissues causes inhibition of respiration [70, 71]. However, in tissues, such as BAT, that require rapid ATP generation, glycerol-3-phosphate shuttle is used. First, cytosolic glycerol-3-phosphate dehydrogenase (cGPD) converts NADH to NAD while reducing dihydroxyacetone phosphate (DHAP) to glycerol-3-phosphate. Next, mitochondrial glycerol-3-phosphate dehydrogenase (mGPD) at the outer surface of the inner mitochondrial membrane facing cytosol, which is particularly high in BAT, oxidizes glycerol-3-phosphate back to DHAP, reducing FAD to FADH and then election from FADH is transferred to CoQ of mitochondrial ETC. However, there have been conflicting reports on the contribution of mGPD in thermogenesis [72-74]. The mGPD-KO mice did not show impaired thermogenesis, while a second independent mGPD-KO mouse model maintained on high fat diet (HFD) exhibited a more rapid increase in body weight with lower energy expenditure, but this was due to higher circulating thyroid hormone. In this regard, lactate dehydrogenase (LDH) in the cytosol can regenerate NAD by converting pyruvate to lactate, which has been proposed to be important for glycolysis during thermogenesis [65]. However, lactate in BAT is used extensively for oxidation by conversion back to pyruvate to enter TCA cycle and lactate level in BAT does not increase, but decreases during thermogenesis [65].

NDHs (NADH dehydrogenase) that are mainly found in yeast, bacteria and plants are associated with the mitochondrial inner membrane and catalyze the same NADH oxidase reaction as complex I in ETC. There are two main classes of NDHs, NDI (internal NDH) facing the mitochondrial matrix and NDE (external) facing the intermembrane space. In yeast that lacks complex 1, NDI maintains mitochondrial NAD to ensure efficient TCA cycle, while NDE provides cytosolic NAD for glycolysis. NDHs also increase ETC activity and respiration by transferring electrons to CoQ. Thus, ablation of these enzymes leads to high NADH/NAD ratio causing an imbalance in cellular metabolism with defective mitochondrial. In fact, upon environmental cues, NDE has been shown to have much higher turnover numbers of NADH:UQ oxidase activity than mammalian complex I. In mammalian, Aifm2 (Apoptosis inducing mitochondrion associated factor 2 (also called AMID, or Prg3) was discovered to function as an NDH. Aifm2 is a flavoprotein with a NADH/NAD oxidoreductase domain as a lipid-droplet associated protein that is highly and specifically expressed in BAT and is induced upon cold exposure/β-adrenergic stimulation in BAT and iWAT. Upon stimulation, Aifm2 localizes to mitochondria for conversion of NADH to NAD to sustain robust glycolysis, while transferring electrons to mitochondrial ETC in fueling thermogenesis[75]. Remarkably, Aifm2 not only has sequence similarity to yeast NDE1, but also shares the localization and the enzymatic activity. Yeast NDE1 can rescue impaired thermogenesis from Aifm2 deficiency, making Aifm2 to be a mammalian NDE specific to thermogenic tissues (**Fig.2**). Interestingly, search of GWAS database reveals multiple SNPs of Aifm2 to be associated with waist-hip ratio, body mass index and fasting glucose level-related insulin resistance, suggesting a potential role of Aifm2 in human obesity and type 2 diabetes.

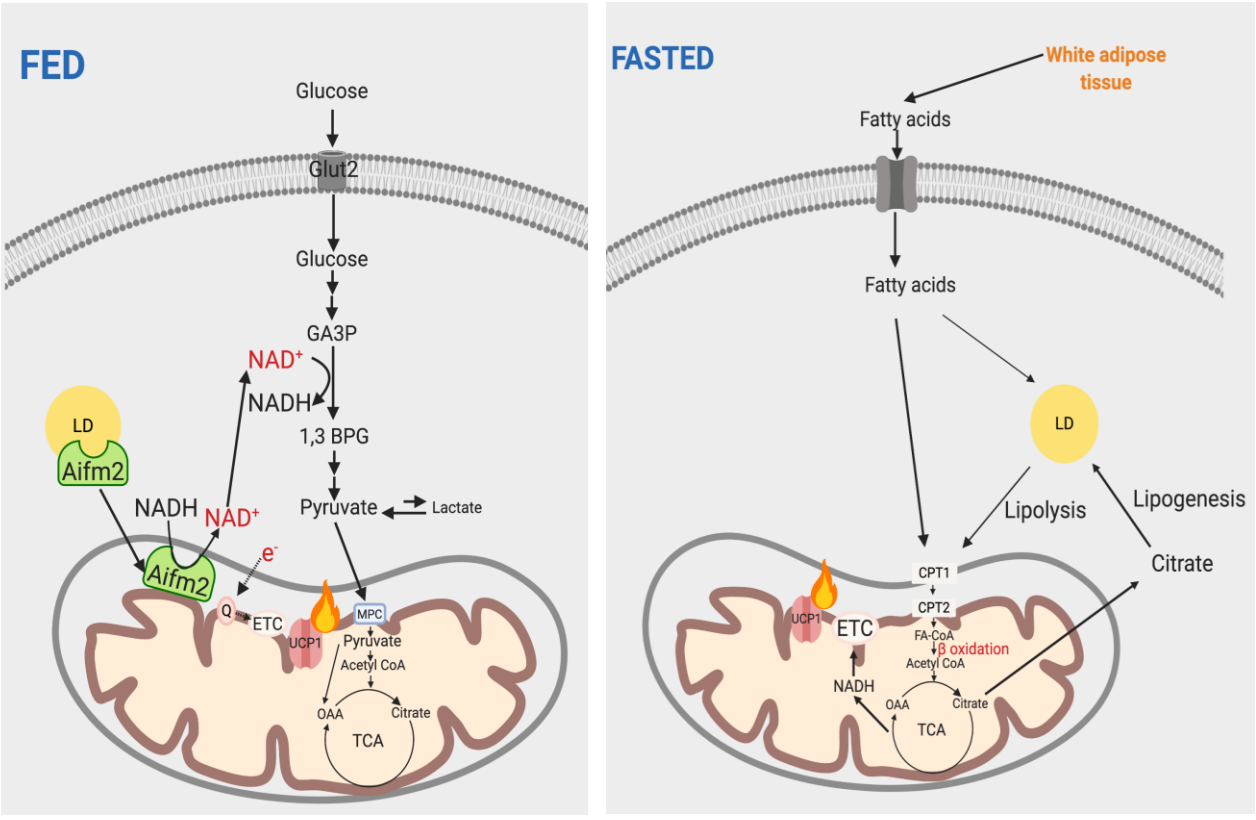

Figure 2. Glucose and fatty acid metabolism supporting thermogenesis in BAT.

Several studies show glucose metabolism is critical for adipocyte differentiation. Wellen *et al.* showed that glucose, required for production of cytosolic acetyl-CoA is used for histone acetylation which results in changes in expression of differentiation programs [50]. Additionally, Shapiro *et al.* al found that Nicotinamide (NAM) is required for PPARγ expression in umbilical cord–derived mesenchymal stem cells differentiation to adipocytes. Similarly, Jackson *et al.* reported glucose and nicotinamide control adipogenesis in mouse 3T3-L1 adipocytes [76]. Aifm2 KO resulting in lower glucose oxidation and reduced level of cytosolic NAD could lead to decreased expression of PPARγ. Aifm2 KO BAT showed low level of thermogenic genes such as UCP1 and Dio2. Aifm2 KO results in higher adiposity and WAT-like brown adipocytes. Aifm2 may play an important role in the plasticity of adipocytes, conceivably by providing metabolites that regulate transcriptional activity of regulator of thermogenic programing in BAT.

Conclusion

While WAT plays a critical role by serving as the major energy storage site and by secreting adipokines that control various biological processes, such as appetite, metabolism and insulin sensitivity, BAT has high capacity of glucose and fatty acid (FA) uptake for thermogenesis and all potentially contributing to insulin sensitivity. Understanding both depots development and the underlying to promote "browning" of WAT may provide targets for combatting and preventing obesity and associated diseases. Many studies identified several markers for adipose progenitors/precursors helping uncover the heterogeneity of adipose SVF. However, newly advanced sc-RNA seq would further allow to study of the possible mosaic development of WAT and BAT and to discover any new cell population that might contribute to adipose tissue homeostasis, function and development as well as potential mechanisms for "browing" of WAT. Furthermore, the relationship among transcription factors involved in transitioning from silent chromatin to poised/active chromatin in brown/beige adipocytes needs further investigation. With significant changes of chromatin structure during brown/beige development, the enzymes catalyzing these modifications remains to be elucidated.

Acknowledgement

The work from the authors' laboratory was supported by DK123844 to H.S.S

References

1. Rosen, E.D. and B.M. Spiegelman, *What we talk about when we talk about fat.* Cell, 2014. **156**(1-2): p. 20-44.
2. Ghaben, A.L. and P.E. Scherer, *Adipogenesis and metabolic health.* Nat Rev Mol Cell Biol, 2019. **20**(4): p. 242-258.
3. Jeffery, E., et al., *Rapid depot-specific activation of adipocyte precursor cells at the onset of obesity.* Nat Cell Biol, 2015. **17**(4): p. 376-85.
4. Jeffery, E., et al., *The Adipose Tissue Microenvironment Regulates Depot-Specific Adipogenesis in Obesity.* Cell Metab, 2016. **24**(1): p. 142-50.
5. Kim, S.M., et al., *Loss of white adipose hyperplastic potential is associated with enhanced susceptibility to insulin resistance.* Cell Metab, 2014. **20**(6): p. 1049-58.
6. Macotela, Y., et al., *Intrinsic differences in adipocyte precursor cells from different white fat depots.* Diabetes, 2012. **61**(7): p. 1691-9.

7. Harms, M. and P. Seale, *Brown and beige fat: development, function and therapeutic potential.* Nat Med, 2013. **19**(10): p. 1252-63.
8. Kajimura, S., B.M. Spiegelman, and P. Seale, *Brown and Beige Fat: Physiological Roles beyond Heat Generation.* Cell Metab, 2015. **22**(4): p. 546-59.
9. Inagaki, T., J. Sakai, and S. Kajimura, *Transcriptional and epigenetic control of brown and beige adipose cell fate and function.* Nat Rev Mol Cell Biol, 2017. **18**(8): p. 527.
10. Stanford, K.I., et al., *Brown adipose tissue regulates glucose homeostasis and insulin sensitivity.* J Clin Invest, 2013. **123**(1): p. 215-23.
11. Poher, A.L., et al., *Brown adipose tissue activity as a target for the treatment of obesity/insulin resistance.* Front Physiol, 2015. **6**: p. 4.
12. Li, Y., Y. Meng, and X. Yu, *The Unique Metabolic Characteristics of Bone Marrow Adipose Tissue.* Front Endocrinol (Lausanne), 2019. **10**: p. 69.
13. Rodeheffer, M.S., K. Birsoy, and J.M. Friedman, *Identification of white adipocyte progenitor cells in vivo.* Cell, 2008. **135**(2): p. 240-9.
14. Gupta, R.K., et al., *Transcriptional control of preadipocyte determination by Zfp423.* Nature, 2010. **464**(7288): p. 619-23.
15. Gulyaeva, O., et al., *Sox9-Meis1 Inactivation Is Required for Adipogenesis, Advancing Pref-1(+) to PDGFRalpha(+) Cells.* Cell Rep, 2018. **25**(4): p. 1002-1017.e4.
16. Marcelin, G., et al., *A PDGFRalpha-Mediated Switch toward CD9(high) Adipocyte Progenitors Controls Obesity-Induced Adipose Tissue Fibrosis.* Cell Metab, 2017. **25**(3): p. 673-685.
17. Chau, Y.Y., et al., *Visceral and subcutaneous fat have different origins and evidence supports a mesothelial source.* Nat Cell Biol, 2014. **16**(4): p. 367-75.
18. Sanchez-Gurmaches, J., W.Y. Hsiao, and D.A. Guertin, *Highly selective in vivo labeling of subcutaneous white adipocyte precursors with Prx1-Cre.* Stem Cell Reports, 2015. **4**(4): p. 541-50.
19. Sanchez-Gurmaches, J. and D.A. Guertin, *Adipocytes arise from multiple lineages that are heterogeneously and dynamically distributed.* Nat Commun, 2014. **5**: p. 4099.
20. Billon, N., et al., *The generation of adipocytes by the neural crest.* Development, 2007. **134**(12): p. 2283-92.
21. Min, S.Y., et al., *Diverse repertoire of human adipocyte subtypes develops from transcriptionally distinct mesenchymal progenitor cells.* Proc Natl Acad Sci U S A, 2019. **116**(36): p. 17970-17979.
22. Tontonoz, P., E. Hu, and B.M. Spiegelman, *Stimulation of adipogenesis in fibroblasts by PPAR gamma 2, a lipid-activated transcription factor.* Cell, 1994. **79**(7): p. 1147-56.
23. Wu, Z., et al., *Cross-regulation of C/EBP alpha and PPAR gamma controls the transcriptional pathway of adipogenesis and insulin sensitivity.* Mol Cell, 1999. **3**(2): p. 151-8.
24. Tong, Q., et al., *Function of GATA transcription factors in preadipocyte-adipocyte transition.* Science, 2000. **290**(5489): p. 134-8.
25. Kajimura, S., et al., *Initiation of myoblast to brown fat switch by a PRDM16-C/EBP-beta transcriptional complex.* Nature, 2009. **460**(7259): p. 1154-8.
26. Oishi, Y., et al., *Kruppel-like transcription factor KLF5 is a key regulator of adipocyte differentiation.* Cell Metab, 2005. **1**(1): p. 27-39.
27. Aggarwal, A., et al., *The Circadian Clock Regulates Adipogenesis by a Per3 Crosstalk Pathway to Klf15.* Cell Rep, 2017. **21**(9): p. 2367-2375.

28. Wu, Z. and S. Wang, *Role of kruppel-like transcription factors in adipogenesis.* Dev Biol, 2013. **373**(2): p. 235-43.
29. Payne, V.A., et al., *C/EBP transcription factors regulate SREBP1c gene expression during adipogenesis.* Biochem J, 2009. **425**(1): p. 215-23.
30. Ignotz, R.A. and J. Massague, *Type beta transforming growth factor controls the adipogenic differentiation of 3T3 fibroblasts.* Proc Natl Acad Sci U S A, 1985. **82**(24): p. 8530-4.
31. Sarantopoulos, C.N., et al., *Elucidating the Preadipocyte and Its Role in Adipocyte Formation: a Comprehensive Review.* Stem Cell Rev, 2018. **14**(1): p. 27-42.
32. Tang, W., et al., *White fat progenitor cells reside in the adipose vasculature.* Science, 2008. **322**(5901): p. 583-6.
33. Tseng, Y.H., et al., *Prediction of preadipocyte differentiation by gene expression reveals role of insulin receptor substrates and necdin.* Nat Cell Biol, 2005. **7**(6): p. 601-11.
34. Fox, K.E., et al., *Depletion of cAMP-response element-binding protein/ATF1 inhibits adipogenic conversion of 3T3-L1 cells ectopically expressing CCAAT/enhancer-binding protein (C/EBP) alpha, C/EBP beta, or PPAR gamma 2.* J Biol Chem, 2006. **281**(52): p. 40341-53.
35. Smas, C.M. and H.S. Sul, *Pref-1, a protein containing EGF-like repeats, inhibits adipocyte differentiation.* Cell, 1993. **73**(4): p. 725-34.
36. Smas, C.M., L. Chen, and H.S. Sul, *Cleavage of membrane-associated pref-1 generates a soluble inhibitor of adipocyte differentiation.* Mol Cell Biol, 1997. **17**(2): p. 977-88.
37. Smas, C.M., et al., *Transcriptional repression of pref-1 by glucocorticoids promotes 3T3-L1 adipocyte differentiation.* J Biol Chem, 1999. **274**(18): p. 12632-41.
38. Moon, Y.S., et al., *Mice lacking paternally expressed Pref-1/Dlk1 display growth retardation and accelerated adiposity.* Mol Cell Biol, 2002. **22**(15): p. 5585-92.
39. Villena, J.A., et al., *Resistance to high-fat diet-induced obesity but exacerbated insulin resistance in mice overexpressing preadipocyte factor-1 (Pref-1): a new model of partial lipodystrophy.* Diabetes, 2008. **57**(12): p. 3258-66.
40. Lee, K., et al., *Inhibition of adipogenesis and development of glucose intolerance by soluble preadipocyte factor-1 (Pref-1).* J Clin Invest, 2003. **111**(4): p. 453-61.
41. Wang, Y. and H.S. Sul, *Ectodomain shedding of preadipocyte factor 1 (Pref-1) by tumor necrosis factor alpha converting enzyme (TACE) and inhibition of adipocyte differentiation.* Mol Cell Biol, 2006. **26**(14): p. 5421-35.
42. Mei, B., et al., *Only the large soluble form of preadipocyte factor-1 (Pref-1), but not the small soluble and membrane forms, inhibits adipocyte differentiation: role of alternative splicing.* Biochem J, 2002. **364**(Pt 1): p. 137-44.
43. Kim, K.A., et al., *Pref-1 (preadipocyte factor 1) activates the MEK/extracellular signal-regulated kinase pathway to inhibit adipocyte differentiation.* Mol Cell Biol, 2007. **27**(6): p. 2294-308.
44. Wang, Y. and H.S. Sul, *Pref-1 regulates mesenchymal cell commitment and differentiation through Sox9.* Cell Metab, 2009. **9**(3): p. 287-302.
45. Cao, W., et al., *beta-Adrenergic activation of p38 MAP kinase in adipocytes: cAMP induction of the uncoupling protein 1 (UCP1) gene requires p38 MAP kinase.* J Biol Chem, 2001. **276**(29): p. 27077-82.

46. Iida, S., et al., *PRDM16 enhances nuclear receptor-dependent transcription of the brown fat-specific Ucp1 gene through interactions with Mediator subunit MED1.* Genes Dev, 2015. **29**(3): p. 308-21.
47. Harms, M.J., et al., *Prdm16 is required for the maintenance of brown adipocyte identity and function in adult mice.* Cell Metab, 2014. **19**(4): p. 593-604.
48. Ohno, H., et al., *EHMT1 controls brown adipose cell fate and thermogenesis through the PRDM16 complex.* Nature, 2013. **504**(7478): p. 163-7.
49. Sambeat, A., et al., *LSD1 Interacts with Zfp516 to Promote UCP1 Transcription and Brown Fat Program.* Cell Rep, 2016. **15**(11): p. 2536-49.
50. Lee, Y.H., et al., *Cellular origins of cold-induced brown adipocytes in adult mice.* Faseb j, 2015. **29**(1): p. 286-99.
51. Kleiner, S., et al., *Development of insulin resistance in mice lacking PGC-1alpha in adipose tissues.* Proc Natl Acad Sci U S A, 2012. **109**(24): p. 9635-40.
52. Kong, X., et al., *IRF4 is a key thermogenic transcriptional partner of PGC-1alpha.* Cell, 2014. **158**(1): p. 69-83.
53. Yi, D., et al., *Zc3h10 Acts as a Transcription Factor and Is Phosphorylated to Activate the Thermogenic Program.* Cell reports, 2019. **29**(9): p. 2621-2633.e4.
54. Ahmadian, M., Y. Wang, and H.S. Sul, *Lipolysis in adipocytes.* Int J Biochem Cell Biol, 2010. **42**(5): p. 555-9.
55. Brasaemle, D.L., *Thematic review series: adipocyte biology. The perilipin family of structural lipid droplet proteins: stabilization of lipid droplets and control of lipolysis.* J Lipid Res, 2007. **48**(12): p. 2547-59.
56. Duncan, R.E., et al., *Regulation of lipolysis in adipocytes.* Annu Rev Nutr, 2007. **27**: p. 79-101.
57. Jaworski, K., et al., *AdPLA ablation increases lipolysis and prevents obesity induced by high-fat feeding or leptin deficiency.* Nat Med, 2009. **15**(2): p. 159-68.
58. Ahmadian, M., et al., *Desnutrin/ATGL is regulated by AMPK and is required for a brown adipose phenotype.* Cell Metab, 2011. **13**(6): p. 739-48.
59. Blondin, D.P., et al., *Inhibition of Intracellular Triglyceride Lipolysis Suppresses Cold-Induced Brown Adipose Tissue Metabolism and Increases Shivering in Humans.* Cell Metab, 2017. **25**(2): p. 438-447.
60. M, U.D., et al., *Postprandial Oxidative Metabolism of Human Brown Fat Indicates Thermogenesis.* Cell Metab, 2018. **28**(2): p. 207-216 e3.
61. Lee, J., J.M. Ellis, and M.J. Wolfgang, *Adipose fatty acid oxidation is required for thermogenesis and potentiates oxidative stress-induced inflammation.* Cell Rep, 2015. **10**(2): p. 266-79.
62. Schreiber, R., et al., *Cold-Induced Thermogenesis Depends on ATGL-Mediated Lipolysis in Cardiac Muscle, but Not Brown Adipose Tissue.* Cell Metab, 2017. **26**(5): p. 753-763 e7.
63. Shin, H., et al., *Lipolysis in Brown Adipocytes Is Not Essential for Cold-Induced Thermogenesis in Mice.* Cell Metab, 2017. **26**(5): p. 764-777 e5.
64. Symonds, M.E., et al., *Recent advances in our understanding of brown and beige adipose tissue: the good fat that keeps you healthy.* F1000Res, 2018. **7**.
65. Jeong, J.H., J.S. Chang, and Y.H. Jo, *Intracellular glycolysis in brown adipose tissue is essential for optogenetically induced nonshivering thermogenesis in mice.* Sci Rep, 2018. **8**(1): p. 6672.

66. Hao, Q., et al., *Transcriptome profiling of brown adipose tissue during cold exposure reveals extensive regulation of glucose metabolism.* Am J Physiol Endocrinol Metab, 2015. **308**(5): p. E380-92.
67. Winther, S., et al., *Restricting glycolysis impairs brown adipocyte glucose and oxygen consumption.* Am J Physiol Endocrinol Metab, 2018. **314**(3): p. E214-e223.
68. Barquissau, V., et al., *White-to-brite conversion in human adipocytes promotes metabolic reprogramming towards fatty acid anabolic and catabolic pathways.* Mol Metab, 2016. **5**(5): p. 352-365.
69. Yu, X.X., et al., *Cold elicits the simultaneous induction of fatty acid synthesis and beta-oxidation in murine brown adipose tissue: prediction from differential gene expression and confirmation in vivo.* FASEB J, 2002. **16**(2): p. 155-68.
70. Kauppinen, R.A., T.S. Sihra, and D.G. Nicholls, *Aminooxyacetic acid inhibits the malate-aspartate shuttle in isolated nerve terminals and prevents the mitochondria from utilizing glycolytic substrates.* Biochim Biophys Acta, 1987. **930**(2): p. 173-8.
71. Barron, J.T., L. Gu, and J.E. Parrillo, *Malate-aspartate shuttle, cytoplasmic NADH redox potential, and energetics in vascular smooth muscle.* J Mol Cell Cardiol, 1998. **30**(8): p. 1571-9.
72. Brown, L.J., et al., *Normal thyroid thermogenesis but reduced viability and adiposity in mice lacking the mitochondrial glycerol phosphate dehydrogenase.* J Biol Chem, 2002. **277**(36): p. 32892-8.
73. DosSantos, R.A., et al., *Evidence for a compensated thermogenic defect in transgenic mice lacking the mitochondrial glycerol-3-phosphate dehydrogenase gene.* Endocrinology, 2003. **144**(12): p. 5469-79.
74. Alfadda, A., et al., *Mice with deletion of the mitochondrial glycerol-3-phosphate dehydrogenase gene exhibit a thrifty phenotype: effect of gender.* Am J Physiol Regul Integr Comp Physiol, 2004. **287**(1): p. R147-56.
75. Nguyen, H.P., et al., *Aifm2, a NADH Oxidase, Supports Robust Glycolysis and Is Required for Cold- and Diet-Induced Thermogenesis.* Mol Cell, 2020. **77**(3): p. 600-617.e4.
76. Jackson, R.M., et al., *Glucose availability controls adipogenesis in mouse 3T3-L1 adipocytes via up-regulation of nicotinamide metabolism.* J Biol Chem, 2017. **292**(45): p. 18556-18564.

Chapter 2:

ST2 is the receptor of Pref-1

ST2 is the receptor of Pref-1

ABSTRACT

We originally cloned Pref-1 as adipose tissue specific gene that is expressed highly in preadipocytes, but not mature fat cells. Soluble Pref-1 can activate ERK and upregulate Sox9, which in turn suppresses C/EBPβ and C/EBPδ and inhibits adipogenesis. In understanding mechanism of Pref-1 action, we recently have identified ST2, a known receptor of IL-33 as the putative Pref-1 receptor by employing an improved and more sensitive method of crosslinking in live cells. We found that, a high level of plasma membrane ST2 present in 3T3-L1 preadipocytes and adipose precursors from WAT. Here, we showed that Pref-1 binds directly to ST2 at the plasma membrane of adipose precursor cells to activate phosphor-ERK and inhibit adipogenesis. We also found that Pref-1 also requires ST2 downstream signaling molecules including IL1Rap, Myd88, TRAF6, and IRAK1. Moreover, our ST2 ablation in Pref-1 expressing cells mouse model clearly demonstrate *in vivo* evidence of ST2 requirement for Pref-1 to exert its effects on adipogenesis.

INTRODUCTION

White adipose tissue (WAT) plays a critical role by serving as the major energy storage site and by secreting adipokines that control various biological processes, such as food intake, metabolism and insulin sensitivity. In modern society, excess WAT leading to obesity has become an epidemic and is closely associated with metabolic diseases, such as type 2 diabetes. WAT deficiency, such as lipodystrophy, also manifests as insulin resistance (IR) with ectopic lipid accumulation in tissues, such as liver, underscoring the importance of maintaining the proper WAT mass [1, 2]. WAT can expand not only through increased adipocyte volume but also by increased adipocyte number (adipogenesis) [3]. A cascade of transcription factors is involved in adipose differentiation. Notably, PPARγ and C/EBPα are the key drivers of adipogenesis, while C/EBPβ and C/EBPδ are expressed early in differentiation to induce C/EBPα and PPARγ. Moreover, several growth factors have been shown to affect adipogenesis [4-7]. Understanding how adipogenesis is regulated may help in developing therapeutic strategies against obesity/lipodystrophy.

We originally cloned Preadipocyte factor-1 (Pref-1) as an adipose tissue-specific gene, expressed in preadipocytes, but not in mature adipocytes in adults [8]. During embryogenesis, however, Pref-1 is detected in several embryonic tissues, but extinguished postnatally and is restricted mainly to preadipocytes of adipose tissue [9]. In adipose tissue, Pref-1 is highly expressed before adipose conversion but is downregulated during adipogenesis, Pref-1 level inversely correlating with the degree of differentiation [10-14]. Hence, Pref-1 is used widely as a preadipocyte marker [8, 10, 15]. By lineage tracing, we showed that Pref-1 marks very early adipose progenitors during embryogenesis and that they are required for adipose development and expansion in mice [15]. Pref-1 is synthesized as a transmembrane protein with a N-terminal signal sequence and a single transmembrane-spanning domain. Transmembrane form of Pref-1 is cleaved at the juxtamembrane region [16], releasing the biologically active soluble Pref-1. Soluble Pref-1 activates ERK [17]. Upon activating ERK, Pref-1 upregulates Sox9 which, in turn, suppresses C/EBPβ and C/EBPδ, to inhibit adipogenesis [18]. In understanding mechanism underlying Pref-1 action, the most critical component missing at present is the plasma membrane receptor required for binding of soluble Pref-1 for intracellular signaling.

Pref-1 contains 6 tandem EGF-repeats which was originally described for EGF, TGFα and HB-EGF that all bind the EGF receptor [19]. However, none of the EGF-repeats of Pref-1 maintain the exact spacing of EGF, nor contain the amino acid residues critical for EGF receptor binding [20-22]. Another class of EGF-repeat proteins are Notch and its ligands, Delta, Serrate and Lag-2 (DSL) [23-25]. The spacing of cysteines and the conserved amino acid residues in Pref-1 are similar to those of Delta, and thus Pref-1 was also named Delta-like 1 (Dlk1) [26]. Yet, Pref-1 does not contain the DSL domain required for Notch interaction. Moreover, reports have been contradictory that Pref-1 has been reported either to antagonize or act synergistically with Notch [27]. Regardless, we could not detect Pref-1 binding to Notch [28], nor could we detect Pref-1 effect on expression of Hes-1, a well-studied downstream Notch target [29, 30]. Even though, we reported that fibronectin, an extracellular protein, interacts and modulates Pref-1 signaling [28], Fibronectin is unlikely the receptor for Pref-1, but may modulate Pref-1 signaling, similar to known fibronectin function for several growth factors.

In order to identify the plasma membrane receptor for Pref-1, we employed a new improved and more sensitive crosslinking in live cells. Remarkably, we have identified ST2 (also called IL1RL1 (IL-1 receptor-like protein 1) as the Pref-1 receptor. ST2 is known as the receptor for IL-33 that belongs to the interleukin-1 (IL-1) family of inflammatory cytokines [31-33]. IL-33 does not contain a signal sequence and is found in the nucleus, but is released into the extracellular space from necrotic cells during cell and tissue damage to act as an endogenous danger signal to alert adjacent cells [32] to maintain tissue homeostasis. Thus, although ST2 is found in various tissues, it is found mainly in mast cells and Th2 cells [34] for type 2 immunity. We found a high level of plasma membrane ST2 in 3T3-L1 preadipocytes and in Lin^- preadipocytes of SVF from WAT and that, similar to the expression pattern of Pref-1, ST2 is downregulated during adipocyte differentiation, while its known ligand, IL-33, is upregulated during differentiation. Here, we demonstrate Pref-1 binds to ST2 and ST2 functions as Pref-1 receptor to activate MEK/ERK to induce Sox9 and suppress adipogenesis in vitro and in vivo, Taken together, our study clearly illustrates evidence of ST2 act as Pref-1 receptor to exert Pref-1 effects on adipogenesis.

EXPERIMENTAL PROCEDURES

Plasmids and reagents

All plasmids, reagents and antibodies used are provided in Table 2.

Animals

All animal studies were carried out in accordance with UC Berkeley ACUC and OLAC regulations. Both ST2 global KO mice and ST2 floxed mice were kindly provided by Dr. Ari Molfosky at UCSF. ST2-PreASKO was generated by crossing ST2 floxed mice withs Pref-1-rtTA mice that we previously were reported. Mice were housed in a 12:12 light-dark cycle and chow and water were provided *ad libitum*. Dox was provided in chow at 600 mg/kg.

Metabolic measurements

Fat and lean mass was determined by echoMRI-100V. CT Scan was performed on Trifoil eXplore RS9 microCT system.

EdU injection

EdU was injected subcutaneously at 4 wk-old mice at 10 ug/g of body weight and EdU incorporation into SVF cells from WAT was assessed by FACS 3 days later according to manufacturer's protocol.

Cell culture

Cells were grown in standard condition with 5% CO^2, at 37°C. Primary SVF cells were isolated from 4 wk-old male mice of indicated genotype. Adipocyte differentiation of SVF cells was performed as previously described [15]/ Cells were then harvested for RNA isolation or protein extraction or fixed with formalin for ORO staining. To generate CRIPRS KO cell lines, 3T3–L1 cells were transfected with Lipofectamine 3000 and plasmid pCRISPR-CG01 containing Cas9, GFP and 2 independent sgRNA targeting mouse ST2. Cells were then FACS by GFP.

ELISA

Pathscan Phospho-p44/42 MAPK (7177) and total p44/42 MAPK (7050) ELISA kits were used to calculate the pERK/ERK ratio.

SVF and adipocyte fraction isolation

SVF fractionation was carried out as previously described [15]. Briefly, mouse WAT was minced and digested with Collagenase type II (Sigma) in KREBs buffer at 37°C for 45 min with shaking. Cell suspension was then passed through 100 μm mesh, span at 300 g for 5 min, floating adipocyte fraction was collected for RNA or DNA extraction, whereas cell pellet was resuspended in KREBS buffer, passed through 70 μm and 40 μm mesh and subjected to FACS and *in vitro* differentiation, or lysed with RIPA buffer for immunoblotting or with TRIzol for RNA isolation.

RNA isolation and RT-qPCR

Total RNA from SVF cells were extracted using TRIzol and RNA from adipose tissue were extracted using RNeasy Lipid kit. Reverse transcription was performed with 1 μg of total RNA using Superscript II or with 10–100 ng from sorted cells using Superscript Villo. qRT-PCR was performed on ABI PRISM 7500 (Applied Biosystems) using Sybr Green or TaqMan (Invitrogen). The primers are listed in table 1.

Whole mount staining

1mm piece of tissue was excised, fixed with 1% PFA, incubated with UCP1 antibody, LipidTox Red Reagent (Thermo Fisher) and DAPI. Tissues were immobilized on a slide with mounting medium and visualized using a confocal microscope.

Immunoblotting and Immunostaining

For immunoblotting, tissues or cells were lysed in RIPA buffer. Proteins (5-100 μg) were separated on SDS-PAGE gel, transferred on a nitrocellulose membrane and incubated with indicated antibodies (see Table 2 for list of antibodies). For whole-mount tissue immunostaining, a 1mm piece of WAT or BAT was excised, incubated with LipidTOX Green Reagent (Thermo Fisher) and DAPI, immobilized on a slide with mounting medium and imaged using confocal microscope. Cell number and size was calculated using ImageJ software.

Pref-1 and antibody administration in animals

Mice were injected intraperitoneal with 30-50ug of neutralizing ST2 antibody. After 48 hr, the same mice were injected with 10ug of Pref-1 Fc or Fc.

Statistical analysis

Statistical analysis was performed using two tailed t-test. The error bars represent standard error mean (SEM). Data are expressed as mean +/- SD and p value <0.05 was considered statistically significant. Number of mice or replicates used in each experiment was indicated in figure legends. Experiments were repeated at least three times.

RESULTS

Pref-1 directly binds to-ST2

To identify the Pref-1 receptor, soluble Pref-1 corresponding to aa 1-329 with a N-terminal His-tag was overexpressed in HEK293 cells in serum free media and was purified by HIS-PUR resin. The soluble Pref-1 was then crosslinked by using the recently developed diazirine photo-reactive linker method. The heterobifunctional linker enables two-step reactions in which Pref-1 is labeled by an amine reactive NHS ester followed by UV-activated crosslinking with a diazirine moiety to target any nearby amino acid side chain or peptide backbone. We used cell surface protein crosslinkers, Sulfo-SDA (Sulfo-NHS (N-hydroxysuccinimide) -Diazirine, 3.9 Å spacer) (Fig. 4A, left) and Sulfo-sBED with longer cleavable spacer and biotin handle (Thermo-Fisher) (Fig. 4B, left). Purified His-tagged soluble Pref-1 was incubated with a crosslinker at 1:10 molar ratio for 30 mins at 4°C. After quenching, excess crosslinker was removed by using zebra desalting column. The labeled Pref-1 was then mixed with 3T3-L1 preadipocytes in serum free media and crosslinked by exposing the cells with 320 nm UV for 5 mins. The Pref-1-receptor complex was then purified by His-tag beads and subjected it to SDS-PAGE. The band corresponding to the crosslinked Pref-1 complex visualized by using Pref-1 antibody was excised out and subjected to MS analysis. In order to distinguish the bona fide Pref-1 receptor, the 10 candidate proteins thus identified were overexpressed in Cos7 cells. In Cos7 cells, Pref-1 could not phosphorylate and activate ERK, an indication of absence of Pref-1 receptor. Forty-eight hrs post transfection of candidate genes, cells were treated with purified His-tagged Pref-1 or tag peptide only. P-ERK/ERK ratio in cell lysates was quantified by using ELISA kit. As expected, Pref-1 treatment of 3T3-L1 preadipocytes resulted in a 6-fold increase in P-ERK/ERK and it did not affect P-ERK/ERK in Cos7 cells. More importantly, among all the candidates, only ST2 transfected Cos7 cells showed an approximately 3.5-fold increase in P-ERK/ERK upon Pref-1 treatment (Fig. 3A). To further verify ST2 as the Pref-1 receptor, each candidate gene was knock-downed by transducing shRNA lentivirus in 3T3-L1 cells which then were treated with Pref-1. Indeed, only ST2 KD effectively prevented ERK activation by Pref-1 (Fig. 3B). These results suggest that ST2 might function as the Pref-1 receptor.

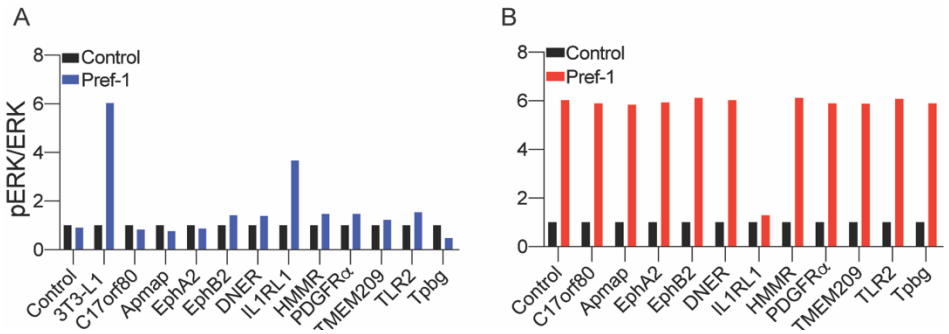

Figure 3. Pref-1 receptors candidate screening
pERK/ERK ELISA assay was perform on lysates collected from Cos7 cells (A) overexpressing the candidates or from 3T3-L1 (B) with the candidates KD

To verify binding of Pref-1 to ST2, we performed in situ crosslinking of the soluble Pref-1 to 3T3-L1 or Cos7 cells by the same method used for identification of candidate proteins. 3T3-L1 cells express substantial endogenous ST2, while Cos7 cells do not express significant levels of ST2. Purified His-tagged soluble Pref-1 was added to 3T3-L1 or Cos7 cells in serum free media for crosslinking by using Sulfo-SDA, a short non-cleavable photo-crosslinker. After washing, the crosslinked cell lysates and media were immunoprecipitated (IP) by poly-histidine

antibody to detect the Pref-1-ST2 complex. In the non-crosslinked control sample, Pref-1 was detected in the media as 50 kD band. In contrast, a larger Pref-1-ST2 complex of approximately 110 kD in size was detected only in 3T3-L1 cells, but not in Cos7 cells (Fig. 4A). Next, we transfected Cos7 cells with Myc-tagged ST2 and the cells were crosslinked with His-tagged Pref-1 by using Sulfo-SBED with a cleavable spacer. After IP with His antibody, the complex was cleaved by β-mercaptoethanol. Immunoblotting revealed presence of Pref-1 and ST2 in the complex as detected as individual band at their predicted size of 50 kD (Fig. 4B, middle) and 63 kD (Fig. 4B, right), respectively. We also used the same cleavable spacer to crosslink Pref-1 Fc to cells of stromal vascular fraction isolated from iWAT. Immunoblotting for ST2 detected the endogenous ST2 upon IP of Pref-1 Fc (Fig. 4C). Overall, these results clearly demonstrate that Pref-1 interacts with ST2 in live cells.

We further examined the Pref-1-ST2 interaction by Co-IP. For this experiment, IL-33, a known ligand for ST2, was employed as a control. His-tagged IL-33 or His-tagged Pref-1 was transfected individually, or co-transfected with Myc-tagged ST2, into Cos7 cells. Upon transfection, we detected expression of His-Pref-1 and His-IL-33 in Cos7 cells. Lysates were then immunoprecipitated using Myc antibody, followed by IB with His antibody. When lysates of the IL-33- or Pref-1-treated control cells were used for IP with myc antibody, there was no detectable IL-33 or Pref-1 band by IB with His antibody. When lysates of cells that were cotransfected with IL-33 and ST2, IB with His antibody detected IL-33 at the predicted size of approximately 18 kD. More importantly, when lysates of cells cotransfected with Pref-1 and ST2, IB with His antibody clearly detected Pref-1 band at predicted size of 50 kD (Fig. 4D). We next examined the interaction between Pref-1 and ST2 in 3T3-L1 cells. After 3T3-L1 cells were treated with purified Pref-1, lysates were IP with ST2 antibody followed by IB with Pref-1 antibody. We again detected Pref-1 in Co-IP sample but not in the control IP sample (Fig. 4E, left). We also injected Pref-1 Fc and control, Fc into mice. SVF cells from iWAT were collected after 48 hrs. When lysates were IP with ST2 antibody, immunoblotting for Pref-1 revealed the Pref-1 band in Pref-1 Fc, but not control Fc injected sample (Fig. 4E, right).

Next, to study the direct interaction between Pref-1 and ST2, purified Pref-1 and ST2 extracellular domain were utilized in *in vitro* pulldown assay. Purified His-tagged Pref-1 or His-tagged IL-33 was incubated with Fc-tagged ST2 in the binding buffer at 4^{o}C for overnight. The complex formed was then purified by using the Protein A/G magnetic beads and subjected to IB with His antibody. Again, IL-33 and Pref-1 were detected at their predicted sizes, when IP with ST2 (Fig. 4F). This clearly demonstrates that, like IL-33, Pref-1 directly interacts with ST2 in vitro. Since we detected direct binding of Pref-1 to ST2, we next examined the relationship between Pref-1 and IL-33 in their binding to ST2. Purified His-tagged Pref-1 and His-tagged IL-33 each alone or together was incubated with Fc-tagged ST2 at a molar ratio of 1:1 or 1:3 (Pref-1:IL-33). When ST2 was incubated with Pref-1 alone, IP with ST2 followed by IB using His antibody showed Pref-1 band at the expected size. At 1:1 molar ratio of Pref-1 and IL-33, IL-33 band was detected as expected. However, Pref-1 signal was decreased significantly compared to Pref-1 alone sample. Remarkably, at 1:3 ratio, Pref-1 was no longer detected, and only IL-33 band was detected. In addition, IL-33 signal at 1:3 ratio was much higher than that in sample of 1:1 ratio (Fig. 4G). These results demonstrate that Pref-1 and IL-33 bind ST2 in a competitive manner.

We also tested in situ live cell imaging of Pref-1 interaction with ST2 at the cell surface by Proximity Ligation Assay (PLA) using the DuoLink kit. His-tagged Pref-1 and Myc-tagged ST2 were co-transfected into Cos7 cells. Secondary antibodies against rabbit IgG for His-tag and

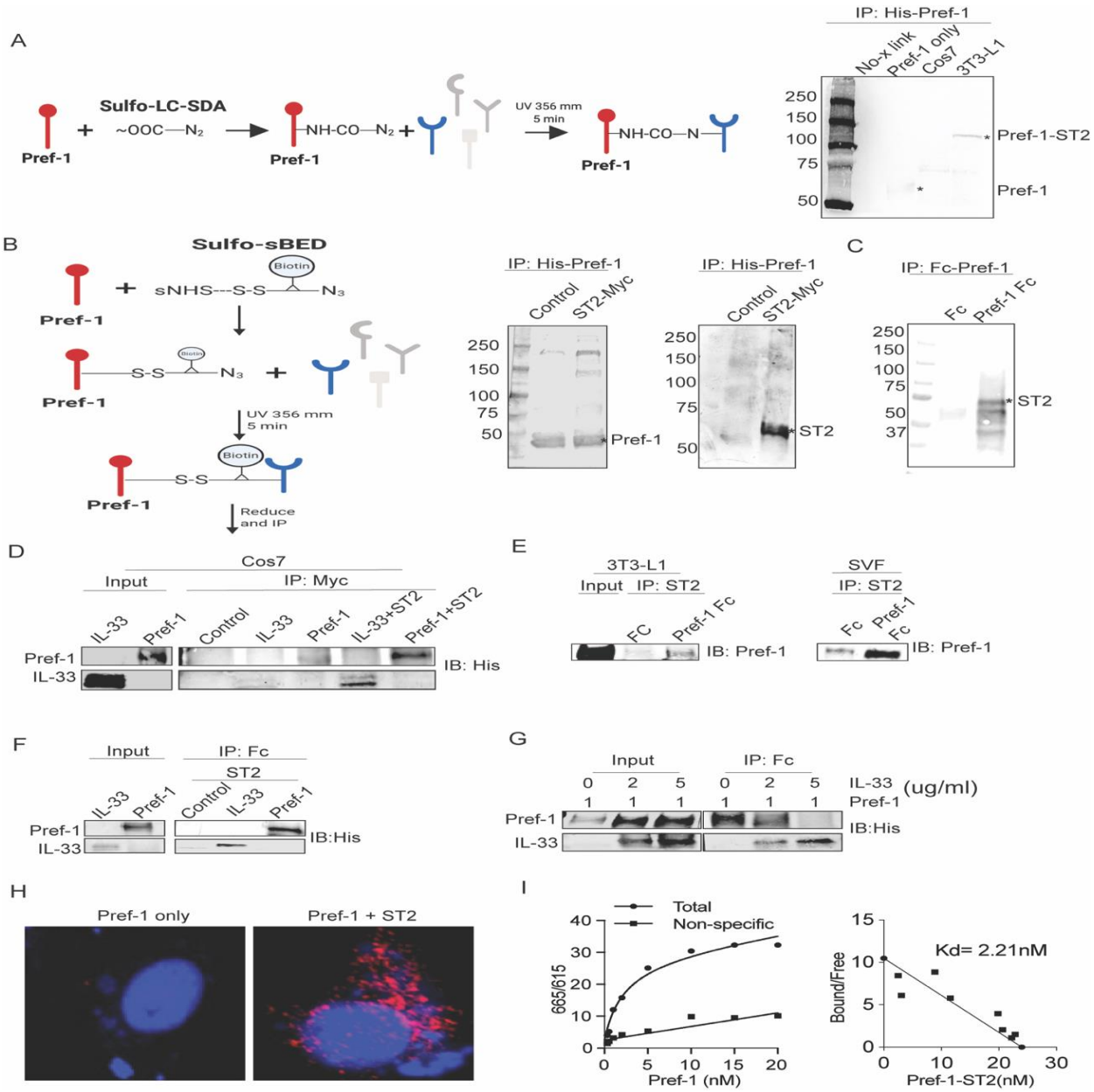

Figure 4. ST2 directly interacts with Pref-1

(A) Schematic irreversible crosslinking his-tagged Pref-1with live 3T3-L1 or Cos7 cells and immunoblotted (IB) for His * Pref-1 and crosslinked product of Pref-1+ST2. (B) Schematic reversible crosslinking his-tagged Pref-1with myc-tagged ST2 overexpressed in Cos7 cells, * 50kD Pref-1 and 60kD ST2. (C) IB for ST2 after crosslinking Pref-1 Fc or Fc with SVF cells collected from WAT., *. 60kD ST2 band. (D) Lysates from HEK293 cells expressing ST2-myc were incubated with His-Pref-1 or His-IL-33 followed by IP with αMyc and IB for His. (E) 3T3-L1 lysates (right) or SVF lysates (right) were IP with aST2 and IB for Pref-1. (F) Purified His-Pref-1 or His-IL-33 were incubated with ST2-Fc, followed by IB for His. (G) ST2-Fc were incubated with indicated amount of His-Pref-1 and His-IL-33, followed by IP with aFc and then IB for His, (H) Visualization of Pref-1 binding to ST2 overexpressing Cos7 cell by PLA. (I) FRET assay for Pref-1 binding to ST2 and Scatchard plot with Kd.

mouse IgG for Myc-tag were used as PLA probes. As shown by red fluorescence, Pref-1-ST2 interaction was detected in live cells by PLA, while no fluorescence was detected in Pref-1 only transfected cells (Fig. 4H,J). This in situ interaction further establishes the Pref-1-ST2 binding. We also employed FRET detection system for in situ Pref-1-ST2 interaction and the interaction in situ was quantified. First, Myc-tagged ST2 was transfected into Cos7 cells. These ST2 overexpressing cells were then incubated with His-tagged Pref-1 at increasing concentrations of 0.1 nM to 20 nM. We then treated the cells with His-antibody labeled with donor, europium (EU) and Myc antibody labeled with acceptor, allophycocyanin (APC). The energy transfer from complex formation after excitation of EU at 340 nm was measured with time-resolved fluorometry by APC emission at 665 nm. Indeed, we clearly detected the saturable binding of Pref-1 to ST2 in live cells. Analysis of the binding by Scatchard plot showed the binding affinity (Kd) between Pref-1 and ST2 to be 2.88 nM, an indicative of tight binding (Fig. 4I). Overall, we conclude that Pref-1 directly binds to ST2.

ST2 is highly expressed in adipose precursor cells

By RT-qPCR, we found ST2 to be expressed highly in various adipose depots, especially in iWAT compared to other tissues including liver, muscle, kidney, heart, and brain (Fig. 5A). Gene analysis revealed, like Pref-1, ST2 was mainly expressed in SVF but not in adipocytes in iWAT (Fig. 5B). This expression indicates that ST2 might be expressed in preadipocytes/adipose precursors but not in adipocytes. However, ST2 has been shown to be expressed in endothelial cells, as well as immune cell types, including subset of Treg and ILC2 cells, cell types found in SVF of WAT. Therefore, we investigated whether ST2 is expressed also in preadipocytes/adipose progenitors present in SVF. By FACS based on their surface markers, SVF cells were first sorted into lineage negative (Lin^-) ($CD45^-$, $Ter1119^-$, $CD31^-$) and lineage positive cells (Lin^+). ILC2 cells were selected by cells that were $CD25^+$ $CD127^+$ $CD161^+$. In Lin^- SVF cells were further sorted in adipocyte precursor cells ($CD34^+$, CD29+, $PDGFR\alpha^+$ and $Sca1^+$) [13]. For Lin^+ population, Treg cells were isolated by using $CD4^+$, $CD25^+$, and $Foxp3^+$ surface markers. In all adipose depots, the number of $ST2^+$ cells in APC population was comparable to the number of $ST2^+$ cells in ILC2 population. Among adipose depots, iWAT had the highest number of $ST2^+$ cells (Fig. 5C, left). Moreover, in both iWAT and pWAT, 93-98% of APC and ILC2 cells were $ST2^+$ cells. More importantly, percent of $ST2^+$ cells detected in both APC and ILC2 populations were comparable (Fig. 2C, right). In addition, percent of $ST2^+$ cells in total Treg population was also similar to both $ST2^+$ APC and $ST2^+$ ILC2 cells (data not shown). During adipocyte differentiation of 3T3-L1 cells, similar to Pref-1, ST2 mRNA levels were decreased by 95% at Day 3 of differentiation (Fig. 5D, left), in contrast to the signficant increase in PPARγ and FABP4 mRNA levels during differentiation. ST2 protein levels were

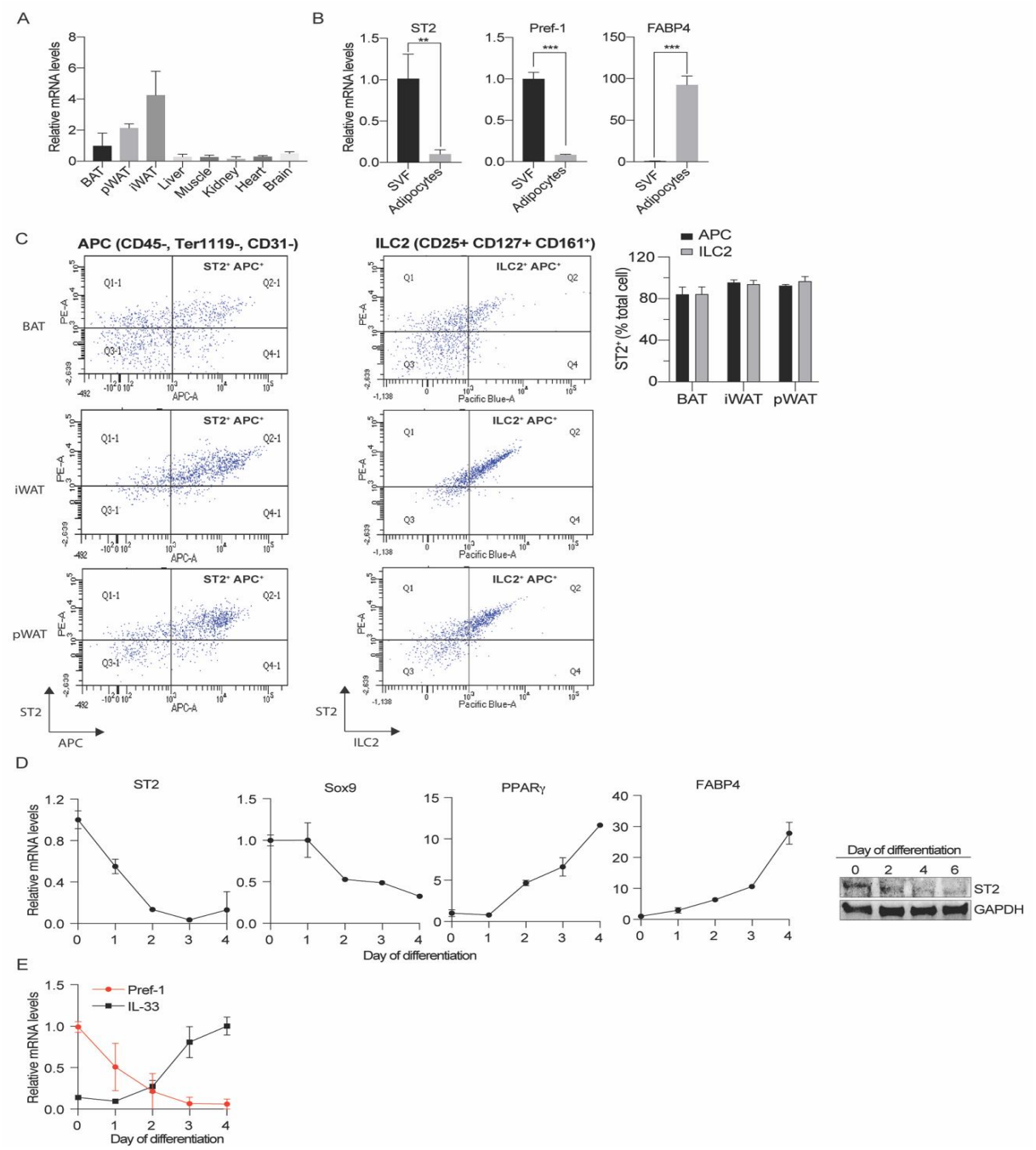

Figure 5. ST2 is present in adipose precursors
(A)ST2 expression in various tissues. (B) ST2 mRNA levels in SVF and adipocytes fraction in iWAT, (C) FACS analysis of ST2 in adipocytes progenitors and ILC2 cells. (D) ST2 mRNA and protein levels as well as Pref-1 and IL-33 mRNA levels during 3T3-L1 adipocyte differentiation.

markedly decreased also during adipocyte differentiation (Fig. 2D, right). Surprisingly, in contrast to the expression pattern of Pref-1 and ST2, IL-33 mRNA levels were very low in preadipocytes and were significantly induced during adipocyte differentiation (Fig. 5E). Overall, the parallel expression pattern of Pref-1 and ST2 is consistent with the concept that ST2 functions as the Pref-1 receptor during adipocyte differentiation.

ST2 is required for Pref-1 mediated ERK activation

If Pref-1 functions by binding to ST2, it is predicted that ST2 should be required for Pref-1 effects, including ERK activation, Sox9 induction and its downstream suppression of C/EBPβ and C/EBPδ, and ultimately inhibition of adipocyte differentiation. First, in addressing whether ST2 is required for ERK activation by Pref-1, we employed Cos7 cells that do not express endogenous Pref-1 or ST2 at a significant level. Cos7 cells were transfected with the full-length ST2. Forty-eight hrs post transfection, cells maintained in serum-free media for 1hr, were treated with Fc, Fc-tagged Pref-1. Cell lysates were subjected to IB by using antibodies against P-T^{202}/Y^{204}-ERK1/2 and total ERK1/2. We also used commercially available ELISA kit (Cell signaling) to quantify the P-ERK/ total ERK ratio. Pref-1 treatment in control Cos7 cells did not significantly increase ERK phosphorylation or P-ERK/total ERK ratio. In contrast, in ST2 transfected Cos7 cells, Pref-1 brought ERK phosphorylation significantly to increase P-ERK/total ERK by approximately 4-fold (Fig. 6A).

To address whether ST2 is required for Pref-1 mediated ERK activation in preadipocytes, we employed 3T3-L1 cells. As expected, Pref-1 increased ERK phosphorylation in 3T3-L1 preadipocytes that has endogenous ST2, as detected by IB (Fig. 6B, left) and P-ERK/total ERK was increased by approximately 4-fold. When we transfected Myc-tagged ST2 in 3T3-L1 cells, P-ERK signal was increased even at a higher degree by Pref-1, P-ERK/ERK increasing by 14-fold (Fig. 6B, right). These results clearly demonstrate the role of ST2 in Pref-1 mediated ERK activation. Next, we employed ST2 neutralizing antibody to test the requirement of ST2 in activation of ERK by Pref-1. 3T3-L1 cells were first pre-incubated with either IgG or ST2 antibody at 15 times of molar concentration of Pref-1 and the cells were subsequently treated with Pref-1 for 15 mins. In the control, IgG treated cells, ERK phosphorylation increased by Pref-1 treatment. In contrast, in preadipocytes pretreated with ST2 antibody, P-ERK was not detected (Fig. 6C, left).To further test the requirement of ST2 for Pref-1 action, two different ST2-KO pools of 3T3-L1 cells by CRISPR-Cas9 system were generated. Two different gRNA sequences targeting ST2 exon 1 and 3 was transfected into Cas9 stably expressing 3T3-L1 cells. The KO pools were selected by maintaining these cells in puromycin-containing selection media. By RT-qPCR, pools of ST2 KO cells showed nearly 70% reduction in the levels of ST2 mRNA (Fig. 6D, left). IB for P-ERK showed that, unlike in control 3T3-L1 cells, Pref-1 did not increase ERK phosphorylation in both pools of ST2 CRISPR KO cells (Fig. 6D, middle). ELISA showed that, while control cells showed an approximately 4-fold increase in P-ERK/ERK, Pref-1 failed to increase P-ERK/ERK in pools of ST2KO 3T3-L1 cells (Fig 6D, right).

We next examined whether ST2 is required for Pref-1 mediated ERK activation in preadipocytes *in vivo settings*. immunocompromised mice were pretreated with either IgG or ST2 neutralizing antibody at 20 times in concentration of Pref-1 before administration of a single dose of Fc or Pref-1-Fc administration**.** Twenty-four hr post injection, WAT depots were collected. Immunoblotting for ERK phosphorylation showed that, in control IgG treated mice, Pref-1-Fc administration but not control Fc, increased P-ERK in both iWAT and pWAT significantly. Remarkably, in ST2 neutralizing antibody pre-treated mice, Pref-1 failed to induce ERK phosphorylation (Fig. 6E)**.** We also examined ERK phosphorylation in primary culture of preadipocytes of SVF of WAT, SVF from WT and global ST2-KO mice were isolated and cultured. These cells were treated with varying concentrations of Pref-1 from 0.5 to 5 ug/ml in serum free media. As expected, ERK phosphorylation by IB showed that in wild type cells, Pref-1 increased P-ERK in a dose dependent manner. In contrast, in ST2-KO cells, Pref-1 did not

induce ERK phosphorylation (Fig. 6F). Overall, these results demonstrate the requirement of ST2 for Pref-1 mediated ERK activation.

Since IKK phosphorylation is reported to activate via ST2 by IL-33, we check P-IKK level in 3T3-L1 upon Pref-1 treatment. Interestingly, Pref-1 did not increase IKK phosphorylation for NF-κB activation in IgG treated samples. Similar to IB, P-ERK/ERK ELISA showed an increase in the ratio of approximately 3-fold by Pref-1 treatment in both control and IgG pre-incubated cells. However, this activation of ERK was completely prevented by ST2 antibody (Fig. 6C left).

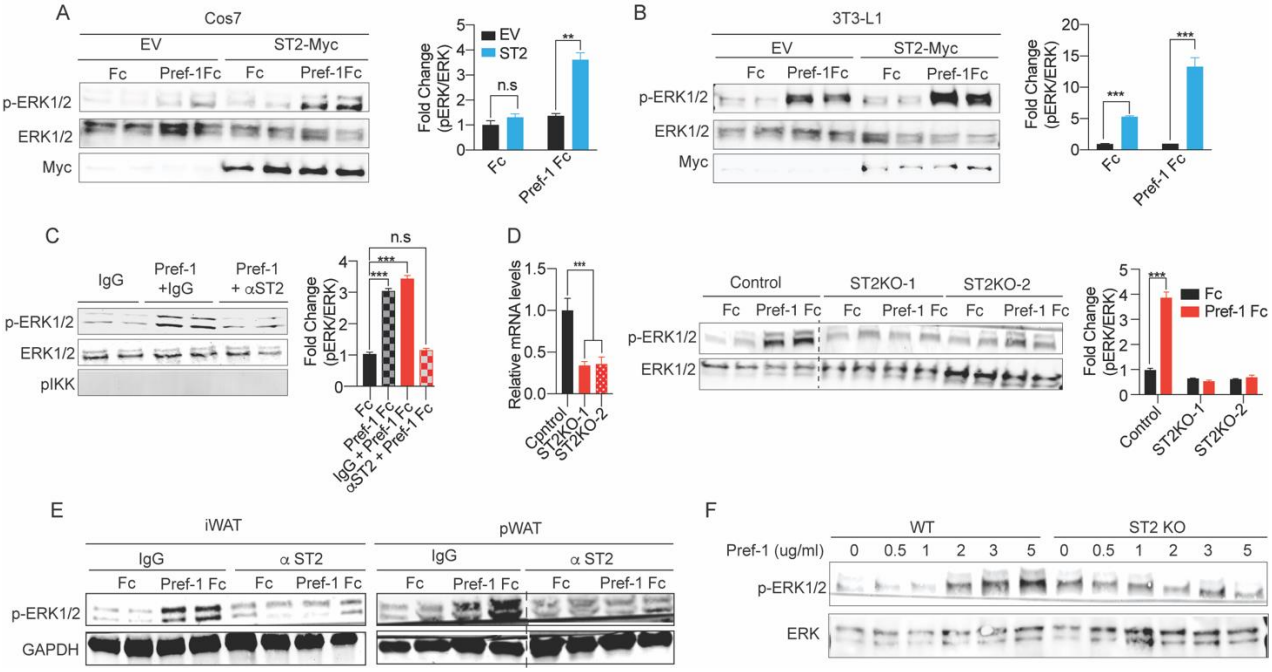

Figure 6. ST2 is required for Pref-1 mediated ERK activation
IB and ELISA for phospho-ERK and total ERK after Cos-7 (A) or 3T3-L1 (B) overexpressing ST2 were treated with Pref-1. (C) 3T3-L1 preadipocytes treated with either IgG or neutralizing ST2 antibody and Pref-1. (D) CRIPR ST2-KO 3T3-L1 cells. (E) iWAT and pWAT lysates from mice that were pretreated with IgG or ST2 ab prior to Pref-1 injection. (F) SVF cells isolated from either WT or ST2 KO mice that were treated with Pref-1.

Requirement of ST2 for Pref-1 inhibition of adipocyte differentiation

We originally identified Pref-1 as an inhibitor of adipocyte differentiation by activating MEK/ERK. To examine whether ST2 is required for Pref-1 inhibition of adipocyte differentiation, full length ST2 was overexpressed in 3T3-L1 cells. The cells were then treated with either Fc or Pref-1 Fc before treating them with adipogenic cocktail. As expected, Oi Red O staining showed greatly lower lipid staining in the control cells treated with Pref-1(Fig. 7A). In contrast, in ST2 overexpressing cells Pref-1 had no inhibitory effect on lipid accumulation. Additionally, there is a significantly lower lipid staining in ST2 overexpressing cells compared to the control cells. This effect might due to presence of the endogenous and FBS derived Pref-1. By RT-qPCR, Fc treated control cells showed an increase in adipogenic genes, such as PPARγ, C/EBPβ, and FABP4, and a decrease in Pref-1 target, Sox9, at Day 3 and Day 6 of differentiation. In control cells, Pref-1 treatment decreased expression of adipogenic genes, while increased Pref-1 target, Sox9. And ST2 overexpression caused significantly reduced mRNA

levels of adipogenic markers while increased Sox9 mRNA levels, compared to control cells. More importantly, Pref-1 treatment in these ST2 overexpressing cells further decreased all the adipogenic genes and increased Sox9 (Fig. 7B). These results indicate the ST2 overexpression enhance Pref-1 inhibitory effect of adipogenesis

We next employed the CRISPR ST2-KO 3T3-L1 cells. Both control and ST2-KO 3T3-L1 cells were treated with control, Fc or Pref-1 Fc prior to adipocyte differentiation. While, as expected, Pref-1 treatment reduced lipid staining in WT cells, there were no significant inhibitory effects of Pref-1 on lipid accumulation in ST2-KO cells (Fig. 7C). Gene analysis revealed that Pref-1 treated control 3T3-L1 cells upon differentiation had much lower levels of PPARγ, C/EBPβ, Plin1, and FABP4 and higher level of Sox9 compared to Fc treated cells. In contrast, there was no differences in expression of these genes between Fc and Pref-1 treatment in ST2 KO cells (Fig. 7D). These data showed that ST2 ablation could prevent inhibition of adipocyte differentiation by Pref-1.

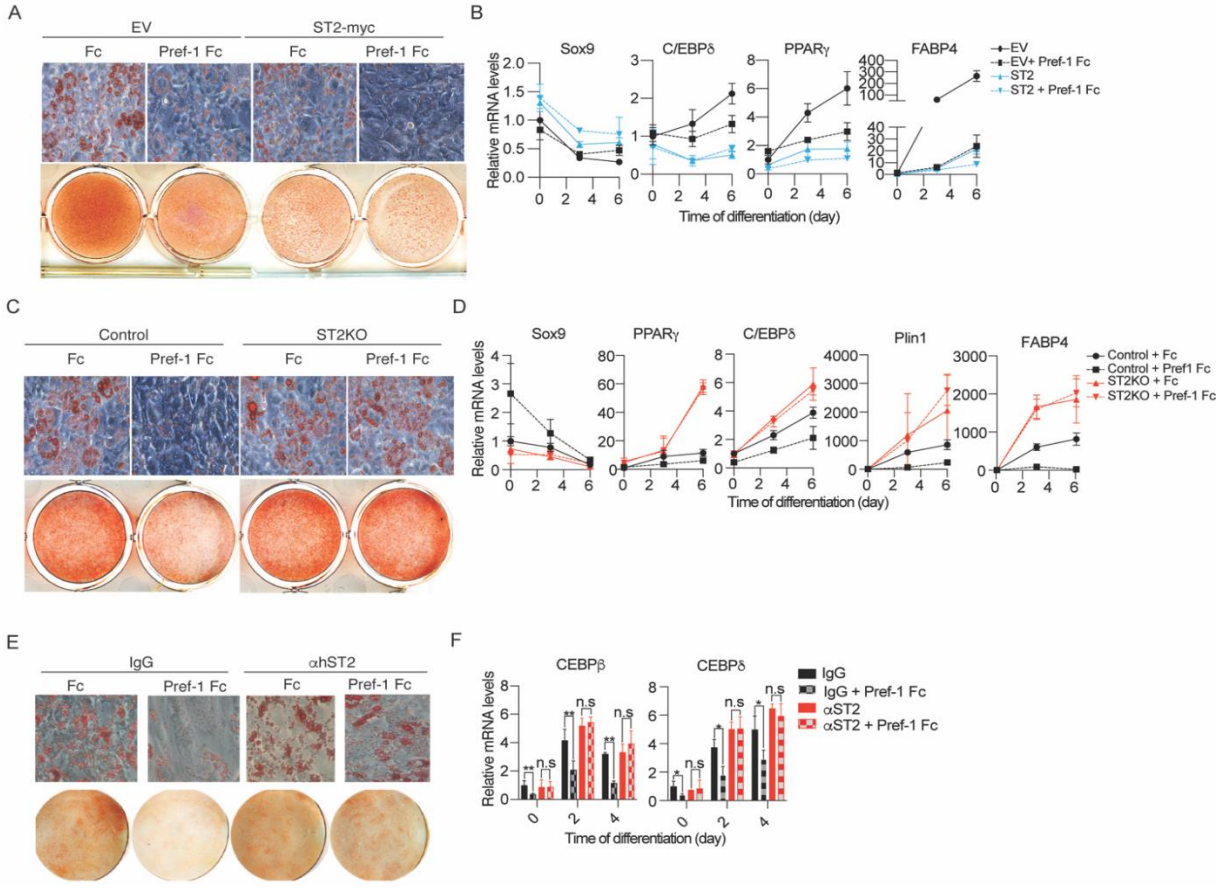

Figure 7. ST2 is critical Pref-1 inhibition of adipocyte differentiation.
3T3-L1 cells overexpressing ST2 were treated with Pref-1 and subjected for adipocyte differentiation, (A) Oil Red O staining and (B) adipogenic genes by RT-qPCR. ST2-KO 3T3-L1 preadipocytes treated with Pref-1 and then subjected for adipocyte differentiation, (C) Oil Red O staining and (D) adipogenic genes by RT-qPCR. Human preadipocytes pretreated with ST2 ab or IgG were then differentiated into adipocytes in the presence of Pref-1(E) Oil Red O staining and (D) C/EBPβ and C/EBPδ mRNA.

We also examine Pref-1 effect in cultured human primary preadipocytes using human ST2 neutralizing antibody. Similar to the results from 3T3-L1 cells, by Oil Red O staining, Pref-1 Fc compared to control Fc, treatment reduced the lipid staining. In contrast, Pref-1 treatment in ST2 antibody treated cells showed no significant decrease in lipid staining (Fig. 7E). Treatment with Pref-1 Fc, compared to control Fc, showed decreased expression of C/EBPβ and C/EBPδ in control IgG pre-treated human preadipocytes at Day 2 and Day 4 of differentiation. More importantly, in human preadipocytes pretreated with ST2 antibody, there were no differences in expression of C/EBPβ and C/EBPδ between Pref-1 Fc and control Fc treatment (Fig. 7F). Overall, in both mouse and human preadipocytes in culture, Pref-1 mediated inhibition of adipocyte differentiation was prevented in ST2 deficiency by ST2 neutralizing antibody treatment or by genetic ablation of ST2. Overall, we conclude that Pref-1 requires ST2 to exert inhibitory effect on preadipocyte differentiation into adipocytes.

IL1RAP/Myd88/IRAK1/TRAF6 axis for Pref-1 function

As stated before, ST2 is the known IL-33 receptor and IL-33-ST2 signaling pathway has been studied extensively. IL-33 binding to ST2 causes heterodimeric complex formation of ST2 and IL-1 receptor accessary protein (IL1RAP), while the herterodimer formation is not required for IL-33 binding to ST2. IL-33-ST2-1L1RAP complex then recruits MyD88 via its direct interaction with IL1RAP, that in turn recruits IRAK1/4 (IL-1 Receptor-Associated Kinase), followed by recruitment of TRAF-6 (TNF Receptor-Associated Factor), leading to activation of the NF-κB and MAPK pathways (Fig. 8A). Since Pref-1 binds ST2 to activate MEK/ERK for inhibition of adipogenesis, we predicted that some or all the signaling components of IL-33-ST2 may also be involved in Pref-1-ST2 signaling. We therefore tested this by measuring Pref-1 mediated P-ERK upon knockdown of each component in 3T3-L1 cells.

First, we tested whether IL1RAP that recruits downstream molecules of IL-33 signaling, is required for Pref-1 action. 3T3-L1 cells were transfected with IL1RAP shRNA and the knockdown cells were selected by using puromycin. The cells were pre-incubated with serum free media before treatment with Pref-1 Fc. IL-33 Fc and Fc alone were used as a positive and negative control, respectively. Gene analysis showed IL1RAP mRNA and protein levels to be reduced by approximately 80% (Fig. 8B, left). As previously shown, Pref-1 significantly increased ERK phosphorylation. IL-33 also increased P-ERK in 3T3-L1 cells, but in a lesser degree than that upon Pref-1 treatment. In the IL1RAP KD cells, Pref-1 and IL-33 both failed to induce P-ERK, while there were no significant changes in ERK protein levels between all the treatments (Fig. 8B, right). These result show that as in the case of IL-33, IL1RAP is required for Pref-1 activation of ERK. Thus, it is probable that ST2 interacts with IL1RAP upon Pref-1 binding to ST2.

We next employed shRNA-mediated KD of Myd88, IRAK1, and TRAF6 to examine whether they also are required for Pref-1 action. By RT-qPCR, Myd88, IRAK1, and TRAF6 mRNA levels were found to be decreased by 90%, 80% and 65%, respectively (Fig.5C, D, E left panels). Like IL1RAP, KD of Myd88 or IRAK1 prevented Pref-1 and IL-33 to increase P-ERK (Fig. 8C, E). Interestingly, Pref-1 did not increase P-ERK upon TRAF6 KD, while IL-33 could still activate ERK in these cells (Fig.8D). These results show that Pref-1 induces ERK phosphorylation by binding to ST2 through IL1RAP-Myd88-TRAF6 axis. In this regard, IL-33 mediated activation of NF-kB and ERK, the two downstream events of IL-33-ST2, has been reported to diverge, as TRAF6 is required for NF-kB, but not for ERK activation [35]. To examine whether IRAK1 is required for Pref-1 inhibitory effect on adipogenesis, we subjected

both control and IRAK1 KD preadipocytes in the presence of Pref-1 to adipocyte differentiation. Similar to ST2 KO, IRAK1 KD cells had slightly higher lipid accumulation than control cells and Pref-1 did not show inhibitory effect on these cells (Fig. 8F, top). Gene analysis showed similar results as ST2 KO. Unlike control cells, Pref-1 did not inhibit the adipogenic genes including C/EBPβ, C/EBPδ, PPARγ, and FABP4 (Fig. 8F, bottom). Taken together, Pref-1 activates P-ERK to inhibit adipocyte differentiation through ST2/IL1RAP/Myd88/TRAF6 axis.

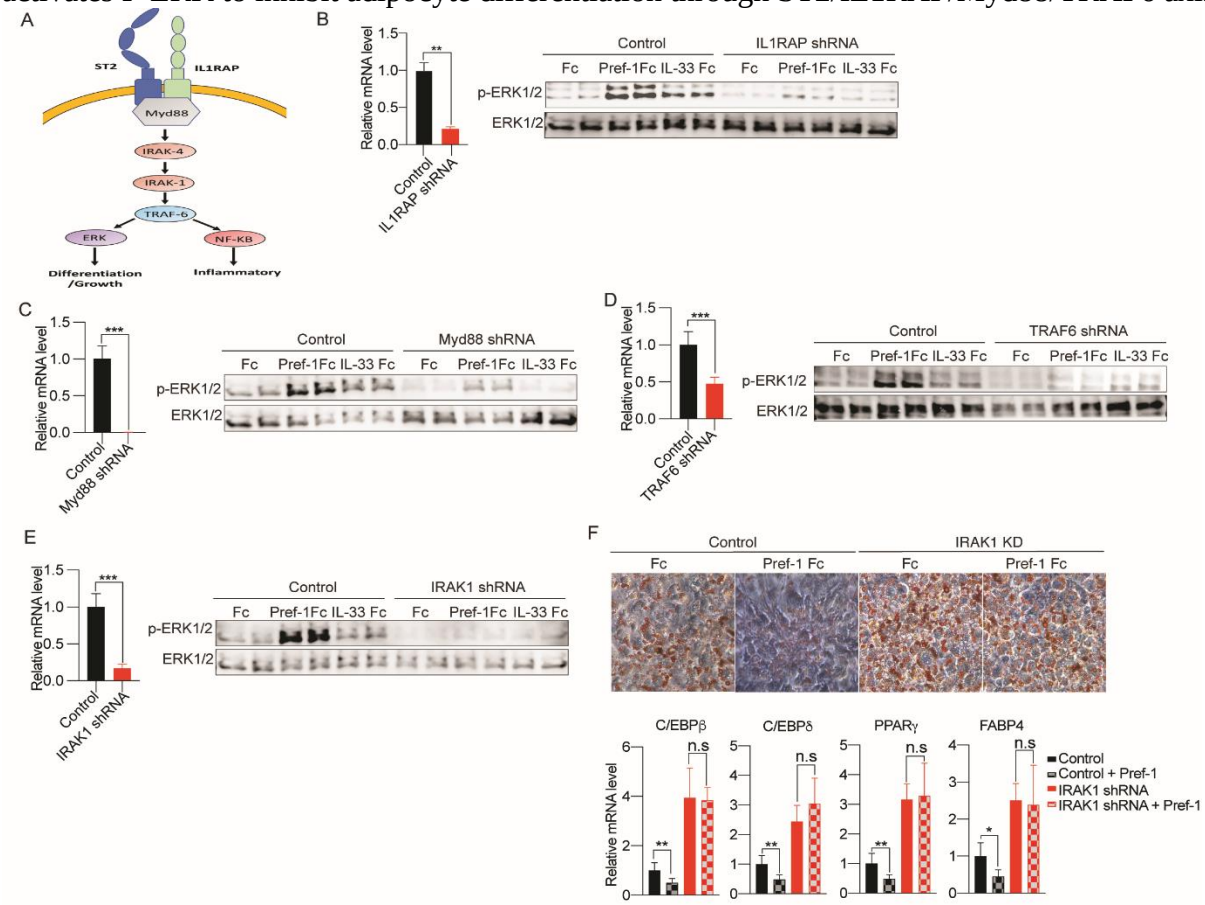

Figure 8. IL1RAP/Myd88/IRAK1/TRAF6 axis is required for Pref-1 function
(A) ST2 signaling pathway. RT-qPCR and IB for phosphor-ERK and total ERK in cells of IL1RAP KD (B), Myd88 KD (C), TRAF6 KD (D), and IRAK1 KD (E) treated with Fc, Pref-1 Fc, or IL-33 Fc. (F) IRAK1 KD cells were subjected to adipocyte differentiation in the presence of Pref-1, Oil Red O staining (top) and RT-qPCR (bottom).

Pref-1 inhibitory effect is prevented by ST2 antibody treatment and ST2 KO

We previously generated and studied loss- and gain-of function mouse models for Pref-1 to demonstrate Pref-1 function in WAT development *in vivo*; Pref-1-KO mice showed ab increase in adipose tissue mass due to lack of inhibitory effect of Pref-1 on adipogenesis. Conversely, Pref-1 overexpressing transgenic mice were lean with partial lipodystrophy. Here, we tested whether ST2 functions as the plasma membrane receptor for Pref-1. We predicted that, in the absence ST2, Pref-1 cannot inhibit adipogenesis in mice. First, immunocompromised mice were pretreated with either ST2 neutralizing antibody or normal IgG at 20 times higher concentration before a single dose of Pref-1 Fc or control, Fc administration. 3-wk post injection, in IgG pre-treated group, Pref-1 Fc injected mice had approximately 4 g lower body weight (BW) compared

to Fc group. In contrast, in the ST2 pretreated mice, Pref-1 Fc administration had no difference in BW compared to Fc treatment (Fig. 9A). By dissection and weighing, we found that Pref-1 Fc treatment reduced WAT mass in control mice pretreated with normal IgG, but it failed to reduce WAT mass in mice pretreated with ST2 neutralizing antibody. Moreover, Pref-1 treatment to normal IgG treated mice caused a 2-fold increase in expression of Sox9, a Pref-1 target gene, and a significant decrease in C/EBPβ, C/EBPδ and PPARγ in both iWAT and pWAT. More importantly, all these Pref-1 mediated changes in gene expression detected in normal IgG group were not observed in ST2 antibody treated mice (Fig. 9B). Incidentally, ST2 antibody pretreatment alone also increased BW and WAT mass with higher expression of adipogenic markers, probably due to the blocking of endogenous Pref-1 action. These data demonstrate that blocking ST2 prevents the inhibitory effect of Pref-1 on adipogenesis.

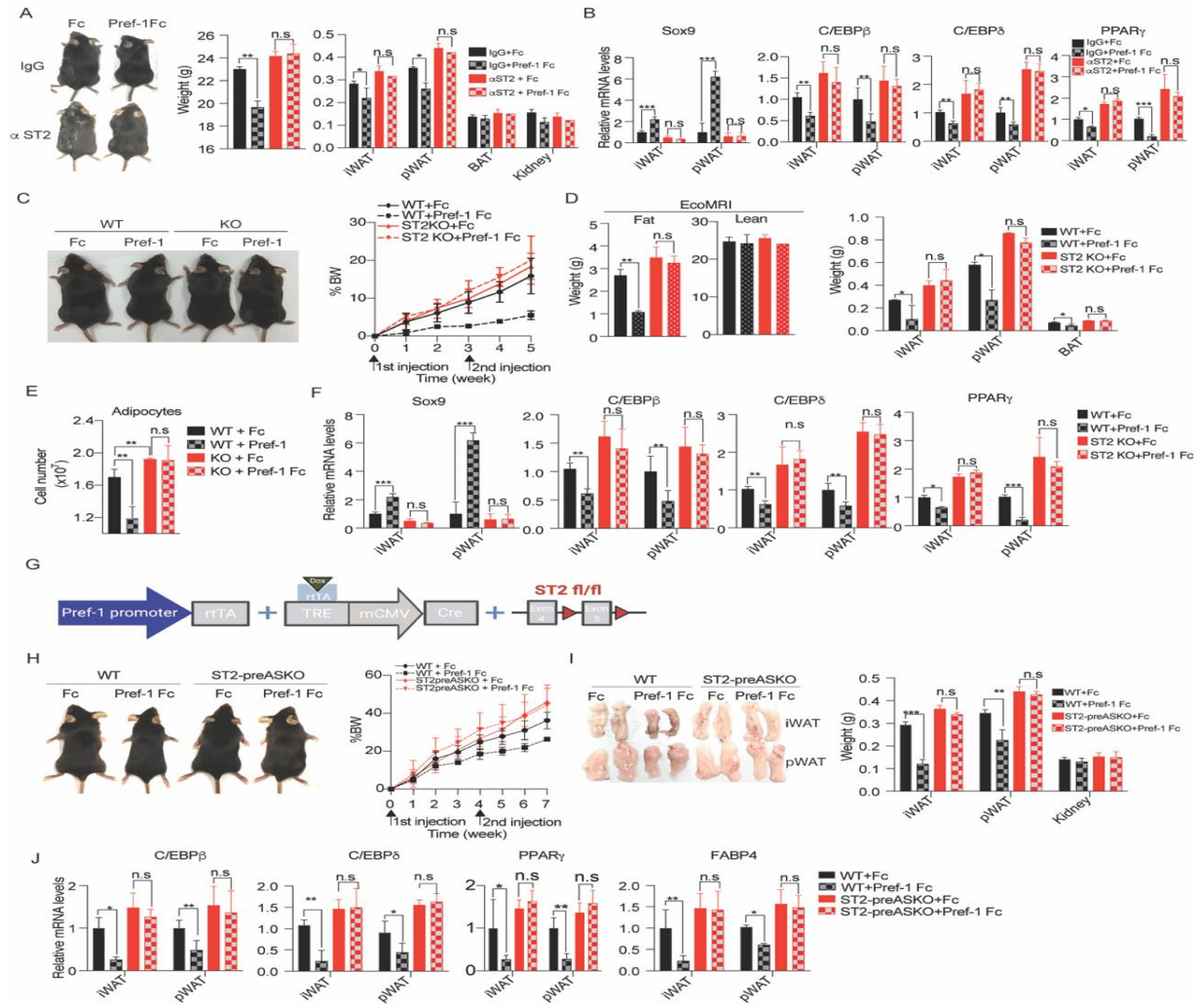

Figure 6. ST2 ablation blunts Pref-1 inhibition on adipogenesis *in vivo*

Immuno-compromised mice were injected with ST2 antibody or IgG, followed by Pref-1 Fc or Fc: (A) Body weight, fat mass. (B) RT-qPCR. ST2-KO and WT mice treated with Pref-1 Fc or FC: (C) Body weight gain. (D) Fat mass. (E) Adipocyte numbers of WT and ST2-KO mice. (F) RT-qPCR. ST2 KO in Pref-1 expressing cells mice (ST2-PreASKO) were treated with Pref-1 Fc or Fc: (G) schematic of generating ST2-preASKO. (H) Body weight gain. (I) fat mass. (J) RT-qPCR.

To further test the requirement of ST2 for Pref-1 action on adipogenesis, 9-wk old global ST2-KO and WT mice were injected with Fc or Pref-1 Fc every three wks. Prior to Pref-1 treatment, ST2 KO mice had somewhat higher BW and with higher WAT mass, again probably due to the lack of endogenous Pref-1 action. After 3 wks of the initial injection, in WT mice, Pref-1 treatment causes a decrease in % weight gain compared to control, Fc. At 5 wks, Pref-1 treated WT mice were approximately 13% lower BW than Fc mice. In contrast, there was no significant differences in % BW gain between Pref-1 Fc and Fc injected ST2 KO mice throughout 5-wks of treatment (Fig. 9C). EcoMRI showed that Pref-1 injected WT mice had approximately 2 g lower fat mass than those of Fc treated mice. In contrast, Pref-1 treatment did not lower fat mass in ST2 KO mice. Pref-1 administration lowered fat mass in WT mice while it had no effect on ST2-KO mice (Fig. 9D). We also quantified the number of adipocytes in iWAT from mice by staining adipocyte fraction with DAPI and LipidTox (lipid stain), followed by FACS. Indeed, number of adipocytes per depot was significantly decreased by Pref-1 treatment in WT mice. Notably, there was no significant decrease in number of adipocytes in Pref-1-treated ST2 KO mice (Fig. 9E). Additionally, Pref-1 treatment in ST2-KO mice did not show any increase of Sox9 mRNA levels by which increased 2-fold higher than Fc treatment in WT mice. In WT mice, Pref-1 injection also decreased mRNA levels of C/EBPβ, C/EBPδ, and PPARγ In contrast, Pref-1 injection did not affect these genes in ST2-KO mice. Also, somewhat lower Sox9 and higher expression of C/EBPs in Fc treated WT mice compared to Fc-treated ST2-KO mice were detected as the endogenous Pref-1 action would be blocked in ST2-KO mice (Fig. 9F). Overall, these data indicate that inhibition of adipogenesis by Pref-1 observed in WT mice was lost upon ST2 ablation.

Next, to demonstrate the requirement of ST2 for Pref-1 function specifically in preadipocytes, we generated ST2 KO in Pref-1 expressing cells by crossing ST2-floxed mice with -6 kb Pref-1 promoter-rtTA/TRE-Cre mice that we originally generated for inducible and conditional ablation. As we previously reported, upon doxycycline (Dox) administration, Pref-1-rtTA/TRE-Cre ablates ST2 in Pref-1 expressing adipose precursors (ST2-PreASKO), but not in adipocytes or in other cell types such as immune cells. Thus, observed differences in phenotype between our ST2-PreASKO and WT mice after Pref-1 administration would reflect the direct effect of Pref-1 on adipose precursors, but not indirect effects arising from other tissues or other cell types, if any. We performed the same studies using these ST2-PreASKO mice, as we performed in global ST2-KO mice. WT and ST2-PreASKO mice were administered with Dox at E0 and kept on Dox throughout the adulthood. At 7 wks old, these mice were injected with either Fc or Pref-1 Fc every 3 wk. In WT mice, Pref-1 Fc injection showed a much lower weight gain compared to Fc treatment. At 7-wks, Pref-1 Fc injected WT mice gained approximately 15% BW less than the control Fc treatment group. In contrast, in ST2-PreASKO mice, BW showed no difference between Pref-1 Fc and Fc injected mice (Fig. 9H). Pref-1 Fc compared to Fc treated mice had 3-fold and 2-fold lower tissue weight in iWAT and pWAT, respectively. Similar to ST2 global KO, Pref-1 Fc treatment in ST2-PreASKO mice did not show differences in WAT depot weights compared to Fc treated mice (Fig. 9I). Additionally, ST2-PreASKO mice without Pref-1 treatment already showed a somewhat higher BW as well as WAT mass compare to control Fc treated WT mice, again probably due to the lack of anti-adipogenic effect of endogenous Pref-1. Pref-1 Fc also decreased expression of adipogenic markers, including C/EBPβ, C/EBPδ, PPARγ, and FABP4, in WT mice. Pref-1 treatment failed to do so in ST2-PreASKO mice (Fig.9J). Overall, the observed effect of Pref-1 on ST2-PreASKO mice was

similar to that on global ST2-KO mice, suggesting the Pref-1 function on adipose precursors. Overall, these results clearly show that ST2 is required for Pref-1 inhibition of adipogenesis in vivo.

DISCUSSION

Pref-1 is a widely used preadipocyte marker that we originally cloned and identified. Pref-1 has been shown to mark adipose progenitors that are required for white adipose tissue development and expansion. By using recently developed diazirine photo-reactive linker combined with robust NHS-ester chemistry in live cells, we found that Pref-1 directly binds to the plasma membrane ST2 for its downstream signaling. We also showed that the known ST2 ligand, IL-33 and Pref-1 binding to ST2 is competitive. In addition, we found plasma membrane ST2 is highly expressed in both SVF and 3T3-L1 preadipocytes. Furthermore, we found that ST2 and its downstream signaling axis are required for Pref-1 signaling for ERK activation, inhibition of adipocyte differentiation and expression of Pref-1 targets, such as Sox9, C/EBPβ and C/EBPδ both *in vitro* and *in vivo*.

In understanding mechanism underlying Pref-1 action, we had been searching for the critical missing component of Pref-1 signaling pathway. Previously, in order to identify Pref-1 receptor, structural feature of Pref-1 was considered. However, EGF-repeats of Pref-1 do not maintain the exact spacing of EGF and are missing of aa critical for EGF receptor binding. Even though mammalian Pref-1 was previously reported to bind to and act synergistically with Notch, we did not find Pref-1 interact directly with Notch or Pref-1 effects in Notch downstream targets such HES-1[28]. We only reported that fibronectin interacts and modulates Pref-1 signaling. In order to the bona fide plasma membrane receptor of Pref-1, we employed much improved and more sensitive diazirine photo-reactive linker method of crosslinking in live cells. Remarkably, we have identified ST2 as the putative Pref-1 receptor.

ST2 (also called IL1RL1 (IL-1 receptor-like protein 1)) is found in various tissues, but mainly in mast cells and Th2 cells for type 2 immunity. Importantly, ST2 is the receptor for IL-33 that belongs to the interleukin-1 (IL-1) family of inflammatory cytokines. Interestingly, IL-33 does not contain a signal sequence and is found in the nucleus but is released into the extracellular space from necrotic cells during cell and tissue damage and can act as an endogenous danger signal to alert adjacent cells [32, 36]. Through ST2, IL-33 is involved in Th2-mediated immune response and is closely related to inflammatory diseases [37-39]. In contrast, Pref-1 made as transmembrane protein is cleaved at the juxtamembrane region in releasing soluble Pref-1. Even though ST2 has been shown to be expressed in endothelial cells, as well as immune cell types, including subset of Treg and ILC2 cells [37, 40, 41], we found the plasma membrane form of ST2 highly expressed in the SVF of WAT. Moreover, after FACS of SVF cells, we clearly detected $ST2^+$ cells that were Lin^- ($CD45^-$, $Ter1119^-$, $CD31^-$). In fact, a higher percentage of Lin^- cells in comparison to Lin^+ cells were $ST2^+$, when sorted according to Rodeheffer et al. [13]. Moreover, during 3T3-L1 adipocyte differentiation, both Pref-1 and ST2 were downregulated. In contrast, IL-33 expression was very low in preadipocytes and induced during adipocyte differentiation. Moreover, both ST2 and Pref-1 are expressed in embryonic stage, and IL-33 is not known to be secreted during embryogenesis [42][42][40][39]. Overall, the parallel expression pattern of Pref-1 and ST2 is consistent with the concept of ST2 functioning as the Pref-1 receptor during adipocyte differentiation.

In our study, we found that Pref-1 can directly bind to ST2. Interestingly, we found that Pref-1 and IL-33 showed competitive binding to ST2. This is likely due to ST2 only relatively

small binding pocket which contains 3 extracellular immunoglobulin (Ig)-like domains. In fact, there are other receptors having more than one ligand. As mentioned, EGF, HB-EGF, and TGFα, all function by binding to EGF receptor [43]. Delta, Serrate and Lag-2 are all ligands for Notch while RAGE, the receptor for advanced glycation end products, has multiple ligand [44-46]. Recently G-coupled receptor for chemokines (MIP1 and Rantes), CCR5, also functions as a HIV receptor and blocking CCR5 is the only known cure for HIV [47-49].

As Pref-1 functions via binding to ST2, we predicted ST2 to be required for Pref-1 function. Indeed, ST2 deficiency prevented Pref-1 mediated activation of ERK, induction of Sox9 and its downstream suppression of C/EBPβ and C/EBPδ, and inhibition of adipocyte differentiation. We also found that Pref-1 requires ST2 downstream signaling molecules to activate ERK and inhibit adipogenesis. We showed that IL-1 receptor accessary protein (IL1RAP), myeloid differentiation primary response protein MyD88, and IL-1 Receptor-Associated Kinase (IRAK)1/4, followed by recruitment of TNF Receptor-Associated Factor (TRAF) 6 are all required for Pref-1 ERK activation and adipogenesis inhibition.

Pref-1 is highly expressed before adipose conversion but is downregulated during adipogenesis, Pref-1 level inversely correlating with the degree of differentiation. Pref-1 is used widely as a preadipocyte marker and Pref-1 level increases greatly in murine models of lipodystrophies, while it is significantly lower in obesity mouse models and human. We found a high level of plasma membrane ST2 in 3T3-L1 preadipocytes and in Lin^- preadipocytes of SVF from WAT. Our loss-of-function in 3T3-L1 cells indicated that Pref-1 binds to ST2 at the plasma membrane of preadipocytes to activate ERK and inhibit adipogenesis. In addition, using various mouse models including ST2-treated neutralizing antibody, ST2 global KO, and ST2 ablation in Pref-1 expressing cells clearly demonstrate *in vivo* evidence of ST2 requirement for Pref-1 to exert its effects on adipogenesis and that ST2 as the de facto Pref-1 receptor.

ACKNOWLEDGEMENTS

The work was supported in part by NIDDK grant to H.S.S. Imaging was supported in part by NIH S10RR026866-01. The content is solely the responsibility of the authors and does not necessarily represent the official views of the NIH. The authors declare no competing financial interests.

RERFERENCES

1. Melvin, A., S. O'Rahilly, and D.B. Savage, *Genetic syndromes of severe insulin resistance.* Curr Opin Genet Dev, 2018. **50**: p. 60-67.
2. Araujo-Vilar, D. and F. Santini, *Diagnosis and treatment of lipodystrophy: a step-by-step approach.* J Endocrinol Invest, 2018.
3. Jo, J., et al., *Hypertrophy and/or Hyperplasia: Dynamics of Adipose Tissue Growth.* PLoS Comput Biol, 2009. **5**(3): p. e1000324.
4. Rosen, E.D. and B.M. Spiegelman, *Molecular regulation of adipogenesis.* Annu Rev Cell Dev Biol, 2000. **16**: p. 145-71.
5. Gregoire, F.M., C.M. Smas, and H.S. Sul, *Understanding adipocyte differentiation.* Physiol Rev, 1998. **78**(3): p. 783-809.
6. Cristancho, A.G. and M.A. Lazar, *Forming functional fat: a growing understanding of adipocyte differentiation.* Nat Rev Mol Cell Biol, 2011. **12**(11): p. 722-34.
7. Mota de Sa, P., et al., *Transcriptional Regulation of Adipogenesis.* Compr Physiol, 2017. **7**(2): p. 635-674.

8. Smas, C.M. and H.S. Sul, *Pref-1, a protein containing EGF-like repeats, inhibits adipocyte differentiation.* Cell, 1993. **73**(4): p. 725-34.
9. Sul, H.S., *Minireview: Pref-1: role in adipogenesis and mesenchymal cell fate.* Mol Endocrinol, 2009. **23**(11): p. 1717-25.
10. Sarantopoulos, C.N., et al., *Elucidating the Preadipocyte and Its Role in Adipocyte Formation: a Comprehensive Review.* Stem Cell Rev, 2018. **14**(1): p. 27-42.
11. Tang, W., et al., *White fat progenitor cells reside in the adipose vasculature.* Science, 2008. **322**(5901): p. 583-6.
12. Tseng, Y.H., et al., *Prediction of preadipocyte differentiation by gene expression reveals role of insulin receptor substrates and necdin.* Nat Cell Biol, 2005. **7**(6): p. 601-11.
13. Rodeheffer, M.S., K. Birsoy, and J.M. Friedman, *Identification of white adipocyte progenitor cells in vivo.* Cell, 2008. **135**(2): p. 240-9.
14. Fox, K.E., et al., *Depletion of cAMP-response element-binding protein/ATF1 inhibits adipogenic conversion of 3T3-L1 cells ectopically expressing CCAAT/enhancer-binding protein (C/EBP) alpha, C/EBP beta, or PPAR gamma 2.* J Biol Chem, 2006. **281**(52): p. 40341-53.
15. Hudak, C.S., et al., *Pref-1 marks very early mesenchymal precursors required for adipose tissue development and expansion.* Cell Rep, 2014. **8**(3): p. 678-87.
16. Wang, Y. and H.S. Sul, *Ectodomain shedding of preadipocyte factor 1 (Pref-1) by tumor necrosis factor alpha converting enzyme (TACE) and inhibition of adipocyte differentiation.* Mol Cell Biol, 2006. **26**(14): p. 5421-35.
17. Kim, K.A., et al., *Pref-1 (preadipocyte factor 1) activates the MEK/extracellular signal-regulated kinase pathway to inhibit adipocyte differentiation.* Mol Cell Biol, 2007. **27**(6): p. 2294-308.
18. Wang, Y. and H.S. Sul, *Pref-1 regulates mesenchymal cell commitment and differentiation through Sox9.* Cell Metab, 2009. **9**(3): p. 287-302.
19. Massague, J., *Transforming growth factor-alpha. A model for membrane-anchored growth factors.* J Biol Chem, 1990. **265**(35): p. 21393-6.
20. Ray, P., et al., *Structure-function studies of murine epidermal growth factor: expression and site-directed mutagenesis of epidermal growth factor gene.* Biochemistry, 1988. **27**(19): p. 7289-95.
21. Campbell, I.D., et al., *Structure-function relationships in epidermal growth factor (EGF) and transforming growth factor-alpha (TGF-alpha).* Biochem Pharmacol, 1990. **40**(1): p. 35-40.
22. Burgess, A.W., et al., *Murine epidermal growth factor: structure and function.* Biochemistry, 1988. **27**(14): p. 4977-85.
23. Baron, M., *An overview of the Notch signalling pathway.* Semin Cell Dev Biol, 2003. **14**(2): p. 113-9.
24. Kopan, R. and M.X. Ilagan, *The canonical Notch signaling pathway: unfolding the activation mechanism.* Cell, 2009. **137**(2): p. 216-33.
25. Fortini, M.E., *Notch signaling: the core pathway and its posttranslational regulation.* Dev Cell, 2009. **16**(5): p. 633-47.

26. Laborda, J., et al., *dlk, a putative mammalian homeotic gene differentially expressed in small cell lung carcinoma and neuroendocrine tumor cell line.* J Biol Chem, 1993. **268**(6): p. 3817-20.
27. Bray, S.J., et al., *The atypical mammalian ligand Delta-like homologue 1 (Dlk1) can regulate Notch signalling in Drosophila.* BMC Dev Biol, 2008. **8**: p. 11.
28. Wang, Y., et al., *Pref-1 interacts with fibronectin to inhibit adipocyte differentiation.* Mol Cell Biol, 2010. **30**(14): p. 3480-92.
29. Iso, T., L. Kedes, and Y. Hamamori, *HES and HERP families: multiple effectors of the Notch signaling pathway.* J Cell Physiol, 2003. **194**(3): p. 237-55.
30. Bray, S.J. and M. Gomez-Lamarca, *Notch after cleavage.* Curr Opin Cell Biol, 2017. **51**: p. 103-109.
31. Griesenauer, B. and S. Paczesny, *The ST2/IL-33 Axis in Immune Cells during Inflammatory Diseases.* Front Immunol, 2017. **8**: p. 475.
32. Liew, F.Y., N.I. Pitman, and I.B. McInnes, *Disease-associated functions of IL-33: the new kid in the IL-1 family.* Nat Rev Immunol, 2010. **10**(2): p. 103-10.
33. Chen, Q., H.P. Carroll, and M. Gadina, *The newest interleukins: recent additions to the ever-growing cytokine family.* Vitam Horm, 2006. **74**: p. 207-28.
34. Baba, Y., et al., *Involvement of PU.1 in mast cell/basophil-specific function of the human IL1RL1/ST2 promoter.* Allergol Int, 2012. **61**(3): p. 461-7.
35. Funakoshi-Tago, M., et al., *TRAF6 is a critical signal transducer in IL-33 signaling pathway.* Cell Signal, 2008. **20**(9): p. 1679-86.
36. Miller, A.M., et al., *Interleukin-33 induces protective effects in adipose tissue inflammation during obesity in mice.* Circ Res, 2010. **107**(5): p. 650-8.
37. Rankin, L.C. and D. Artis, *Beyond Host Defense: Emerging Functions of the Immune System in Regulating Complex Tissue Physiology.* Cell, 2018. **173**(3): p. 554-567.
38. Cautivo, K.M. and A.B. Molofsky, *The Skinny: Pancreatic ILC2s Promote Insulin Secretion.* Immunity, 2017. **47**(5): p. 812-814.
39. Molofsky, A.B., A.K. Savage, and R.M. Locksley, *Interleukin-33 in Tissue Homeostasis, Injury, and Inflammation.* Immunity, 2015. **42**(6): p. 1005-19.
40. Zeyda, M., et al., *Severe obesity increases adipose tissue expression of interleukin-33 and its receptor ST2, both predominantly detectable in endothelial cells of human adipose tissue.* Int J Obes (Lond), 2013. **37**(5): p. 658-65.
41. A, S., V.G. J, and S. F, *Mononeuropathies examination diagnosis and treatment.* J Clin Neuromuscul Dis, 1999. **1**(1): p. 51.
42. Pichery, M., et al., *Endogenous IL-33 is highly expressed in mouse epithelial barrier tissues, lymphoid organs, brain, embryos, and inflamed tissues: in situ analysis using a novel Il-33-LacZ gene trap reporter strain.* J Immunol, 2012. **188**(7): p. 3488-95.
43. Singh, B., G. Carpenter, and R.J. Coffey, *EGF receptor ligands: recent advances.* F1000Res, 2016. **5**.
44. Nandagopal, N., et al., *Dynamic Ligand Discrimination in the Notch Signaling Pathway.* Cell, 2018. **172**(4): p. 869-880 e19.
45. Fritz, G., *RAGE: a single receptor fits multiple ligands.* Trends Biochem Sci, 2011. **36**(12): p. 625-32.

46. Megason, S.G., *Dynamic Encoding in the Notch Pathway.* Dev Cell, 2018. **44**(4): p. 411-412.
47. Grande, F., et al., *CCR5/CXCR4 Dual Antagonism for the Improvement of HIV Infection Therapy.* Molecules, 2019. **24**(3).
48. Gupta, R.K., et al., *HIV-1 remission following CCR5Delta32/Delta32 haematopoietic stem-cell transplantation.* Nature, 2019. **568**(7751): p. 244-248.
49. Lopalco, L., *CCR5: From Natural Resistance to a New Anti-HIV Strategy.* Viruses, 2010. **2**(2): p. 574-600.

Chapter 3:

Aifm2, a NADH oxidase, supports robust glycolysis and is required for cold- and diet-induced thermogenesis

Aifm2, a NADH oxidase, supports robust glycolysis and is required for cold- and diet-induced thermogenesis

ABSTRACT

Brown adipose tissue (BAT) is highly metabolically active tissue to dissipate energy via UCP1 as heat, and BAT mass is correlated negatively with obesity. The presence of BAT/BAT-like tissue in humans renders BAT as attractive target against obesity and insulin resistance. Here, we identify Aifm2, a NADH oxidoreductase domain containing flavoprotein, as a lipid droplet (LD) associated protein highly enriched in BAT. Aifm2 is induced by cold, as well as by diet. Upon cold or β-adrenergic stimulation, Aifm2 associates with the outer side of the mitochondrial inner membrane. As a unique BAT-specific first mammalian NDE (external NADH dehydrogenase)-like enzyme, Aifm2 oxidizes NADH to maintain high cytosolic NAD levels in supporting robust glycolysis and to transfer electrons to ETC for fueling thermogenesis. Aifm2 in BAT and subcutaneous WAT promotes oxygen consumption, uncoupled respiration and heat production during cold- and diet-induced thermogenesis. Aifm2, thus, can ameliorate diet-induced obesity and insulin resistance.

INTRODUCTION

Obesity, characterized by the excess accumulation of white adipose tissue (WAT), has become a global epidemic. In contrast to WAT that serves as the main energy storage organ, brown adipose tissue (BAT) dissipates energy via non-shivering thermogenesis to maintain body temperature when exposed to cold. Moreover, upon cold exposure, subcutaneous WAT becomes BAT-like via so-called browning or beiging [1]. Presence of BAT and BAT-like tissue in human adults has been established and BAT activity is known to increase upon cold exposure to inversely correlate with adiposity [2-6]. Unlike white adipocytes that have unilocular lipid droplet (LD), brown adipocytes contain numerous small LDs and a high number of mitochondria. Although it may not be an exclusive mechanism, UCP1 at the inner mitochondrial membrane of BAT dissipates proton gradient from mitochondrial electron transport chain (ETC) to generate heat [7]. In addition, BAT has also been known to dissipate heat in response to diet or food intake, known as diet-induced thermogenesis. Thus, even at thermoneutrality, UCP1 KO mice are heavier than their WT counterparts and UCP1 has also been shown to increase from consuming obesogenic diets [8]. A better understanding of the regulation of BAT metabolism and thermogenic process may provide future therapeutic targets for obesity and related metabolic diseases, such as type 2 diabetes.

Thermogenesis is a highly energetic process and, classically, FAs derived from intracellular lipolysis are presumed to be used as the energy source [9]. Upon cold exposure, norepinephrine released from the sympathetic innervation in BAT stimulates β_3-adrenergic receptor increasing intracellular lipolysis involving ATGL and HSL [10]. FAs thus generated are utilized for oxidation in addition to directly binding and activating UCP1 [6]. Recently, however, it was reported that FAs taken up from circulation are used for thermogenesis, especially in fasted condition [11, 12]. Glucose uptake increases in BAT of both rodents and humans after cold exposure or β-adrenergic stimulation [13, 14]. And proteins/enzymes involved in glucose uptake and catabolism, such as Glut1 and Hexokinase, are induced in BAT upon cold exposure [15]. And BAT has the highest glucose uptake among different tissues and, thus, the presence of BAT or BAT-like tissue in adults has been evidenced by the ^{18}F-glucose uptake of PET-CT scan [13]. Interestingly, glycolysis was reported to be critical for optogenetically induced

thermogenesis [16]. Yet, neither the role nor the significance of glycolysis and its downstream metabolism during thermogenesis have been well studied.

Glucose taken up by various tissues undergoes glycolysis to generate ATP and NADH. To sustain robust glycolysis, cytosolic NAD is critical in supporting glyceraldehyde-3-phosphate dehydrogenase reaction in the glycolytic pathway [17]. Inner mitochondrial membrane is impermeable to NADH or NAD. Thus, in most tissues, malate-aspartate shuttle transfers NADH produced from glycolysis into mitochondria for ETC and returns NAD to cytosol for glycolysis. In BAT, that require rapid ATP generation, glycerol-3-phosphate shuttle is presumed critical [17, 18]. However, contribution of mtGPD in thermogenesis could not be demonstrated in KO mouse models in vivo. The original mtGPD-KO mouse model did not show impaired thermogenesis, whereas a second independent mtGPD-KO mouse model maintained on a high fat diet (HFD) exhibited a more rapid increase in body weight with lower energy expenditure, but this was due to higher circulating thyroid hormone levels [19, 20]. Lactate dehydrogenase (LDH) reaction in the cytosol can regenerate NAD by converting pyruvate to lactate. However, lactate in BAT can be used for oxidation by converting back to pyruvate to enter TCA cycle, and lactate levels in BAT do not increase but rather decrease during thermogenesis [16] [21]. Therefore, BAT may have a unique, yet to be identified means of NAD generation for glycolysis.

NDHs (NADH dehydrogenase) that are mainly found in yeast, bacteria and plants are associated with the mitochondrial inner membrane and catalyze the same NADH oxidase reaction as complex I in ETC [22]. There are two main classes of NDHs, NDI (internal NDH) facing the mitochondrial matrix and NDE (external) facing the intermembrane space [23]. In yeast that lacks complex 1, NDI maintains mitochondrial NAD to ensure efficient TCA cycle, while NDE provides cytosolic NAD for glycolysis. NDHs also increase ETC activity and respiration by transferring electrons to CoQ [24]. Thus, ablation of these enzymes leads to high NADH/NAD ratio causing an imbalance in cellular metabolism with defective mitochondrial respiration [25]. In fact, upon environmental cues, NDE has been shown to have much higher turnover numbers of NADH:UQ oxidase activity than mammalian complex I [26]. There has been no NDHs reported in the mammalian system.

We recently have discovered that Aifm2 (Apoptosis inducing mitochondrion associated factor 2 (also called AMID, or Prg3), a flavoprotein with a NADH/NAD oxidoreductase domain as a lipid-droplet associated protein that is highly and specifically expressed in BAT and is induced upon cold exposure/β-adrenergic stimulation in BAT and iWAT. Although Aifm2 was previously reported to a be a p53 target and predominantly cytosolic to promote caspase-independent cell death [27, 28], Aifm2 cannot induce apoptosis in BAT cells. Rather, upon stimulation, Aifm2 localizes to mitochondria for conversion of NADH to NAD to sustain robust glycolysis, while transferring electrons to mitochondrial ETC in fueling thermogenesis. Remarkably, Aifm2 not only has sequence similarity to yeast NDE1, but also shares the localization and the enzymatic activity. Yeast NDE1 can rescue impaired thermogenesis from Aifm2 deficiency, making Aifm2 to be a mammalian NDE specific to thermogenic tissues. Interestingly, search of GWAS database reveals multiple SNPs of Aifm2 to be associated with waist-hip ratio, body mass index and fasting glucose level-related insulin resistance, suggesting a potential role of Aifm2 in human obesity and type 2 diabetes [29-31].

EXPERIMENTAL PROCEDURES

Plasmids and reagents

All plasmids, reagents and antibodies used are provided in Table 2.

Animals

All animal studies were carried out in accordance with UC Berkeley ACUC and OLAC regulations. Generation of Aifm2 KO mice was created by injecting Cas9 mRNA and an in vitro transcribed guide RNA target sequence, CTTCCCTGGCAAGTTTAACG, corresponding to aa113-120 at the third exon of Aifm2 into zygotes. Aifm2 was first inserted into plasmid in which the chicken β-actin promoter driving tagged zsGreen and the bovine growth hormone poly A signal at the 3' end. The vector also contains LoxP-STOP-LoxP cassette at 5' end of the Aifm2 coding sequence. Generation of Aifm2 floxed mice was carried out by microinjected into embryos. Aifm2 TG mice were generated by crossing these mice with UCP1-Cre mice. Aifm2 floxed mice using CRISPR-Cas9 Nickase system. A pair of the gRNAs target sequences, ACCAGCGGCTCGAGCCTCTCAGG and GTAAATCTCAGGACAGCGCTAGG, corresponding to 5' and 3' end of Exon 2 of the Aifm2 gene, respectively, with Cas9 Nickase mRNA, and DNA donor containing Exon2 flanked by LoxP sites were injected into zygotes. Mice were housed in a 12:12 light-dark cycle and chow and water were provided *ad libitum*, when not specified.

Metabolic and thermogenic measurements

Fat and lean mass was determined by echoMRI-100V. CT Scan was performed on Trifoil eXplore RS9 microCT system. Metabolic cage experiments to measure physical activity were carried out on CLAMS System (Columbus). Body temperatures were assessed using a RET-3 rectal probe for mice (Physitemp). CL316,243 (Sigma) was intraperitoneally injected into mice at 1mg/kg. FLIR E5 series infrared camera was employed to capture thermography.

Human tissues

Human cDNA array containing cDNA from 48 samples covering all major human normal tissues at different locations (Origene, HRMT104) were used for RT-qPCR and human tissue lysates (Thermo) were utilized immunoblotting.

Cell culture

Brown adipocyte differentiation was performed as described in Kajimura et al., 2009. To induce thermogenic genes, cells were treated for 6 hrs with 10 μM isoproterenol or CL-316,248. Cells were then harvested for RNA isolation or protein extraction or fixed with formalin for ORO staining. For adenoviral transduction, sub-confluent BAT cells were transduced with vehicle (ViraQuest) or Aifm2 (Abmgood) adenovirus with 0.5 μg/ml polyLysine at MOI=100. For Aifm2 knockdown, BAT adipocytes were transduced by Aifm2 shRNA lentivirus at MOI=200.

Mitochondrial and lipidTox analysis

MitoTracker Red was added into the culture media at final concentrations of 300nM. The cells were incubated under normal culture conditions for 15 min. LipidTox Red was added into the culture media at 1:200 dilution. The cells were incubated under normal culture conditions for 30 min. These cells were mounted with Duolink Mounting medium with DAPI, and then visualized by fluorescence microscopy.

Plasmid Constructs

Aim2 N-terminal and C-terminal deletion constructs were created by PCR amplifying the non-deleted part of the vector and reinserting into either pCDNA3.1 or pEGFP-N1. Aifm2 D285N

and G2A mutants were created by site directed mutagenesis using the following primers:
D285N: ATGCCATTGGTAACTGTGCCGATACCAAG
R: CTTGGTATCGGCACAGTTACCAATGGCAT. G2A F: AATTCGGTACCATGGGGTCCC AGGTCTCG. R: CGAGACCTGGGACCCCATGGTACCGAAT

Separation of SVF and Adipocyte fraction

SVF fractionation was carried out as previously described[12]. Briefly, mouse WAT and BAT were minced and digested with Collagenase type II (Sigma) in KREBs buffer at 37° C for 45 min with shaking. Cell suspension was then passed through 100 μm mesh, span at 300g for 5 min, floating adipocyte fraction was collected for RNA, DNA, or protein extraction, whereas cell pellet was resuspended in KREBS buffer, passed through 70 μm and 40 μm mesh and subjected to FACS and *in vitro* differentiation, or lysed with RIPA buffer for immunoblotting or with TRIzol for RNA isolation.

RNA isolation and RT-qPCR

Total RNA from cells were extracted using TRIzol and RNA from adipose tissue were extracted using RNeasy Lipid kit (Qiagen). Reverse transcription was performed with 1 μg of total RNA using Superscript II (Invitrogen) or with 10-100 ng from sorted cells using Superscript III (Invitrogen). RT-qPCR was performed on ABI PRISM 7500 (Applied Biosystems). Statistical analysis was performed using ddct method with U36B4 primers as control (see primer sequences in Supplementary Table S1.

Cold-induced Thermogenesis

Cold exposed mice were housed for 10 days at thermoneutrality before cold exposure at 4°C. Core body temperature was determined using a Physitemp BAT-12 probe. CL-316,243 (Sigma) was injected intraperitoneally into mice at 1mg/kg.

Whole mount staining

1mm piece of tissue was excised, fixed with 1% PFA, incubated with UCP1 antibody, LipidTox Red Reagent (Thermo Fisher) and DAPI. Tissues were immobilized on a slide with mounting medium and visualized using a confocal microscope.

Immunoblotting and Immunostaining

For immunoblotting, tissues or cells were lysed in RIPA buffer. Proteins (5-100 μg) were separated on SDS-PAGE gel, transferred on a nitrocellulose membrane and incubated with indicated antibodies (see Supplementary Table S2 for list of antibodies). For whole-mount tissue immunostaining, a 1mm piece of WAT or BAT was excised, incubated with LipidTOX Green Reagent (Thermo Fisher) and DAPI, immobilized on a slide with mounting medium and imaged using confocal microscope. Cell number and size was calculated using ImageJ software.

AAV and lentivirus administration in animals

Mice were anesthetized with ketamine (100 mg/kg). For BAT and WAT administrations, a longitudinal incision in the skin at the interscapular or inguinal area was performed. To distribute the vector in the whole depot, each interscapular BAT (iBAT) or inguinal WAT (iWAT) received four injections of 20μL AAV or Aifm2 shRNA solution using a Hamilton syringe. For the systemic administration, AAV vectors were diluted in 200 μL saline and injected into the lateral tail vein.

Subcellular fractionation

Mitochondria fractions were isolated with 50 mg of brown adipose tissue or $2x10^7$ using Mitochondria Isolation Kit for Tissue or Culture Cells (Thermo Scientific). LD and cytosolic fractions were isolated as described in [33].

Mitochondria and mitoplast isolation

Intact mitochondria from adipose tissues or BAT cells were isolated using Mitochondria Isolation Kit for Tissue or Mitochondria Isolation Kit for Cultured Cells (Thermo Scientific). Mitochondrial extract was collected using 2% CHAPS lysis buffer. Intact mitoplast was isolated by treating purified mitochondria with digitonin (0.25mg/ml) for 20 min.

NAD/NADH and NADH oxidase activity

NAD/NADH in cell/ tissue lysates was measured with colorimetric NAD/NADH (K337). Oxidoreductase activity assay was carried out by using spectrophotometer, as described in Miramar et al, 2001. The assay buffer was 100 mM potassium phosphate pH, 8.0 containing 100 mM NaCl and 0.1mM FAD. Enzyme was mixed in the assay buffer for 15 min prior to adding NADH to final concentration of 0.25mM. The absorbance at 340mm was measuring at 25^{o}C.

JC-1 and ERthermAC

BAT cells ($1X10^{6}$ cells/ml) were treated with JC-1 (2□M) for 30 min, and cells were then washed 2 times with PBS and and subjected to FACS analysis. For ERthermAC, BAT cells were treated with the dye (250nM) for 30 mins prior to FACS analysis.

Statistical analysis

Statistical analysis was performed using two tailed t-test. The error bars represent standard error mean (SEM). Data are expressed as mean +/- SD and p value <0.05 was considered statistically significant. Number of mice or replicates used in each experiment was indicated in figure legends. Experiments were repeated at least three times.

RESULTS

Aifm2 is expressed specifically in BAT and is induced by cold.

Brown adipocytes contain multiple small lipid droplets which are different from a unilocular LD found in white adipocytes [32]. In an attempt to identify BAT-specific proteins associated with smaller LDs by proteomic mass spectrometry, we used a protocol adapted from [33] to isolate LD fraction from perigonadal WAT (pWAT) or BAT from mice. Proteins isolated from LD fraction of both adipose depots were analyzed by LC/MS. We discovered that Aifm2 as a lipid droplet associated protein and was highly enriched in BAT (Fig.10A,B). Aifm2 did not possess signal sequence but contained N-terminal hydrophobic/membrane domain (aa1-27), NADH oxidoreductase domain (aa81-285) and FAD domain (aa286-308) (Fig. 11A). Using Aifm2 primers detecting both human and mouse Aifm2, gene analysis by RT-qPCR in various mouse tissues from 6-wk-old C57BL/6 mice and commercially available human tissue cDNA array revealed that Aifm2 is the highest in mouse BAT, approximately 60-fold higher than mouse iWAT and human subcutaneous fat. Similarly, immunoblotting for Aifm2 showed the highest Aifm2 in mouse BAT and very low level in both mouse iWAT and human subcutaneous fat, and undetectable in other tissues (Fig. 10B). In addition, Aifm2 expression from representative databases for mice and human tissues indicate Aifm2 expression mainly in BAT in mice and in WAT in humans (BAT not included) (Fig. 10C,D). Interestingly, microarray data provided by Tseng Lab comparing mRNA levels in human interscapular BAT and WAT from 10 patients showed approximately 10-fold higher Aifm2 mRNA levels in human BAT compared to WAT. Also RNA seq data by Virtanen Lab examining transcripts in both human interscapular WAT and BAT revealed Aifm2 expression were positively correlated with UCP1 mRNA levels, significantly higher in BAT than WAT (Fig. 11C) [3]. In mouse BAT, Aifm2 mRNA was approximately 7-fold higher in adipocyte fraction than stromal vascular fraction (SVF) containing various cell types including pre-brown adipocytes (Fig. 11D). During brown adipocyte differentiation, Aifm2 mRNA was markedly increased, 7-fold higher at Day 3 than

Day 0 (Fig. 10E, left). Similarly, Aifm2 protein was significantly increased during brown adipogenesis (Fig. 2E, right).

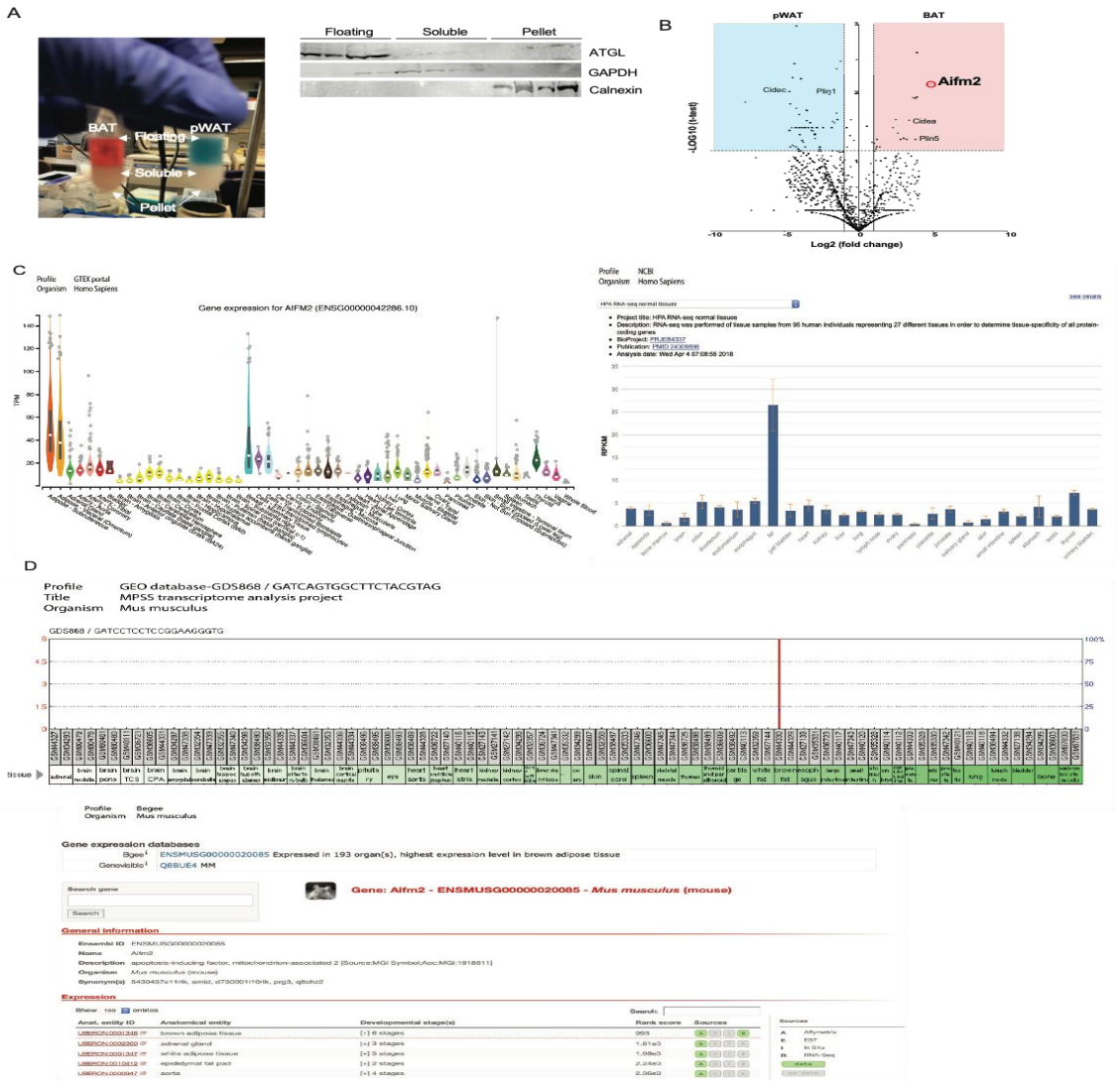

Figure 10. Lipid droplets associated protein screening and Aifm2 expression in human and mouse databases. (A) Immunoblot for ATGL, GAPDH, and Calnexin. (B) Volcano plot from MS data demonstates magnitude and significance of LD associated proteins of BAT compared to pWAT. (C) human Aifm2 tissue expression in GTEX and NCBI. (D) mouse Aifm2 tissue expression in GEO (GDS868) anf Begee.

We next examined whether Aifm2 expression might be induced during thermogenesis. Mice were kept at either 30^{o}C or cold-exposed at 4^{o}C for 3 hrs. By RT-qPCR, like UCP1, Aifm2 mRNA levels were greatly increased after cold exposure (4^{o}C) compared to thermoneutrality (30^{o}C) by approximately 9- and 25-fold, respectively, in both BAT and iWAT, a subcutaneous WAT that can undergo browning. Aifm2 protein level in BAT and iWAT of the cold exposed mice was also higher (Fig. 11F). Similarly, when mice were injected with either saline (control) or CL-31,248. Aifm2 mRNA was increased by 12- and 4-fold respectively in iWAT and BAT in

mice administered with a β3-adrenergic agonist, CL-316,248. Aifm2 protein in both BAT and iWAT were significantly increased by CL-316,248 treatment (Fig. 11G). We also identified a CRE located at -442 bp upstream of the Aifm2 start site. Co-transfecting CREB with -1500 Aifm2 promoter-luciferase resulted in a 4-fold increase in the promoter activity (Fig. 11H). Overall, these results demonstrate that Aifm2 is highly expressed in BAT and increased during brown adipogenesis and that Aifm2 expression is induced in BAT and iWAT in response to cold.

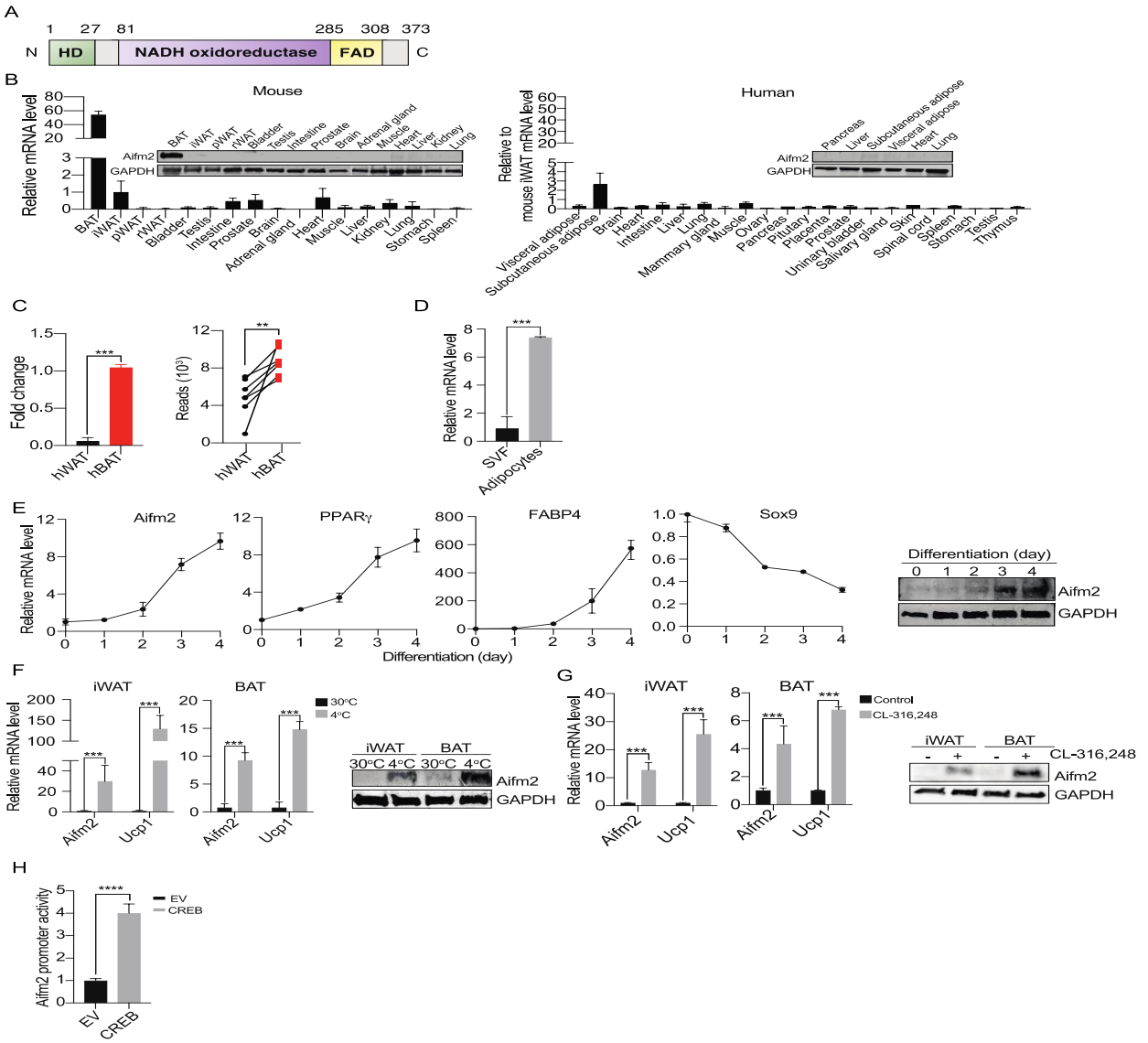

Figure 11. Aifm2 is specifically expressed in BAT and is induced by cold and β-agonist
(A) Aifm2 structure. (B) RT-qPCR/immunoblotting for Aifm2 in mouse tissues (left), human tissues (right). (C) Aifm2 expression in human BAT and WAT by microarray (left) and by RNA seq (right). (D) Aifm2 mRNA in SVF and adipocyte. (E) RT-qPCR/immunoblotting during BAT cell differentiation (n=6). (F) Aifm2 and UCP1 in iWAT and BAT of mice at 30°C or 4°C. (G) Aifm2 and UCP1 in iWAT and BAT of mice at 30°C injected with control or CL-316,248. (H) Luciferase activity using Aifm2-luc and either empty vector or CREB. Data are mean ± SD. *p<0.05, ** p< 0.01, *** p<0.001.

Aifm2 translocates to mitochondria upon cold exposure/β-adrenergic stimulation

To examine intracellular localization of Aifm2, we first tested the presence of Aifm2 in LD of differentiated BAT cells by immunoblotting. Supernatant from lysates of BAT cells was subjected to centrifugation through sucrose step gradient of 60, 20 and 5%. The top floating layer was collected as LD [33]. In the basal condition, Aifm2 was detected at a high level in LD but also found at a very low level in 5-20% fraction composed of mainly cytosolic fraction with some mitochondria contamination as detected by low level of Tom20 (Fig. 12A, left panel). Thus, we further separated cytosolic fraction without mitochondrial contamination by classic differential centrifugation. Under control treatment, Aifm2 was undetectable in the cytosolic fraction and was detected at low level in the mitochondrial fraction (Fig. 12A, right panel). Thus, in basal condition, Aifm2 is present mainly in LD. However, when BAT cells were treated with CL-316,248, Aifm2 was no longer detectable in LD, but was mainly found in the mitochondrial fraction (Fig. 12A, right panel). Similarly, Aifm2 was detected at a high level in LD, and at a very low level in mitochondrial fraction of BAT in mice maintained at thermoneutrality. In contrast, upon cold exposure, Aifm2 was barely detectable in LD, but was found mainly in mitochondrial fraction of BAT (Fig. 12B).

We next attempted to visualize Aifm2 in live cells. Using lentivirus, GFP-tagged Aifm2 was overexpressed in differentiated BAT cells. Immunofluorescence imaging showed that Aifm2 was detected around LDs as evidenced by colocalization of GFP with LipidTox or Mitotracker Red. GFP was also detected as punctates in the cytoplasm, an indication of potential mitochondrial association of Aifm2 (Fig. 12C, left panel). However, with the isoproterenol treatment, Aifm2 was no longer localized around LDs, but detected only as cytoplasmic punctates (Fig. 12C, left). GFP and lipidTox colocalization showed approximately 95% Aifm2 GFP signal surrounding lipid droplets in the basal condition. In contrast, Aifm2-GFP and lipidTox colocalization was reduced approximately to 21% in isoproterenol treatment. When visualizing the Aifm2-GFP with Mitotracker Red, in the control treatment, Aifm2-GFP was mainly detected in ring-shaped structures assuming LDs. However, upon isoproterenol treatment, Aifm2-GFP was colocalized completely with Mitotracker Red (Fig. 12C, right). GFP signal and Mitotracker Red colocalization was approximately 8% in the control treatment and it increased to 87% in isoproterenol. Overall, these results point toward translocation of Aifm2 from LD to mitochondria in BAT upon cold or β-AR stimulation.

Next to identify the domains that are responsible for Aifm2 association with LDs and mitochondria, multiple Aifm2 deletion and mutation constructs were generated and then overexpressed in differentiated BAT cells. Deletion constructs of Aifm2 N-terminal hydrophobic region aa1-27 (Aifm2 ΔN) and C-terminal aa308-373 (Aifm2 ΔC) were tagged with GFP. Aifm2 has been found to be myristolated at the N-terminal a-amino group of glycine residue, thus Aifm2 G2A was also created by site-directed mutagenesis [34]. Using similar differential centrifugation methods, immunoblotting for Aifm2 revealed that Aifm2 G2A was present mainly in the mitochondria fraction in the basal condition. Whereas Aifm2ΔN was found in cytosolic fraction. Similar Aifm2 WT, Aifm2ΔC was detected mainly in the LD fraction like Aifm2 WT (Fig. 12D, top panels). In live BAT cells, like immunoblotting, GFP-fusion Aifm2 G2A mutant was detected as punctates that were co-stained with MitoTracker Red, but not with LipidTox (Fig. 12D, bottom left panels), indicating mitochondrial localization. Moreover, whereas Aifm2 ΔC-GFP did not affect Aifm2 localization, Aifm2 ΔN-GFP was detected mainly in the cytosol (Fig. 12D, bottom right panels). Taken together, N-terminal domain is required for both LD and mitochondrial localization and N-myristylation is essential for LD binding of Aifm2.

To further investigate localization of Aifm2 in the mitochondria, by ultracentrifugation of digitonin-treated mitochondria, we prepared the mitoplasts stripped of outer mitochondrial membrane from BAT cells. Mitoplast pellet and the supernatant containing solubilized mitochondrial outer membrane and intermembrane space (OM+IMS) were collected. In the basal condition, we could not detect Aifm2 in either mitoplasts or OM+IMS fraction. However, when we used BAT cells treated with CL-316,248, Aifm2 appeared highly in the mitoplast fraction, but was absent in the OM+IMS fraction (Fig. 12E, left). In BAT from mice maintained at thermoneutrality, Aifm2 was present at a very low level in mitoplasts, which was increased significantly in mitoplasts from BAT of cold-exposed mice (Fig. 12E, right). Aifm2 was not detected in the OM+IMS fraction in mice maintained either at thermoneutrality or cold-exposed. We conclude that, even without mitochondrial targeting signal sequence, Aifm2 can be found in mitoplasts upon cold exposure and probably associated with outside of the inner mitochondrial membrane.

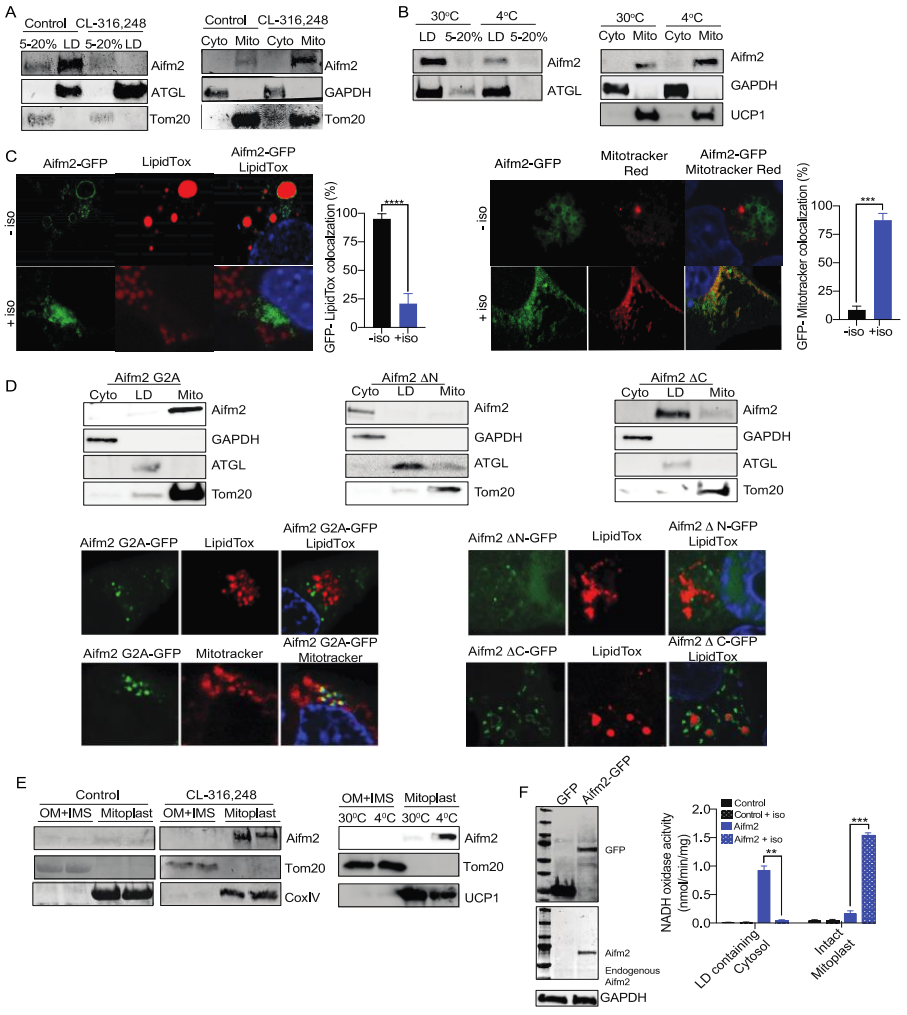

Figure 12. Aifm2 translocates from LD to mitochondria during thermogenesis. (A) Immunoblotting in indicated fraction. (B) BAT collected from mice at 30°C or 4°C and immunoblotting in indicated fraction. (C) Confocal fluorescence of Aifm2-GFP (green) in BAT cells treated in either control or isoproterenol with LD stained by LipidTOX (red) (left) or with mitochondria stained by Mitotracker Red (right). (D) Localization of Aifm2 G2A mutant, Aifm2 ΔN, Aifm2 ΔC in BAT cells by immunoblotting in various fractions (Top). (BOTTOM) Confocal fluorescence of Aifm2 G2A-GFP, ΔN and (ΔC) (green) with either LipidTox or Mitrotracker Red. (E) Immunoblotting in solubilized mitochondrial outer membrane and inner membrane space (OM+IMS) fraction and mitoplast fraction using BAT cells treated (left) and BAT from mice (right). (F) Immunoblotting for Aifm2-GFP of transfected HEK293 cells (left), NADH oxidase activity of Aifm2 in HEK293 by spectrophotometry at 340nm. Data are mean ± SD. *p<0.05, ** p< 0.01, *** p<0.001.

Next, we compared NADH oxidase activity in various subcellular compartments to correlate with Aifm2 localization. HEK293 cells, expressing low endogenous Aifm2 were transfected with Aifm2, then treated with oleate (Fig. 12F, left). It was reported that HEK293 responses to isoproterenol and increases cAMP due to endogenous β-receptor [35]. We employed the cytosolic fraction containing LDs and intact mitoplasts and OM+IMS, to measure NADH oxidase activity by monitoring the remaining NADH levels spectrophotometrically at 340 nm using NADH as substrate. The reaction was started by adding the enzyme-containing samples preincubated with FAD. We found that under basal condition, NADH oxidase activity in cytosolic fraction of Aifm2 OE cells was higher by approximately 9-fold compared to that of control cells. NADH oxidase activity of intact mitoplasts, representing that of outer side of mitoplasts, was greatly lower in Aifm2 transfected or control cells (Fig. 12F). After isoproterenol, NADH oxidase activity in intact mitoplasts of Aifm2 transfected cells was higher by 10-fold compared to that of control cells. NADH oxidase activity of solubilized mitoplasts increased by only 1.5-fold, probably due to the presence of the same high NADH oxidase activity from complex I and III of ETC in transfected and control cells (Data not shown). The very low NADH oxidase activity detected in the cytosolic fraction remained unchanged between transfected and control cells (Fig. 12F). These results indicate that NADH oxidase activity of cytosolic and intact mitoplast fraction is mainly from Aifm2 and that Aifm2 resides in LD in basal condition and, upon β-AR stimulation or cold-exposure, it associates with mitochondrial inner membrane facing the intermembrane space, where it oxidizes NADH to NAD.

Aifm2 maintains NAD to support glycolysis in BAT cells during thermogenesis

Classically, FAs have been known to be oxidized for supporting ETC, in addition to directly binding and activating UCP1 during thermogenesis. However, BAT recently has been proposed to be metabolically flexible to use not only FAs but also glucose [36]. We propose that glucose may serve as the main fuel source for thermogenesis, especially in the fed condition with high circulating glucose. In order to sustain robust glycolysis, BAT must maintain a NAD pool in the cytoplasm. We thus investigated whether Aifm2, with its NADH oxidase activity, affects cellular NAD/NADH by Aifm2 loss- and gain-of function experiments. In determining NAD/NADH levels, we used a biochemical assay based on lactate dehydrogenase cycling in which newly formed NADH reduces formazan reagent. BAT cells were treated with either control shRNA or Aifm2 pooled shRNA lentivirus. In the control BAT cells, NAD/NADH ratio increased 3-fold in response to isoproterenol. Aifm2 KD in BAT cells reduced NAD/NADH by 20% compared to control cells. Importantly, Aifm2 KD prevented the increase in NAD/NADH upon β-AR stimulation (Fig. 13A). Conversely, when His-tagged Aifm2 was overexpressed BAT cells by adenoviral transduction, NAD/NADH was increased by approximately 30%. In response to isoproterenol, the NAD/NADH further increased by approximately 2.5-fold in Aifm2 OE cells (Fig. 13B). In order to determine intracellular compartment-specific NAD/NADH, we next studied changes in NAD/NADH in situ. We co-expressed cytoplasmic Peredox, a fluorescent biosensor of NADH/NAD redox state in HEK293 cells with Aifm2 and cells were then with or without isoproterenol. Peredox contains a circularly permuted GFP T-Sapphire with mCherry-fused bacterial NADH-binding protein, Rex [37]. Indeed, cytoplasmic NADH/NAD state was reduced in control HEK293 cells in response to isoproterenol treatment (Fig. 13C, left). Aifm2 OE caused NADH/NAD in the cytoplasm to decrease by approximately 2-fold which was decreased further by 3-fold upon isoproterenol treatment (Fig. 13C, left). There was a slight but

significant increase in NAD/NADH in control HEK293 cells upon isoproterenol treatment. Moreover, NAD/NADH, which was increased approximately 2-fold in Aifm2 transfected cells, further increased by 3-fold in response to β-AR stimulation (Fig. 13C, right). Overall, these results indicate that Aifm2 increases cytosolic NAD levels in BAT cells.

We next investigated whether the changes in NAD levels or NAD/NADH ratio by Aifm2 affect glycolytic rate in BAT cells. We performed extracellular acidification rate (ECAR), a powerful method of monitoring glycolysis. ECAR mainly represents glycolytic flux to lactate. ECAR measured in the presence of a F1//F0 ATP synthase inhibitor, oligomycin, renders maximal glycolytic capacity, due to suppression of mitochondrial ATP production, whereas addition of a hexokinase inhibitor, 2-DG blocks glucose utilization through glycolysis. ECAR measurement using the control BAT cells showed that glycolytic rate and maximal glycolytic capacity were increased by 25% and 40%, respectively, in response to the isoproterenol, whereas Aifm2 KD reduced both fluxes by approximately 25%. And unlike the control cells, Aifm2 KD cells failed to increase glycolytic rate and maximal glycolytic capacity in response to isoproterenol (Fig. 13D, left). Conversely, overexpression of Aifm2 significantly increased both by 25% relative to control cells. With β-AR stimulation, Aifm2 OE BAT cells further increased glycolytic rate and maximal glycolytic capacity by 25% and 40%, respectively (Fig. 13E, left). However, since ECAR can be affected by CO_2 generated by TCA cycle, we also measured intracellular lactate levels in evaluating glycolytic rate. Similar to ECAR, control cells had a 3-fold increase in intracellular lactate levels with isoproterenol treatment.

And Aifm2 KD in BAT cells had lactate levels reduced by 25% compared to control cells. Moreover, Aifm2 KD prevented the increase in lactate production in response to β-AR stimulation (Fig. 13D, right). Conversely, Aifm2 OE in BAT cells increased intracellular lactate levels by 25% relative to control cells. With isoproterenol, the lactate levels were further increased by approximately 7-fold in these Aifm2 OE cells (Fig. 13E, right). The changes in lactate levels were larger than ECAR, which may be due to the fact that we measured intracellular lactate, a direct product of glycolysis, whereas ECAR measures lactate and other acidic substrates secreted into the media. Regardless, results from using both methods clearly demonstrate the effect of Aifm2 on glycolysis in BAT cells. We conclude that with its NADH oxidase activity, Aifm2 generates a NAD pool that allows BAT to maintain high rate of glycolysis.

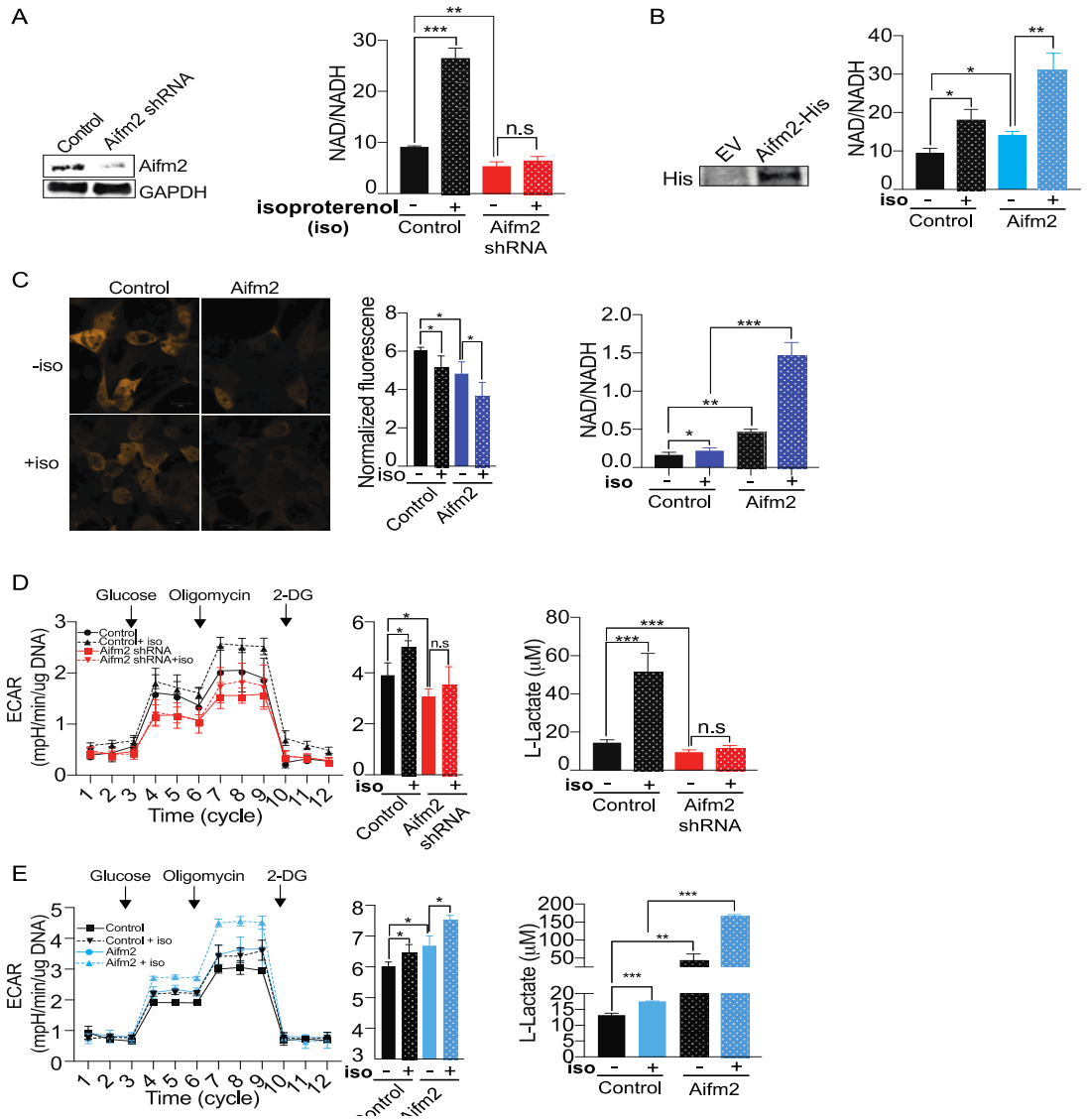

Figure 13. Aifm2 generates NAD in cytosol to increase glycolysis in BAT cells
(A) Immunoblotting for Aifm2 (left) and NAD/NADH ratio (right) in BAT cells transduced by Aifm2 shRNA lentivirus. (B) Immunoblotting for Aifm2 (left) and NAD/NADH ratio (right) in BAT cells transduced by His-Aifm2 adenovirus. (C) Fluorescence images of HEK293 cells overexpressing Peredox (green) with either Aifm2-His or control vector (left), NADH/NAD ratio by quantification of Peredox fluorescence (right). (D) Extracellular acidification rate (ECAR) by XF-24 analyzer (left), glycolytic rate measured by ECAR under oligomycin (middle), and intracellular L-lactate concentration (right) in Aifm2 KD in BAT cells. (E) ECAR (left), glycolytic rate (middle), and intracellular L-lactate (right) in Aifm2 overexpressing BAT cells. Data are mean ± SD. *p<0.05, ** p< 0.01, *** p<0.001.

Aifm2 is required for glycolysis in BAT during thermogenesis

So far, we found that Aifm2, which is expressed specifically in BAT and cold-inducible, associates with mitochondrial inner membrane in stimulated condition and that Aifm2 generates NAD to sustain robust glycolysis. Next, we investigated whether glycolysis promoted by Aifm2

can support thermogenesis in BAT cells. First, we measured mitochondrial membrane depolarization. When ATP synthase or UCP1 is active, protons leak into the matrix to depolarize mitochondria, and mitochondrial depolarization has been correlated with thermogenesis [38]. In measuring mitochondrial potential, we employed a metachromatic dye-based JC-1 fluorescence probe in live cells [39]. In polarized mitochondria, JC-1 aggregates in the mitochondrial matrix to emit light in the orange/red region, whereas in depolarized mitochondria, JC-1 monomer leaks into the cytosol to display green fluorescence. BAT cells ($1X10^6$ cells/ml) were treated with 2 □m JC-1 for 20 mins prior to FACS analysis. In control cells, isoproterenol led to a 30% decrease in polarization by FACS analysis. Aifm2 KD BAT cells showed a 25% increase in polarization than control cells. Aifm2 KD cells had no decrease in polarization when treated with isoproterenol (Fig. 14A, left). In contrast, Aifm2 overexpression caused an approximately 25% decrease in polarization. Isoproterenol treatment in Aifm2 OE cells further decreased polarization by another 25% (Fig. 14B, left). In addition, we also utilized TMRM (tertramethylrhodamine, methyl ester) to examine mitochondrial potential in Aifm2 KD BAT cells. Similar to JC-1, TMRM is cell-permeant fluorescent dye that accumulated in polarized mitochondrial and ceases its signal or disappears in depolarized mitochondria. In Aifm2 KD BAT cells, TMRM positive cell population is 20% higher than control cells. When treated with isoproterenol, positive TMRM control BAT cells decreased by 30% while positive TMRM BAT cells with Aifm2 KD showed no change. These results indicate Aifm2 increase mitochondria membrane potential.

Next, using Seahorse XF24, we measured oxygen consumption rate (OCR) in both Aifm2 KD and OE BAT cells. In scrambled shRNA BAT cells, overall OCR was increased significantly upon isoproterenol treatment. OCR under oligomycin treatment, which reflects uncoupled respiration, was also increased by approximately 30% in response to β-AR stimulation. Notably, Aifm2 KD reduced overall OCR and uncoupled OCR by approximately 30%. Furthermore, Aifm2 KD cells did not show any increase in uncoupled OCR by isoproterenol (Fig. 14B, left). Conversely, in BAT cells overexpressing Aifm2, overall OCR was significantly higher than control BAT cells and uncoupled OCR increased approximately by 40%. Isoproterenol caused a further increase in OCR, and the uncoupled OCR was increased by 40% of Aifm2 OE cells (Fig. 14C). These findings clearly show that Aifm2 promotes mitochondrial oxidative metabolism and ETC activity in BAT cells. Since Aifm2 G2A mutant was mainly found in mitochondria, we performed OCR in BAT cell overexpressing this mutant. We found that Aifm2 G2A mutant had higher overall OCR and uncoupled OCR in basal condition. This indicates that Aifm2 association with mitochondria increases ETC activity (Fig. 14C,).

Next, to determine Aifm2 effect on thermogenesis, we utilized a small molecule thermosensitive fluorescent dye, ERthermAC, which can directly monitor temperature changes in live cells [40]. ERthermAC accumulates in the ER and decreases fluorescence, corresponding to an increase in temperature. All cells were treated with 250nM of ERthermAC for 30 mins then washed 2 times with PBS prior to FACS analysis. As expected, there was a large shift in BAT cell distribution to a higher temperature range upon CL-316,248 of control cells. The average fluorescence intensity of ERthermAC upon β-agonist was decreased by approximately 65%, indicating an increase in cell population at a higher temperature range. More importantly, Aifm2 OE increased the cell population of higher temperature by approximately 3-fold. When Aifm2 OE cells were treated with a β-agonist, the cell population with a higher temperature was further increased by approximately 2-fold (Fig. 14D). Altogether, higher oxygen consumption and

uncoupled respiration, as well as heat production, clearly demonstrate promotion of thermogenic activity by Aifm2.

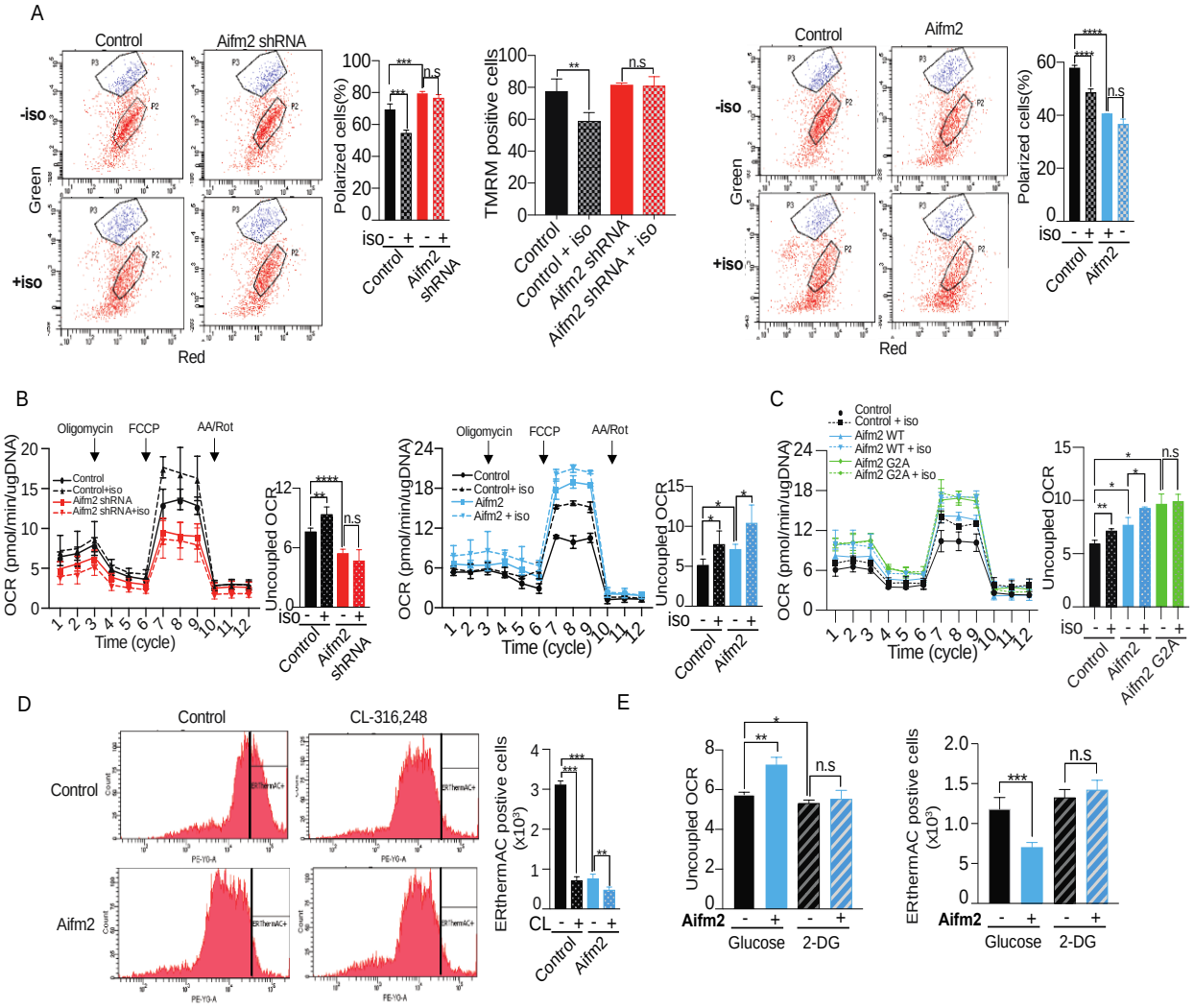

Figure 14. Aifm2 promotes thermogenesis by sustaining glycolysis in BAT cells
(A) FACS analysis of mitochondrial potential by JC-1 and TMRM dye of Aifm2 KD BAT cells (left), and. JC-1 of Aifm2 overexpressing BAT cells (right). (B) Oxygen consumption rate (OCR) by Seahorse XF24 of Aifm2 KD BAT cells (left), and Aifm2 overexpressing BAT cells (right). (C) FACS analysis of ERthermAC. (D) Uncoupled OCR (left), and FACS analysis and quantification of ERthermAC (right) of Aifm2 overexpressing BAT cells treated with 2 deoxyglucose. Data are mean ± SD. *p<0.05, ** p< 0.01, *** p<0.001.

To determine whether Aifm2 function in glycolysis is required for enhancement of thermogenesis, we tested the effect of Aifm2 on uncoupled OCR in the presence of hexokinase inhibitor, 2-DG (2-deoxyglucose), which effectively blocks glycolysis. With isoproterenol stimulation, Aifm2 OE BAT cells had approximately 40% higher overall OCR and uncoupled OCR than control BAT cells. However, the increases in overall and uncoupled OCR by Aifm2 were completely abolished when cells were pre-treated with 2-DG (Fig. 14E, left). We also tested whether inhibiting glycolysis could prevent Aifm2 promotion of heat production in BAT

cells by utilizing ERthermAC. Aifm2 OE BAT cells had a 50% increase in cell population at a higher temperature range compared to the control cells in response to β-agonist. Remarkably, there was no increase in numbers of cells at higher temperature range in Aifm2 OE BAT cells that were pre-treated with 2-DG (Fig. 14E, right). These results confirm that Aifm2 increases overall mitochondrial activity and promotes thermogenesis in BAT cells by maintaining cytosolic NAD to sustain robust glycolysis.

NADH oxidase activity of Aifm2 is required to sustain glycolysis for thermogenesis

We found Aifm2 increases NAD/NADH to promote glycolysis and ultimately thermogenesis in BAT cells. In order to test whether NADH oxidase activity of Aifm2 is required for its effects on glycolysis and thermogenesis, we next performed site-directed mutagenesis of D285N at the putative NADH-binding site of Aifm2. The WT and D285N mutant of Aifm2 were overexpressed in BAT cells (Fig. 15A). Unlike WT Aifm2, D285N mutant containing lysate showed no NADH oxidase activity in vitro as measured by a spectrophotometric assay to monitor absorbance at 340 nm using NADH as substrate (Fig. 15B, left). Aifm2 D285N mutant failed to increase NAD/NADH ratio, where WT Aifm2 increased NAD/NADH approximately 1.8-fold and 3.0-fold in basal and isoproterenol treated conditions, respectively (Fig. 15B, right). While Aifm2 WT OE increased the maximal glycolytic capacity measured by ECAR by approximately 40%, the Aifm2 D285N mutant did not affect glycolysis (Fig. 15C). Additionally, Aifm2 D285N mutant was unable to enhance overall OCR and uncoupled OCR in BAT cells (Fig. 15D). These results show that NADH oxidase is required for Aifm2 effect on glycolysis and thermogenesis.

We next performed rescue experiments using Aifm2 KO cells. Aifm2 KO BAT cells were generated by CRISPR-Cas9. A gRNA targeting exon 5 of Aifm2 was introduced by lentivirus into BAT preadipocytes that stably expresses Cas9. Multiple single clones were selected, and a representative clone was used for these rescue experiments. We transfected WT and D285N mutant Aifm2 into Aifm2-KO cells. Since Aifm2 have relatively high sequence similarity at 42% with yeast NDE1, an external NADH oxidase, we also employed NDE1 for rescue experiments. Overexpression of WT Aifm2, Aifm2 D825N mutant and NDE1 were detected by immunoblotting in Aifm2 KO cells (Fig. 15E). As expected, Aifm2 KO cells had 40% lower of NAD/NADH ratio than control WT cells. Cells expressing Aifm2 WT and NDE1 showed an increase in NAD/NADH ratio, whereas Aifm2 D285N mutant failed to do so (Fig. 15F). Moreover, Aifm2 KO compared to WT cells had 2-fold lower glycolytic capacity measured by ECAR. Expression of Aifm2 WT and NDE1 both increased the glycolytic rate in Aifm2 KO cells, while Aifm2 D285N mutant failed rescue glycolysis in Aifm2 KO cells (Fig. 15G, left). Similarly, lactate level in Aifm2 KO cells was approximately 5-fold lower than control cells and both Aifm2 WT and yeast NDE1 OE increased intracellular lactate level to that in control cells, whereas Aifm2 D285N did not change the lactate levels of Aifm2 KO cells, demonstrating the NADH oxidase activity of Aifm2 is critical for high glycolytic rate in BAT cells (Fig. 15G, right). Furthermore, overall OCR and uncoupled OCR of Aifm2 KO cells, which was 3-fold lower than control cells, was rescued by overexpression of either WT Aifm2 or NDE1, but not D285N mutant Aifm2 (Fig. 15H). Taken together, these results demonstrate that NADH oxidase activity of Aifm2 is critical in sustaining robust glycolysis to support

thermogenesis. We also propose that Aifm2 upon translocation to mitochondria can perform similar function as yeast NDE1.

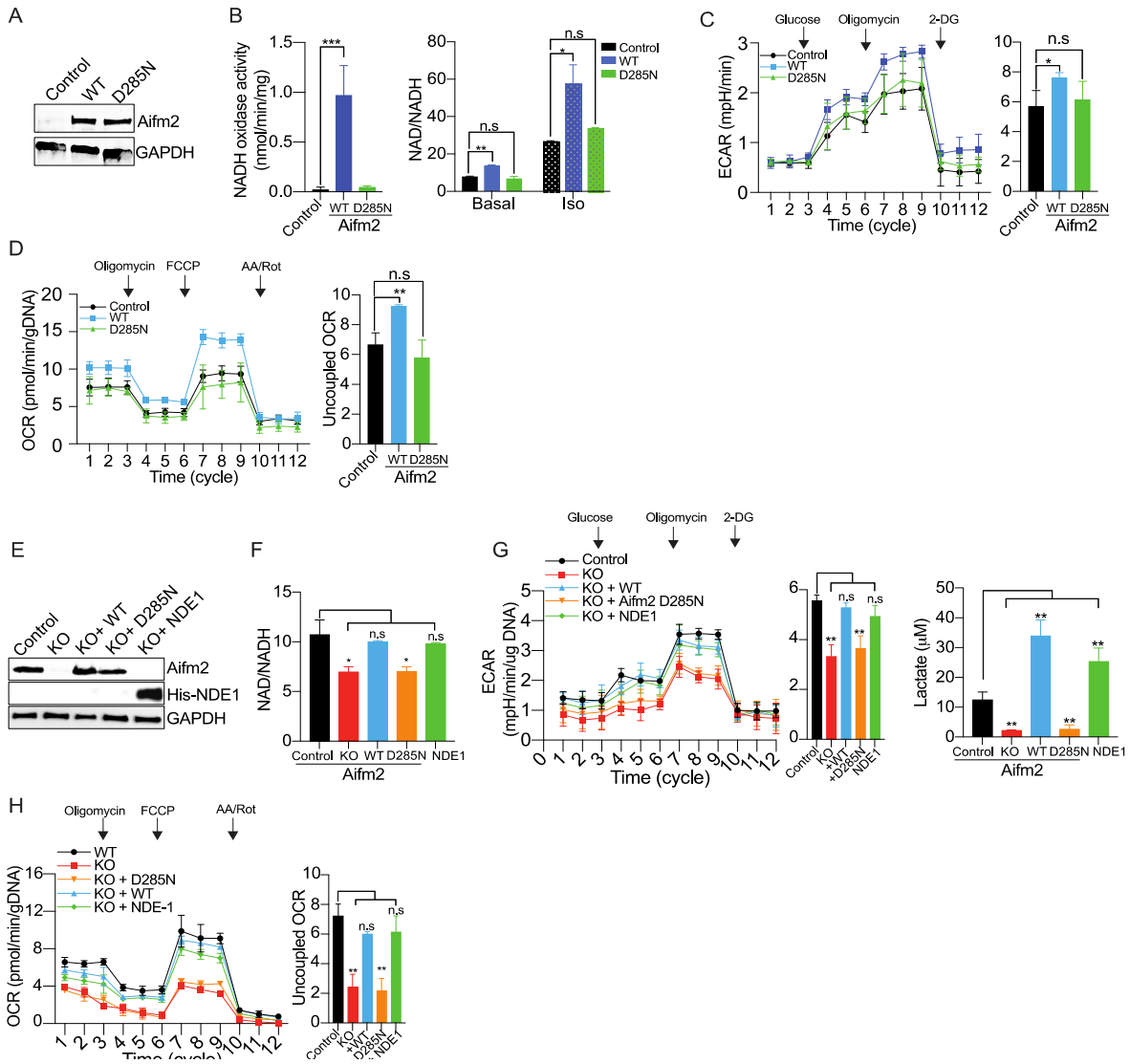

Figure 15. NADH oxidase activity of Aifm2 is required to sustain glycolysis for thermogenesis

Aifm2 WT and D285N mutant were overexpressed in BAT cells. (A) Immunoblotting. (B) NADH oxidase activity of total BAT cell (left), and NAD/NADH ratio (right). (C) Extracellular acidification rate (ECAR) in BAT cells overexpressing Aifm2 WT or D285N. (D) Oxygen consumption rate (OCR) and uncoupled OCR.

Aifm2 WT and D285N mutant, and yeast NDE1 were overexpressed in Aifm2 CRISPR KO BAT cells. (E) Immunoblotting. (F) NAD/NADH ratio. (G) Extracellular acidification rate (ECAR) (left), and intracellular L-lactate (right). (H) Oxygen consumption rate (OCR) and uncoupled OCR. Data are mean ± SD. *p<0.05, ** p< 0.01, *** p<0.001.

Aifm2 is critical for thermogenesis *in vivo* in mice

We next tested the role of Aifm2 on thermogenesis *in vivo.* Aifm2 gain- and loss-of function mouse models could provide us not only the physiologic evidence for the role of Aifm2 in thermogenesis, but also for its downstream effects, such as adiposity. Because Aifm2 is highly expressed only in BAT and not in any other tissues, first, we generated global Aifm2-KO mice, using CRISPR-Cas9 system. We used the gRNA target sequence, CGTTAAACTTGCCAGGGAAG, corresponding to aa113-120 at the third exon of Aifm2 composed of 5 exons encoding a protein of 373 aa in length (Fig. 16A, left). *In vitro* transcribed gRNA and Cas9 mRNA were then injected into zygotes. By genotyping and sequencing of the Aifm2 genomic region, we verified 3 KO lines, including one with a single nucleotide addition, one with a 2 bp deletion and one with a 22 bp deletion in the coding region of the third exon. All lines were confirmed to have complete ablation of Aifm2, and they showed similar phenotypes. Here, the findings from 22 bp deletion KO line were presented. By immunoblotting, Aifm2 was not detectable in BAT or iWAT of Aifm2 KO mice (Fig. 16A, right). The Aifm2 KO mice had significantly higher body weights with greatly increased WAT as determined by EcoMRI (Fig. 16B) and by weighing of dissected WAT depots, while there were no differences in other organ weights (Fig. 17A). Neither were there significant differences in food intake which were collected during CLAMS study (Fig. 17B). Histological analysis of whole mount staining of WAT with LipidTox (red) revealed a larger adipocyte size distribution in adipose depots of Aifm2 KO mice than WT mice. The differences in brown adipocyte size were more apparent in H&E staining (Fig. 17C). Gene analysis revealed that the Aifm2-KO mice compared to WT had greatly reduced expression of thermogenic and BAT-enriched genes, such as UCP1 and Dio2, but interestingly the KO mice had higher expression of adipogenic genes, such as C/EBPβ, C/EBPδ and PPARγ (Fig. 17D). To ensure Aifm2 does not affect brown adipogenesis, Aifm2 was overexpressed in BAT preadipocytes, which was then subjected to differentiation. By RT-qPCR, there was no difference in adipogenic markers such as Sox9, C/EBPβ, C/EBPδ and PPARγ, FABP4 as well as thermogenic genes such as UCP1, Dio2 (Fig. 18A, B). In addition, lipid accumulation showed no change in Aifm2 OE BAT cells comparing to the control cells (Fig. 18C). These results suggest that Aifm2 KO compared to WT mice had higher adiposity due to defective thermogenic program. Thus, unlike WT littermates, the KO mice could not maintain body temperature upon cold, the body temperature of KO mice after 5 hrs of cold exposure being 8^{o}C lower than that of WT mice (Fig. 16C, left). Infrared camera was used to document the heat production by BAT of these mice. The BAT temperature of KO mice after 5 hrs of cold exposure was approximately 6^{o}C lower than that of WT mice (Fig. 16C, middle). When these mice were subjected to chronic cold, after 8 hrs, only 50% of Aifm2 KO mice survived, whereas all WT mice were alive (Fig. 16C, right). Moreover, the whole-body OCR of Aifm2 KO compared to WT littermates measured by CLAMS was significantly lower during the night when mice were kept at thermoneutrality of 30^{o}C, and both during day and night when mice were kept at 23°C. This decrease in OCR in Aifm2 KO mice was even greater in magnitude when mice were exposed to cold at 4°C (Fig. 16D, left). OCR in BAT excised from these KO compared to WT mice were 15% lower as measured by Seahorse XF-24 (Fig. 16D, right). In addition, both BAT and iWAT of Aifm2 KO compared to WT littermates had a significantly lower NAD/NADH ratio (Fig. 16E, left). Intracellular lactate levels in BAT of Aifm2 KO mice were approximately 2-fold lower also (Fig. 16E, right). These results indicate that Aifm2 KO compared to WT mice had lower glycolytic capacity of BAT. We also employed Metabolic Flux Analysis using [U-^{13}C]-glucose. Mice that were fasted for 4 hrs were injected intraperitoneally with uniformly

labeled ^{13}C-glucose. BAT collected after 1 hr were used for methanol extraction for metabolites. The isotopomer levels of metabolites were shown as molar fractions, where M+1, M+2, M+3, etc. represent the number of ^{13}C atoms, while M+0 represent endogenous unlabeled metabolites. These results showed effective ^{13}C incorporation into fructose 1,6-bisphosphate (F1,6BP) (M+6), pyruvate(M+3), lactate(M+3) being the predominant isotopomers. More importantly, these metabolites were approximately 2-fold lower in BAT of Aifm2 KO than WT mice. Additionally, TCA cycles metabolites, such as α-ketoglutarate (M+2), fumarate (M+2), malate (M+2), succinate (M+2), citrate(M+2, M+3, M+5), mainly were detected from uniformly labeled ^{13}C-glucose through pyruvate carboxylase (PC) or pyruvate dehydrogenase (PDH) reactions and they were all significant lower in Aifm2 KO compared to WT mice (Fig. 16F, 8E). These results clearly demonstrate Aifm2 depletion decreased glycolysis in BAT. Overall, we conclude that Aifm2 ablation in mice decreases thermogenesis and energy expenditure, resulting in higher adiposity.

Next, in order to test effect of Aifm2 ablation specifically in BAT and iWAT on thermogenesis, Aifm2 pooled shRNA were injected directly to BAT and iWAT of WT mice via AAV7/9 (10^{12} vg) viruses that are reported to restrict expression in adipose tissue [41]. AAV7/9 viruses carrying scrambled shRNA were used as controls. BAT and iWAT of these mice were evaluated after 2 wks. Transduction efficiency was examined by gene expression analysis showing Aifm2 mRNA levels were approximately 3-fold lower in both BAT and iWAT of Aifm2 shRNA injected mice compared to control mice, while there were no significant differences in pWAT or other tissues, such as testis, heart, and liver. Aifm2 protein level by immunoblotting was lower also in Aifm2 shRNA compared to scrambled control shRNA injected mice (Fig. 15G). When Aifm2 shRNA AAV7/9 injected mice were subjected to 4^{o}C for 4 hrs, their body temperature was 3^{o}C lower than control scrambled shRNA virus injected mice (Fig. 15H, left). Moreover, whole-body OCR of Aifm2 shRNA AAV7/9 virus-injected mice was significantly lower at 23°C than the control scrambled shRNA injected mice, and this decrease in OCR was even more significant in mice at 4°C (Fig. 15H, right).

Similarly, we also injected Aifm2 shRNA pooled lentivirus or scramble shRNA lentivirus directly to BAT and iWAT of WT mice using similar method as mentioned in AAV administration. After 2-weeks, gene analysis by rt-qPCR showed Aifm2 mRNA levels to be approximately 2-fold lower in both BAT and iWAT of Aifm2 shRNA lentivirus injected mice than in control mice, while there was no significant difference in either pWAT or kidney (Fig. 17H). Body temperature of Aifm2 shRNA lentivirus injected mice was 3^{o}C lower than control mice after 4hr at 4^{o}C. BAT temperature detected by infrared imaging of Aifm2 shRNA injected mice was 3^{o}C lower than that of control mice. Moreover, whole-body OCR of Aifm2 shRNA lentivirus injected mice was significantly lower at 23°C than the control mice, and this decrease in OCR were even more significant in mice at 4°C (Fig. 17I). Additionally, gene analysis showed there was no difference in adipogenic and thermogenic markers such as C/EBPβ, C/EBPδ, PPARγ, UCP1, and Dio2 between Aifm2 shRNA injected mice and control mice. These results indicate Aifm2 effect is due to its functions in glycolysis, but not adipocyte differentiation. (Fig. 17J).

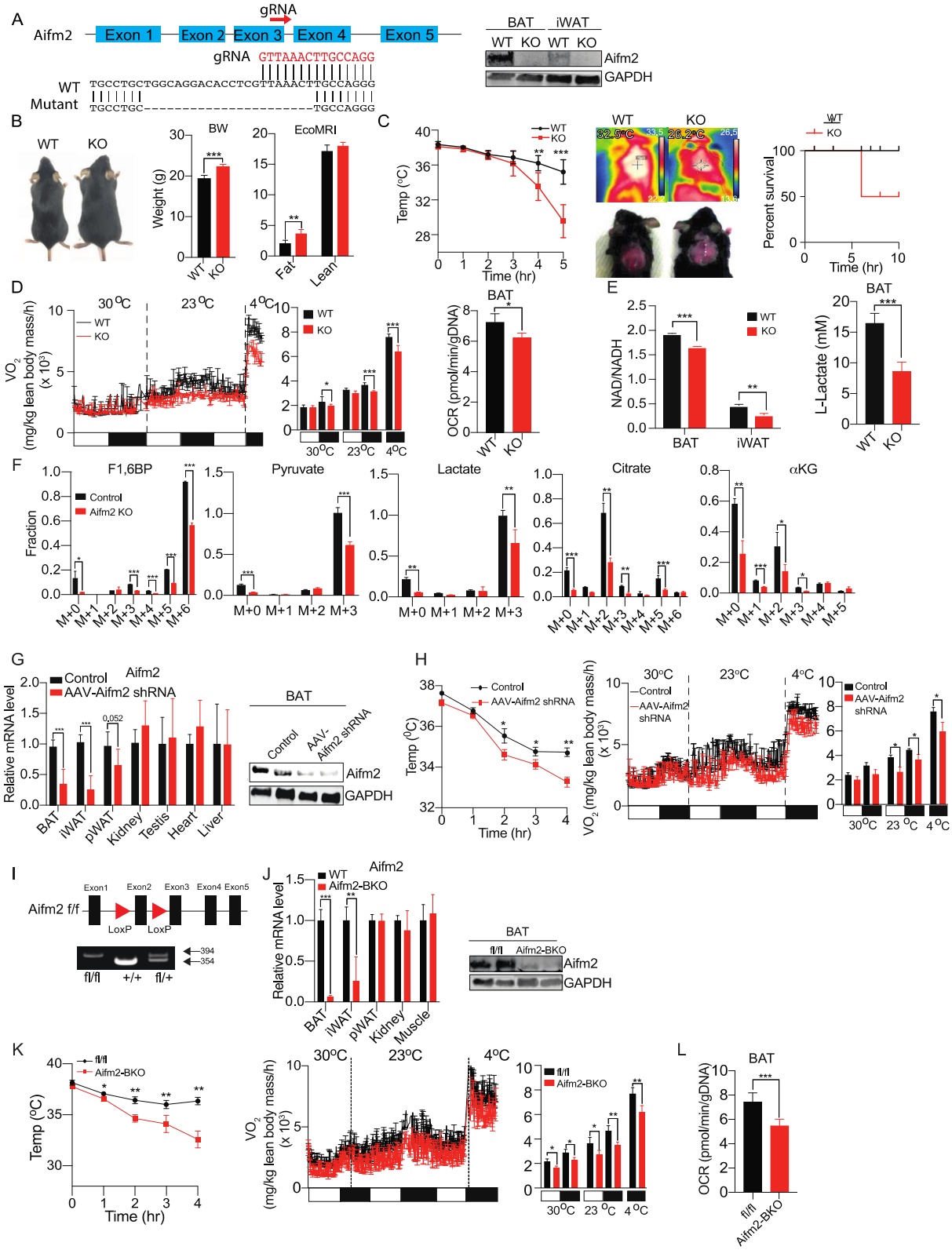

Figure 16. Aifm2 deficiency in BAT impairs thermogenesis in mice

(A) Schematic diagram of generation of Aifm2 CRISPR KO mice (left), and immunoblotting for Aifm2 (right). (B) Representative photograph of WT and Aifm2 KO mice, body weights and body composition. (C) Rectal temperature of mice (left). Infrared thermography (middle), and

survival curve of mice (n=6) (right). (D) VO_2 assayed using CLAMS (left) and OCR measured in BAT from mice (right) (n=5-7). (E) NAD/NADH measured in BAT and iWAT(left), and intracellular L-Lactate level in BAT (right) (n=5-6). (F) Metabolic Flux Analysis (MFA) using [U-^{13}C] glucose. Representative glycolysis and TCA intermediates, M+1, M+2, M+3, etc. represent the number of ^{13}C atoms. (G) rt-qPCR (left) and immunoblotting for Aifm2 (right) in tissues of mice injected directly to BAT and iWAT with either scrambled shRNA or Aifm2 shRNA AAV7 and 9. (H) Rectal temperature (left), and VO_2 assay using CLAMS (right) (n=6-7). (I) Schematic of generation of Aifm2 floxed mice (top), and genotyping of Aifm2 floxed mice (bottom). (J) RT-qPCR (left) and immunoblotting for Aifm2 (right) in BAT of Aifm2 BKO and WT mice. (K) Rectal temperature (left), and VO_2 assay using CLAMS (right) (n=5-6). (L) OCR measured in BAT from Aifm2 BKO mice using Seahorse XF24 (n=4). Data are mean ± SD. *$p<0.05$, ** $p< 0.01$, *** $p<0.001$.

To further determine the role of Aifm2 specifically in BAT *in vivo*, we generated Aifm2 floxed mice using CRISPR-Cas9 Nickase system. We used a pair of the gRNAs target sequences, ACCAGCGGCTCGAGCCTCTCAGG and GTAAATCTCAGGACAGCGCTAGG, corresponding to 5' and 3' end of Exon 2 of the Aifm2 gene, respectively (Fig. 16I, left). To generate BAT specific KO of Aifm2 (Aifm2 BKO), we injected homozygous Aifm2 floxed mice with UCP1-Cre AAV7 virus that we constructed by inserting Cre recombinase into 3' end of the -2.8 kb UCP1 promoter containing both distal enhancer and proximal promoter region to effectively express Cre in UCP1$^+$ cells [42]. Control mice were floxed mice that were injected AVV control virus. Along with the pair of gRNAs, *in vitro* transcribed gRNA and Cas9 Nickase mRNA were injected into zygotes. RT-qPCR showed Aifm2 mRNA to be reduced by 10-fold and 5-fold in BAT and iWAT, respectively, while there was no difference in pWAT, kidney, and muscles. Immunoblotting for Aifm2 in BAT showed a significantly lower Aifm2 protein level in Aifm2-BKO mice (Fig. 16J). When subjecting to 4^{o}C, Aifm2-BKO mice had approximately 4^{o}C lower body temperature than Aifm2 floxed mice. Moreover, whole-body OCR of Aifm2-BKO mice was significantly lower at all temperatures than the floxed mice, the difference being more significant at both 23^{o}C and 4^{o}C than at 30^{o}C (Fig. 16K). When BAT depots were dissected from these mice and subjected to Seahorse, whole-body OCR in BAT of Aifm2 BKO was approximately 33% lower than one in WT mice. Taken together, these results clearly demonstrate Aifm2 ablation specifically in UCP1$^+$ cells resulted in decreased OCR and impaired thermogenesis.

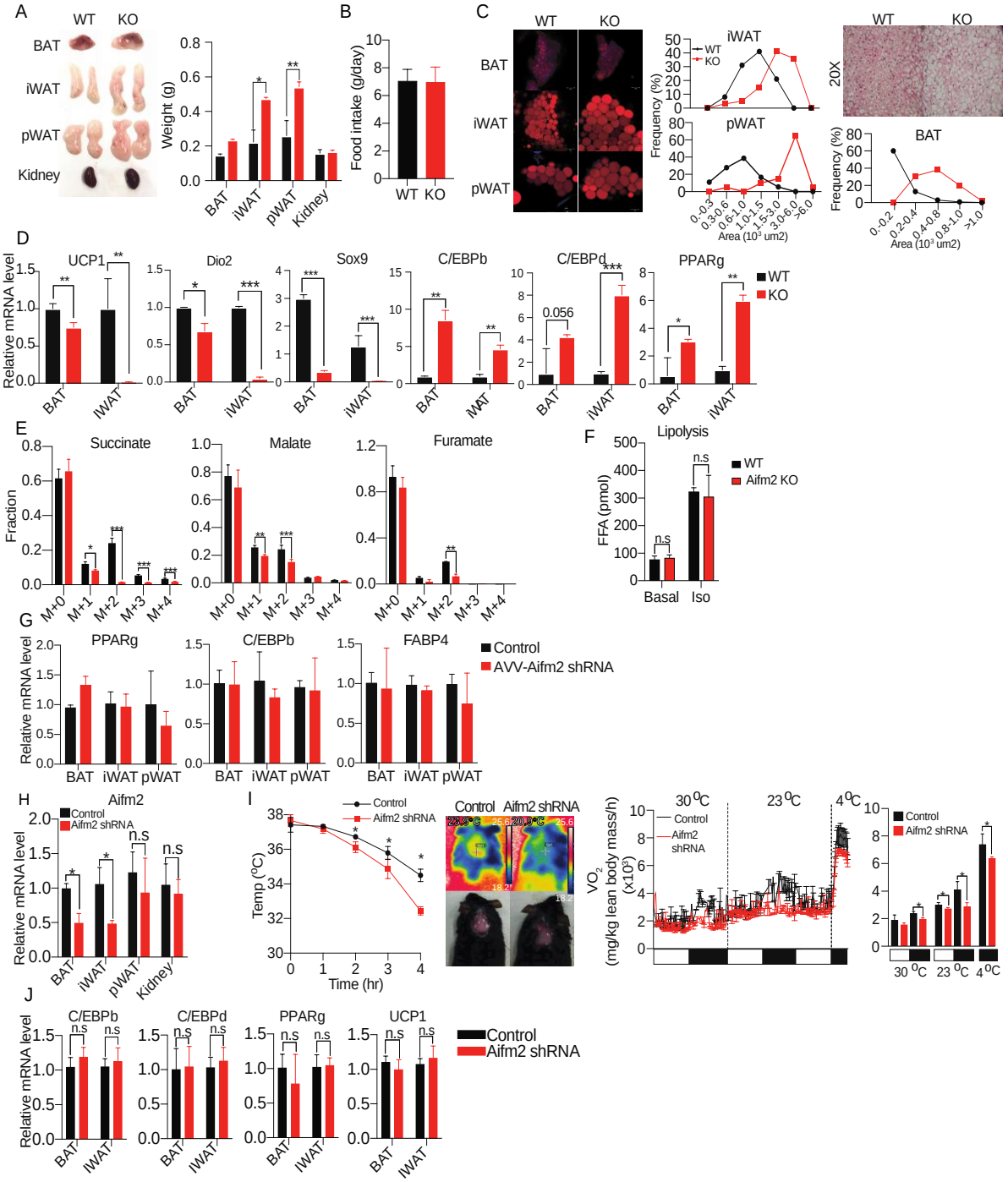

Figure 17. Aifm2 ablation increases adiposity.

(A)Representative photograph and weigh of dissected adipose tissues and kidney. (B) Food intake. (C) Whole-mount staining using LipidTOX (Red) and LD distribution. (D) RT-qPCR. (E) Fractional enrichments. (F) Lipolysis of ex-vivo BAT.

Aifm2 shRNA AAV7 and AAV9 viruses were injected directly into BAT and iWAT

(G) RT-qPCR. (H) RT-qPCR and immunoblotting for Aifm2 (I) Rectal temperature, infrared thermography, and V_{O2} assay using CLAMS. (J) RT-qPCR for adipogenic and thermogenic markers

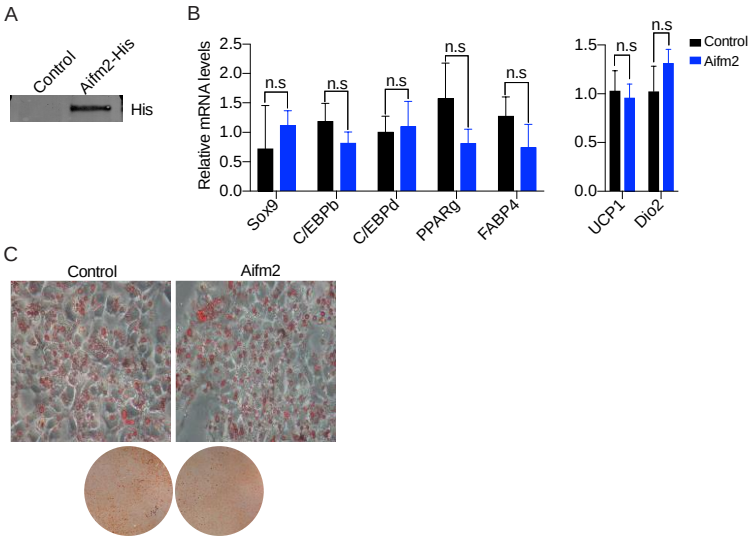

Figure 18.Aifm2 does not affect brown adipogenesis in vitro. Aifm2 was overexpressed in BAT preadipocytes which were then subjected to differentiation (A) RT-qPCR for Aifm2. (B) RT-qPCR for adipogenic genes and BAT-specific genes. (C) Oil-Red O staining.

Next, we generated transgenic mice overexpressing Aifm2 in UCP1^{+} cells for conditional gain-of function studies. We constructed a plasmid in which the chicken β-actin promoter driving the Aifm2 tagged with zsGreen and the bovine growth hormone poly A signal at the 3' end. We inserted LoxP-STOP-LoxP casette at the 5' of the Aifm2 coding sequence to allow Cre-mediated conditional excison of stop codon for Aifm2 expression (Fig. 19A). We obtained several transgenic mouse lines upon microinjection of the insert fragment into embryos, and these mice were crossed with UCP1-Cre mice to overexpress Aifm2 only in UCP1^{+} cells. By rt-qPCR and immunoblotting, Aifm2 shown to be overexpressed in both BAT and iWAT of Aifm2 TG mice (Fig. 19B). Whole body weight and EcoMRI scanning showed that these Aifm2 transgenic mice had significantly lower body weight compared to WT littermates with smaller WAT mass without any differences in lean mass (Fig. 19C). Dissection and weighing of each WAT depots confirmed that Aifm2 TG mice had significantly lower WAT depot weights (Fig. 11A). H&E staining revealed not much difference in morphology of BAT between Aifm2 TG and WT (Fig. 11B). And there was no difference in food intake (Fig. 11C). These TG mice had higher expression of BAT and thermogenic genes, such as UCP1, Dio2 and Cidea, but had lower levels of adipogenic genes, such as C/EBPβ and PPARγ (Fig. 11D). Aifm2 TG mice could maintain body temperature much better than WT littermates when exposed at 4^{o}C. After 5 hrs of cold exposure, body temperature of Aifm2-TG mice was decreased only by 1^{o}C, while that of WT littermates dropped approximately by 4^{o}C (Fig. 19D, left). After 12 hrs of cold exposure, Aifm2 TG mice showed much higher BAT temperature, approximately by 8^{o}C compared to WT mice as detected by the infrared camera. Moreover, 80% of Aifm2-TG mice survived, whereas only 20% WT mice remained after the longer cold exposure (Fig. 19D, right). These Aifm2-TG mice showed a significantly higher whole-body OCR at 30^{o}C during night, and 23°C during both day and night than WT littermates, and the increase in OCR was even more significant at 4^{o}C (Fig. 19E). OCR of both BAT and iWAT of Aifm2 TG mice by Seahorse was also significantly higher than that of WT littermates (Fig. 19F). Moreover, the NAD/NADH ratio was approximately 2-fold higher in both iWAT and BAT of Aifm2 TG mice compared to WT littermates (Fig. 19G, left). In addition, BAT of Aifm2 TG showed 2-fold higher lactate levels than WT BAT (Fig. 19G, right). Taken together, these Aifm2-TG mice had a greater thermogenic capacity and energy expenditure, which led to lower adiposity and leaner phenotype (Fig. 20). Overall, these results from both Aifm2 KO, Aifm2-BKO and TG mice clearly demonstrate *in vivo* evidence for the critical role of Aifm2 in thermogenesis in BAT and in

iWAT. And Aifm2 increases glycolysis and oxygen consumption to enhance thermogenesis resulting in decreased adiposity in mice.

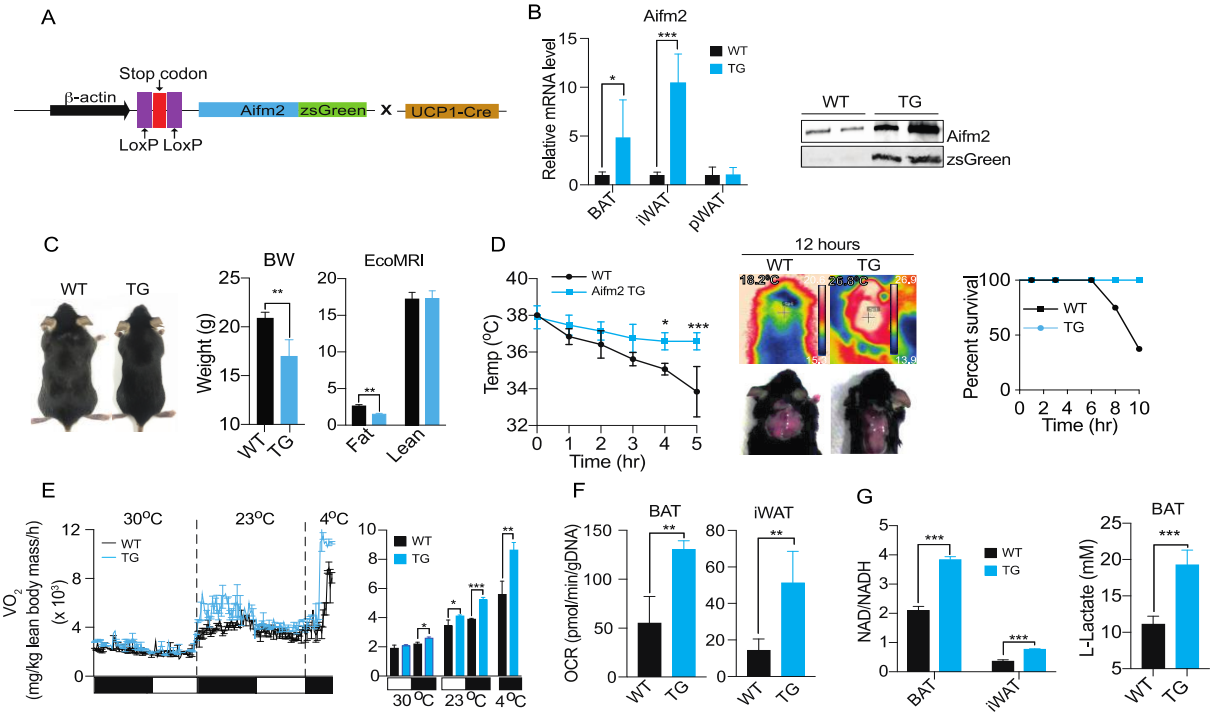

Figure 19. Aifm2 overexpression promotes thermogenesis *in vivo*
(A) Schematic diagram of BAT specific Aifm2 transgenic (TG) mice. (B) RT-qPCR/immunoblotting (right) for Aifm2 in various adipose depots. (C) Representative photograph mice, body weights and body composition. (D) Rectal temperature of mice maintained at 4°C for 5 hrs (left), infrared thermography of 12-hr cold-activated BAT (middle), and survival curve of mice (right) (n=6). (E) VO_2 assayed at indicated ambient temperatures. (F) OCR measured in BAT and iWAT (n=7). (G) NAD/NADH ratio (left), and intracellular L-Lactate level (right) in BAT (n=6). Data are mean ± SD. *p<0.05, ** p< 0.01, *** p<0.001.

Aifm2 promotes glucose oxidation for cold- and diet-induced thermogenesis

With our results that Aifm2 increases glycolysis to fuel thermogenesis, we next tested if Aifm2 functions in response to diet or fed state when glucose is abundant. It is possible that, in contrast to the fasted state in which BAT may primarily use FFA released from WAT lipolysis for thermogenesis, BAT may use glucose for oxidation in the fed state to fuel thermogenesis. We next explored whether thermogenesis promoted by Aifm2 is dependent only on its effect to sustain glycolysis and glucose utilization. Thus, we evaluated substrate preference in fueling thermogenesis in BAT cells. We compared V_{CO2}/V_{O2} from the OCR data from Seahorse in Aifm2 KD and control BAT cells. V_{CO2}/V_{O2} in basal condition was 0.87 and 0.81 in control and Aifm2 KD BAT cells, respectively, showing that Aifm2 depletion shifted the ratio somewhat toward FA oxidation. Remarkably, when treated with isoproterenol, the V_{CO2}/V_{O2} ratio in control BAT cells increased to 0.95, whereas the ratio in Aifm2 KD cells failed to increase (Fig. 21A, left). Conversely, Aifm2 OE in BAT cells shifted V_{CO2}/V_{O2} ratio from 0.87 to 0.90, a slight shift toward glucose oxidation in the basal condition. Notably, isoproterenol treatment of Aifm2 OE cells further shifted V_{CO2}/V_{O2} to 1.00, an indication of exclusive glucose utilization (Fig. 21A, right). Similar to BAT cells in culture, Aifm2 KO mice showed a lower whole-body V_{CO2}/V_{O2}

ratio of 0.76 compared to the WT ratio of 0.84, while Aifm2 TG had V_{CO2}/V_{O2} of 0.9. Aifm2 BKO also had lower whole-body V_{CO2}/V_{O2} of 0.77 than the 0.82 of Aifm2 floxed mice (Fig. 21E). Overall, these data clearly demonstrate that Aifm2 not only increases glycolysis but promotes further oxidation of glucose in BAT during thermogenesis.

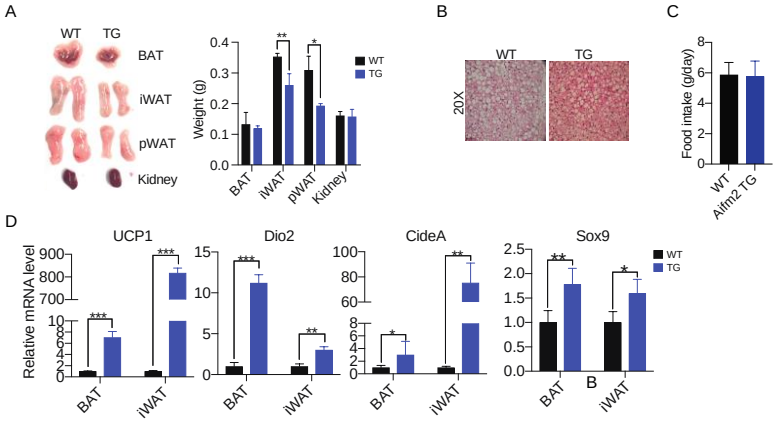

Figure 20. Aifm2 overexpression decreases adiposity *in vivo*
(A) Representative photograph and weigh of dissected adipose tissues and kidney. (B) H&E staining (20X). (C) Food intake. (D) RT-qPCR for adipogenic and thermogenic genes.

To better test whether Aifm2 effect on thermogenesis is due to glucose oxidation, Aifm2 OE BAT cells were treated with UK5009, an inhibitor of mitochondrial pyruvate carrier (MPC), to prevent pyruvate transport into mitochondria. MCP inhibition was also reported to block lactate uptake due to accumulation of intracellular pyruvate. With the β-AR stimulation, Aifm2 OE BAT cells showed a 40% increase in uncoupled OCR, and this increase was lost with the MCP inhibitor treatment. MCP inhibitor also decreased uncoupled OCR in the control cells, indicating glucose oxidation for thermogenesis and Aifm2 effect on thermogenesis as well (Fig. 21B). In contrary, when Aifm2 OE BAT cells were treated with carnitine palmitoyltransferase 1 (CPT1) inhibitor, Etomoxir to prevent FA transport into mitochondria, Aifm2 still increased overall and uncoupled OCR (Fig. 21C). Next, we measured OCR in BAT cells that were maintained in media containing either glucose or FA only. Similar to that observed when cells were maintained in complete media, OCR was higher in Aifm2 OE cells compared to control cells when maintained in glucose only containing media. But this increase in OCR was completely diminished when cells were maintained in palmitate only media (Fig. 21D, left). Using ERthermAC, we next measured the heat production to test the effect of Aifm2 on thermogenesis in BAT cells maintained in glucose or FA only. Indeed, Aifm2 OE BAT cells had higher heat production than control cells in the presence of glucose only, but not in the presence of palmitate only (Fig. 21D, right). These results support the notion that BAT cells can utilize glucose to fuel thermogenesis and that Aifm2 effect on thermogenesis is dependent on its function in glycolysis and thus glucose oxidation.

Our results so far show Aifm2 can sustain glycolysis and glucose utilization to support thermogenesis during cold exposure. Next, we wanted to investigate whether Aifm2 functions not only in cold-induced but also in diet-induced thermogenesis. First, we compared Aifm2

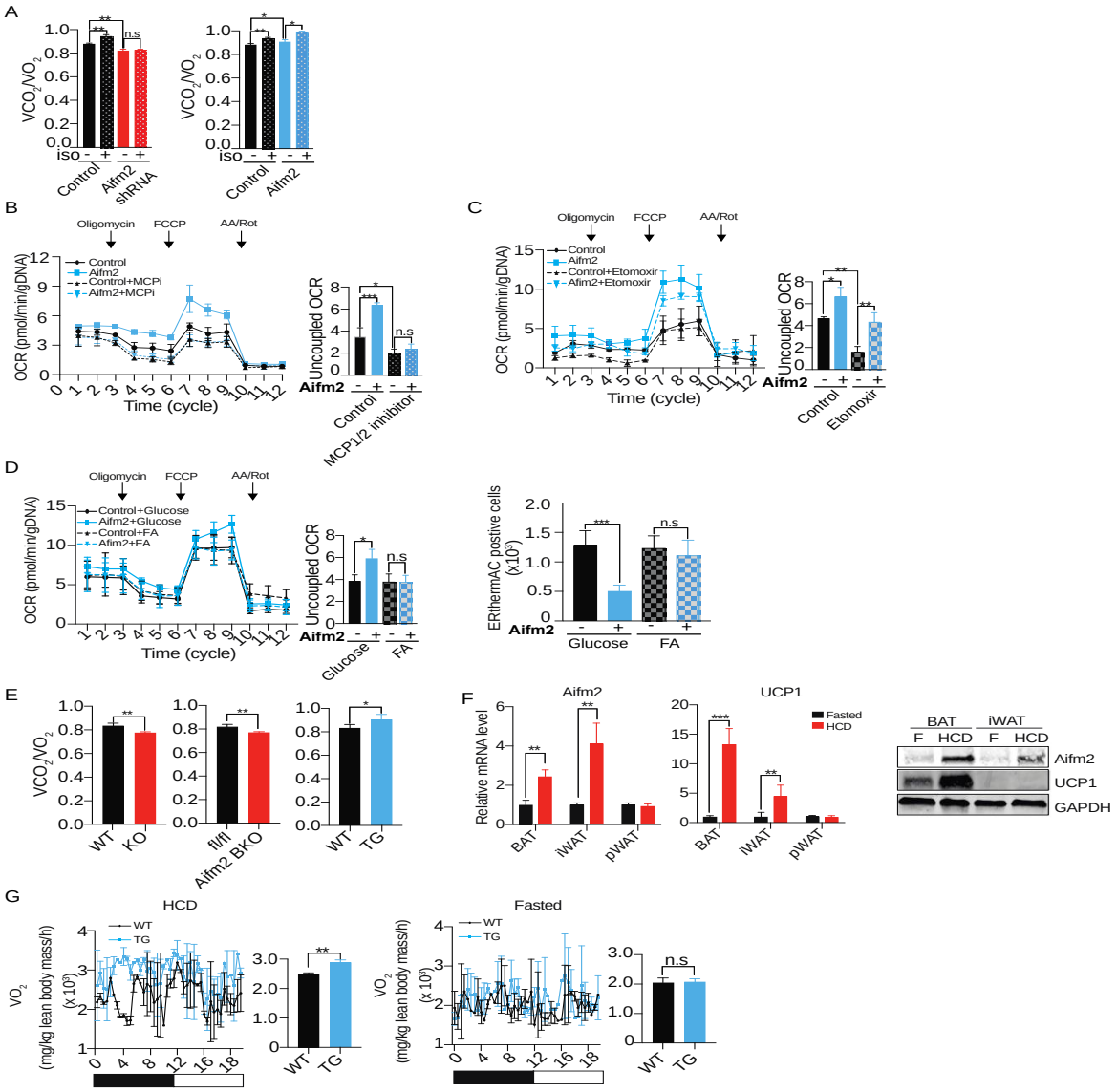

Figure 21. Aifm2 increases glucose oxidation to fuel cold/diet-induced thermogenesis
(A) V_{CO2}/V_{O2} of Aifm2 KD and overexpressing BAT cells. (B) OCR and uncoupled OCR measured in control and Aifm2 overexpressing cells treated with UK5099, an MCP1/2 (mitochondria pyruvate transporter) inhibitor. (C) OCR and uncoupled OCR measured in control and Aifm2 overexpressing cells treated with Etomoxir, CPT1 inhibitor. (D) OCR and uncoupled OCR (left), and quantification of ERthermAC positive cells of Aifm2 overexpressing BAT cells maintained in either glucose only or palmitate only media. (E) V_{CO2}/V_{O2} of Aifm2 KO, Aifm2 BKO and TG mice. (F) RT-qPCR and immunoblotting for Aifm2 and UCP1 in various adipose tissues mice maintained at 30^{o}C either fasted or fed a high-carbohydrate diet (HCD). (G) VO_2 assayed in WT and TG mice maintained at thermoneutrality fed HCD (left) or fasted (right). Data are mean ± SD. *p<0.05, ** p< 0.01, *** p<0.001.

expression in fasted and fed condition. Mice maintained in thermoneutrality were either fasted or given a high carbohydrate diet (HCD) overnight. Indeed, similar to UCP1, we found Aifm2 mRNA to increase by 2- and 4-fold in BAT and iWAT, respectively, when mice were fed HCD compared to fasted mice. Immunoblotting revealed a similar increase in Aifm2 in the fed state at

the protein level (Fig. 21F). Next, WT mice and Aifm2 TG mice were fasted at thermoneutrality for 6 hrs and them half of each group was given HCD. OCR was measured for 20 hrs by CLAMS. Some activity was observed early in HCD treated mice due to the fact they immediately consumed food right after a period of fasting. The data showed that WT mice had lower whole-body OCR during the fasted state than their littermate on HCD. More importantly, Aifm2 TG mice had significant higher OCR than WT mice only in the HCD fed state but failed to maintain the level in the fasted state (Fig. 21G). This indicates that Aifm2 effects on OCR requires glucose. Overall, these results demonstrate that by increasing NAD levels to support robust glycolysis, Aifm2 is critical, not only in cold-induced, but also in diet-induced thermogenesis.

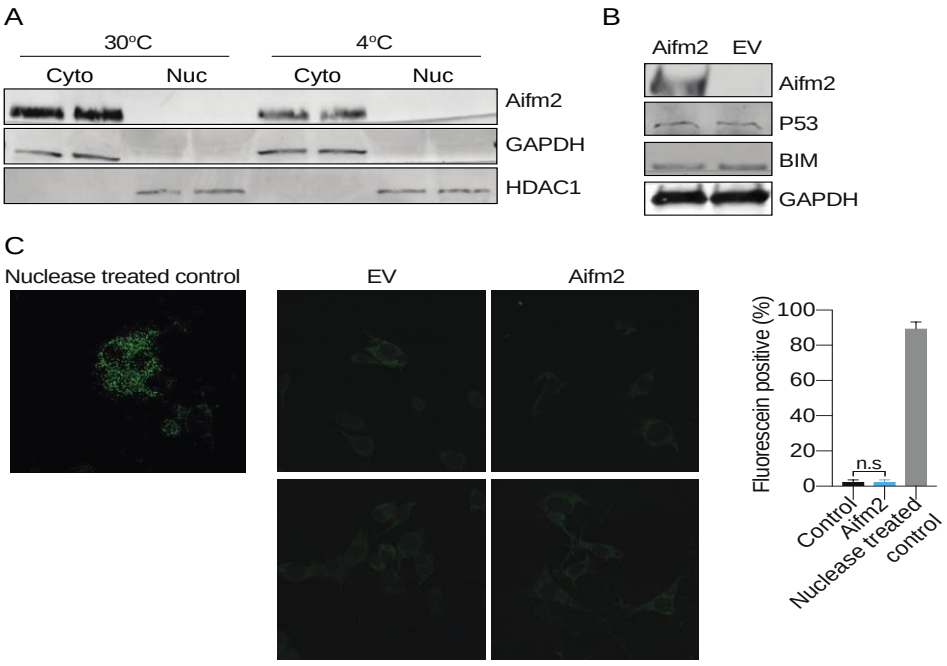

Figure 13. Aifm2 does not induce apoptosis in BAT cells
(A) Immunoblotting for Aifm2
(B) Immunoblotting for p53 and BIM in Aifm2 overexpressing BAT cells.
(C) Representative images of nuclease treated, empty vector, or Aifm2 overexpressing BAT cells and quantification of percent of apoptosis in terms of DNA fragmentation usingTrevigen's TACS® 2 TdT in Situ Apoptosis Detection Kit (TUNEL assay).

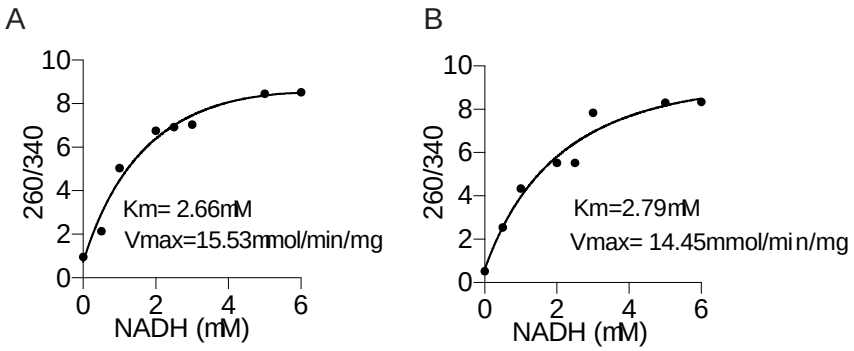

Fig 23. Aifm2 is a LD-associated NADH oxidase.
Aifm2 were overexpressed in BAT cells and LD and mitochondria fractions were isolated and subjected for NADH oxidase assay by spectrophotometry. (A) LD. (B) Mitochondria

DISCUSSION

Aifm2, a FAD dependent NADH/NAD oxidoreductase, belongs to Apoptosis Inducing Factor (AIF) family of proteins, having 22% identity and 44% similarity in amino acid sequence with AIF. AIF was reported to be widely expressed in various organs. However, we found that Aifm2 is very low in many tissues but expressed at a high level in BAT and that Aifm2 in BAT is induced by cold exposure and by diet. Moreover, upon cold-exposure, Aifm2 is induced in subcutaneous WAT, a WAT depot capable of beiging. While the function of Aifm2 in BAT has not been explored previously, the Aifm2 expression pattern points to its potential function in thermogenesis. With its NADH oxidase activity, we uncovered that Aifm2 maintains a robust glycolytic rate by generating NAD in cytosol to promote thermogenesis.

Recent report has shown that free FAs released from WAT, rather than those from intracellular lipolysis, are utilized for thermogenesis, particularly in the fasted state [11, 12]. Our studies also demonstrate BAT utilizes glucose via glycolysis upon cold, especially in the fed state, and that Aifm2 is required for optimal glycolytic rate. In this regard, glucose utilization in BAT was reported to be diminished in UCP1 KO mice treated with norepinephrine [43]. Remarkably, Aifm2 expression is induced not only by cold but also by diet even at thermoneutrality. Although somewhat controversial, recently, diet-induced thermogenesis was reported to be UCP1-dependent [44]. Some studies reported Aifm2 as a p53 target gene to be a tumor suppressor by inducing apoptosis [45, 46]. However, the Aifm2 KO mouse model reported previously did not develop tumor, nor the authors described any phenotypes related to thermogenesis or obesity [45]. Aifm2 overexpression in BAT cells did not significantly induce apoptosis (Fig. 22). In contrary, it is possible that Aifm2 may potentially promote tumor growth by enhancing aerobic glycolysis.

Some studies have proposed that glucose is to be energy source to fuel thermogenesis, particularly in postprandial thermogenesis, with an increase in insulin secretion [13]. However, the fate of glucose metabolism after glycolysis was not clear. Pyruvate produced from glycolysis may be transported into mitochondria to be oxidized via TCA cycle. Moreover, citrate from TCA cycle can then be transported out to cytoplasm for de novo lipogenesis, which can explain how lipogenesis and lipolysis may increase in parallel during thermogenesis [47, 48]. Pyruvate may also be used for anaplerosis to replenish TCA cycle intermediates [49] that might even be required for FA oxidation [15]. In our study, we show glycolysis increase significantly in response to β-AR stimulation and blocking glycolysis and glucose oxidation decreased OCR and

heat production even in the presence of FAs. This notion is supported by our observation that mice that are fasted have much lower OCR and body temperature compared to fed mice (Data not shown). More importantly, effect of Aifm2 on thermogenesis in BAT cells is completely reliant on glucose oxidation since blocking glucose oxidation by inhibiting pyruvate transport into mitochondria diminishes thermogenesis that is promoted by Aifm2 overexpression. These results further demonstrate that Aifm2 sustains glycolysis and increases glucose oxidation to support thermogenesis. These findings also demonstrate that Aifm2 is essential for robust glycolysis and subsequent glucose oxidation to maximize thermogenic capacity.

In order to maintain robust glycolysis during thermogenesis, high cytosolic NAD level is essential for BAT. Interestingly, we found that Aifm2 can translocate to mitochondrial inner membrane facing the interspace and, upon cold exposure or β-AR stimulation, NAD is generated by its NADH oxidase activity of Aifm2. Interestingly, Aifm2 isolated from either LD or mitochondrial fraction of BAT cells showed similar Km and Vmax for NADH oxidase activity (Fig. 23). We propose that Aifm2 translocated from LD to mitochondria, not only to increase cytosolic NAD, but also to support ETC. At this time, the mode of regulation that explains how cold exposure /β-AR stimulation can increase Aifm2 association with mitochondria is not known. In order to explore the regulation of Aifm2 translocation to mitochondria during thermogenesis, we measured ex vivo lipolysis. Although no significant difference in lipolysis between Aifm2 KO and WT mice, as expected, lipolysis was increased in the stimulated compared to basal condition in WT and KO mice (Fig. 17F). It is possible that as lipolysis increases during thermogenesis, LDs get smaller and Aifm2 might translocate from LD to mitochondria due to lacking binding surface. Thus, it should be further explored in the future.

Although mtGPD has been presumed to regenerate cytosolic NAD level in BAT, the role of mtGPD in glycolysis remains unclear, especially since its importance in thermogenesis could not be demonstrated in mtGPD knockout mouse models [20]. We propose that Aifm2 represents a unique BAT specific mechanism for NAD regeneration to sustain high glycolytic flux during thermogenesis and that NADH oxidase activity is critical for Aifm2 to sustain glycolysis for thermogenesis. Interestingly, Aifm2 shares sequence similarity to yeast NDE1, a NADH oxidoreductase that associates with the mitochondrial inner membrane and faces the mitochondrial intermembrane space and maintains cytosolic NAD to support glycolysis [50]. We propose that Aifm2 acts as a mammalian NDE by associating with the mitochondrial inner membrane. With the same enzymatic activity and localization, we argue that Aifm2 might be a mammalian NDE specifically present highly in thermogenic tissues.

By oxidizing NADH to NAD at the mitochondrial inner membrane facing intermembrane space Aifm2 produces electrons and protons as byproducts. Like yeast NDE, while regenerating NAD in the cytosol, Aifm2 potentially contributes to proton gradient, providing electrons to ETC via FAD which subsequently fuels UCP1. This indicates that Aifm2 increases total oxygen consumption and overall ETC activity in BAT, resulting in higher heat production. In this regard, ETC of mitochondria is the main source of reactive oxygen species (ROS), biproducts of electrons leaking during oxidative metabolism of ETC [51, 52]. Recently, ROS or a secondary lipid oxidation product such as 4-HNE, or even direct modification of cysteinyl residues of UCP1, were reported to stimulate uncoupling in BAT [53-55]. In this regard, by using a ROS biosensor in live cells, we detected a significant increase in ROS production in the mitochondria of Aifm2 overexpressing BAT cells (Data not shown). Conversely, Aifm2 KD in BAT cells resulted in a decrease in mitochondrial ROS. Enhancing ROS generation could be an additional mechanism by which Aifm2 increases thermogenesis in BAT.

The phenotype of our loss- and gain-of function mouse models firmly establish the physiological significance of Aifm2 in thermogenesis; Aifm2 total and BAT specific deficiency in mice significantly impairs glycolytic capacity, thermogenesis and cold tolerance which led to decreased energy expenditure and higher adiposity. Conversely, Aifm2 overexpression in BAT enhances thermogenesis, protecting mice from diet induced obesity. Importantly, although mitochondrial Complex I is present in BAT, Aifm2 as a mammalian NDE, can maximize glycolysis and glucose oxidation and also provide elections to ETC to fuel UCP1 for thermogenesis by associating with the mitochondrial inner membrane.

ACKNOWLEDGEMENTS

The work was supported in part by NIDDK grant to H.S.S. Imaging was supported in part by NIH S10RR026866-01. The content is solely the responsibility of the authors and does not necessarily represent the official views of the NIH. The authors declare no competing financial interests.

TABLE 1: List of Primers

Gene Symbol	Primers	Amplicon (bp)
Aifm2	TTG GTG ACT GTG CCG ATA C	176
	GAT CTG ACC CAC GCC ATC AT	
PPARγ	GCC CTT TGG TGA CTT TAT GGA	448
	GCA GCA GGT TGT CTT GGA TG	
C/EBPβ	GAC GGT GGA CAA GCT GAG CG	205
	CCT TGT GCT GCG TCT CCA GG	
C/EBPδ	AAA GTG CAG GCT TGT GGA CT	189
	TTA CTC CAC TGC CCA CCT GT	
Sox9	GTG CAA GCT GGC AAA GTT GA	106
	TGC TCA GTT CAC CGA TGT CC	
UCP1	ACT GCC ACA CCT CCA GTC ATT	123
	CTT TGC CTC ACT CAG GAT TGG	
Dio2	CAG TGT GGT GCA CGT CTC CAA TC	130
	TGA ACC AAA GTT GAC CAC CAG	
CideA	TGC TCT TCT GTA TCA CCC AGT	113
	GCC GTG TTA AGG AAT CTG CTG	
FABP4	ACACCGAGATTTCCTTCAAACTG	88
	CCATCTAGGGTTATGATGCTCTTCA	
Aifm2 G2A	AATTCGGTACCATGGGGTCCC AGGTCTCG	
Aifm2 D285N	ATGCCATTGGTAACTGTGCCGATACCAAG	
Aifm2 promoter	AATACTCGAGCGTTCTTCAGCAGTTCCC	2
	AATAGGTACCAAACCGCTCTTCTCGG	

TABLE 2: List of Antibodies

Name	Vendor	Catalog number
Aifm2	LSBio	LC-C382008
GAPDH	Santa Cruz	SC-25778
Tom20	Abcam	ab56783
ATGL	Cell Signaling	2138
COX-IV	Fisher Scientific	MA515078
HDAC1	Santa Cruz	SC-81598
P53	Abcam	ab31333
Bim	Santa Cruz	SC-374358
ST2	Thermo Fisher	PA5-20077
ERK1/2	Cell signaling	9102
pERK1/2	Cell signaling	9101
p-IKK (S176, S180)	Thermo Fisher	44-714

REFERENCES

1. Bartelt, A. and J. Heeren, *Adipose tissue browning and metabolic health.* Nat Rev Endocrinol, 2014. **10**(1): p. 24-36.
2. Cypess, A.M., et al., *Identification and importance of brown adipose tissue in adult humans.* N Engl J Med, 2009. **360**(15): p. 1509-17.
3. Virtanen, K.A., et al., *Functional brown adipose tissue in healthy adults.* N Engl J Med, 2009. **360**(15): p. 1518-25.
4. Nedergaard, J., T. Bengtsson, and B. Cannon, *Three years with adult human brown adipose tissue.* Ann N Y Acad Sci, 2010. **1212**: p. E20-36.
5. van Marken Lichtenbelt, W.D., et al., *Cold-activated brown adipose tissue in healthy men.* N Engl J Med, 2009. **360**(15): p. 1500-8.
6. Carpentier, A.C., et al., *Brown Adipose Tissue Energy Metabolism in Humans.* Front Endocrinol (Lausanne), 2018. **9**: p. 447.
7. Cannon, B. and J. Nedergaard, *Brown adipose tissue: function and physiological significance.* Physiol Rev, 2004. **84**(1): p. 277-359.
8. Feldmann, H.M., et al., *UCP1 ablation induces obesity and abolishes diet-induced thermogenesis in mice exempt from thermal stress by living at thermoneutrality.* Cell Metab, 2009. **9**(2): p. 203-9.
9. Blondin, D.P., et al., *Inhibition of Intracellular Triglyceride Lipolysis Suppresses Cold-Induced Brown Adipose Tissue Metabolism and Increases Shivering in Humans.* Cell Metab, 2017. **25**(2): p. 438-447.
10. Ahmadian, M., et al., *Desnutrin/ATGL is regulated by AMPK and is required for a brown adipose phenotype.* Cell Metab, 2011. **13**(6): p. 739-48.
11. Schreiber, R., et al., *Cold-Induced Thermogenesis Depends on ATGL-Mediated Lipolysis in Cardiac Muscle, but Not Brown Adipose Tissue.* Cell Metab, 2017. **26**(5): p. 753-763 e7.
12. Shin, H., et al., *Lipolysis in Brown Adipocytes Is Not Essential for Cold-Induced Thermogenesis in Mice.* Cell Metab, 2017. **26**(5): p. 764-777 e5.

13. M, U.D., et al., *Postprandial Oxidative Metabolism of Human Brown Fat Indicates Thermogenesis.* Cell Metab, 2018. **28**(2): p. 207-216 e3.
14. Symonds, M.E., et al., *Recent advances in our understanding of brown and beige adipose tissue: the good fat that keeps you healthy.* F1000Res, 2018. **7**.
15. Winther, S., et al., *Restricting glycolysis impairs brown adipocyte glucose and oxygen consumption.* Am J Physiol Endocrinol Metab, 2018. **314**(3): p. E214-e223.
16. Jeong, J.H., J.S. Chang, and Y.H. Jo, *Intracellular glycolysis in brown adipose tissue is essential for optogenetically induced nonshivering thermogenesis in mice.* Sci Rep, 2018. **8**(1): p. 6672.
17. Barron, J.T., L. Gu, and J.E. Parrillo, *Malate-aspartate shuttle, cytoplasmic NADH redox potential, and energetics in vascular smooth muscle.* J Mol Cell Cardiol, 1998. **30**(8): p. 1571-9.
18. Kauppinen, R.A., T.S. Sihra, and D.G. Nicholls, *Aminooxyacetic acid inhibits the malate-aspartate shuttle in isolated nerve terminals and prevents the mitochondria from utilizing glycolytic substrates.* Biochim Biophys Acta, 1987. **930**(2): p. 173-8.
19. DosSantos, R.A., et al., *Evidence for a compensated thermogenic defect in transgenic mice lacking the mitochondrial glycerol-3-phosphate dehydrogenase gene.* Endocrinology, 2003. **144**(12): p. 5469-79.
20. Alfadda, A., et al., *Mice with deletion of the mitochondrial glycerol-3-phosphate dehydrogenase gene exhibit a thrifty phenotype: effect of gender.* Am J Physiol Regul Integr Comp Physiol, 2004. **287**(1): p. R147-56.
21. Vergnes, L. and K. Reue, *Adaptive thermogenesis in white adipose tissue: is lactate the new brown(ing)?* Diabetes, 2014. **63**(10): p. 3175-3176.
22. Yamashita, T., et al., *Ubiquinone binding site of yeast NADH dehydrogenase revealed by structures binding novel competitive- and mixed-type inhibitors.* Scientific Reports, 2018. **8**(1): p. 2427.
23. Iwata, M., et al., *The structure of the yeast NADH dehydrogenase (Ndi1) reveals overlapping binding sites for water- and lipid-soluble substrates.* Proc Natl Acad Sci U S A, 2012. **109**(38): p. 15247-52.
24. Melo, A.M., T.M. Bandeiras, and M. Teixeira, *New insights into type II NAD(P)H:quinone oxidoreductases.* Microbiol Mol Biol Rev, 2004. **68**(4): p. 603-16.
25. Luttik, M.A., et al., *The Saccharomyces cerevisiae NDE1 and NDE2 genes encode separate mitochondrial NADH dehydrogenases catalyzing the oxidation of cytosolic NADH.* J Biol Chem, 1998. **273**(38): p. 24529-34.
26. Elguindy, M.M. and E. Nakamaru-Ogiso, *Apoptosis-inducing Factor (AIF) and Its Family Member Protein, AMID, Are Rotenone-sensitive NADH:Ubiquinone Oxidoreductases (NDH-2).* J Biol Chem, 2015. **290**(34): p. 20815-26.
27. Marshall, K.R., et al., *The human apoptosis-inducing protein AMID is an oxidoreductase with a modified flavin cofactor and DNA binding activity.* J Biol Chem, 2005. **280**(35): p. 30735-40.
28. Ohiro, Y., et al., *A novel p53-inducible apoptogenic gene, PRG3, encodes a homologue of the apoptosis-inducing factor (AIF).* FEBS Lett, 2002. **524**(1-3): p. 163-71.
29. Dupuis, J., et al., *New genetic loci implicated in fasting glucose homeostasis and their impact on type 2 diabetes risk.* Nat Genet, 2010. **42**(2): p. 105-16.
30. Speliotes, E.K., et al., *Association analyses of 249,796 individuals reveal 18 new loci associated with body mass index.* Nat Genet, 2010. **42**(11): p. 937-48.

31. Heid, I.M., et al., *Meta-analysis identifies 13 new loci associated with waist-hip ratio and reveals sexual dimorphism in the genetic basis of fat distribution.* Nat Genet, 2010. **42**(11): p. 949-60.
32. Betz, M.J. and S. Enerbäck, *Targeting thermogenesis in brown fat and muscle to treat obesity and metabolic disease.* Nature Reviews Endocrinology, 2017. **14**: p. 77.
33. Harris, L.A., et al., *A single centrifugation method for isolating fat droplets from cells and tissues.* J Lipid Res, 2012. **53**(5): p. 1021-5.
34. Suzuki, T., et al., *Strategy for comprehensive identification of human N-myristoylated proteins using an insect cell-free protein synthesis system.* Proteomics, 2010. **10**(9): p. 1780-93.
35. Schmitt, J.M. and P.J.S. Stork, *β2-Adrenergic Receptor Activates Extracellular Signal-regulated Kinases (ERKs) via the Small G Protein Rap1 and the Serine/Threonine Kinase B-Raf.* Journal of Biological Chemistry, 2000. **275**(33): p. 25342-25350.
36. Iwen, K.A., et al., *Cold-Induced Brown Adipose Tissue Activity Alters Plasma Fatty Acids and Improves Glucose Metabolism in Men.* J Clin Endocrinol Metab, 2017. **102**(11): p. 4226-4234.
37. Hung, Y.P., et al., *Imaging cytosolic NADH-NAD(+) redox state with a genetically encoded fluorescent biosensor.* Cell Metab, 2011. **14**(4): p. 545-54.
38. Reers, M., et al., *Mitochondrial membrane potential monitored by JC-1 dye.* Methods Enzymol, 1995. **260**: p. 406-17.
39. Salvioli, S., et al., *JC-1, but not DiOC6(3) or rhodamine 123, is a reliable fluorescent probe to assess delta psi changes in intact cells: implications for studies on mitochondrial functionality during apoptosis.* FEBS Lett, 1997. **411**(1): p. 77-82.
40. Kriszt, R., et al., *Optical visualisation of thermogenesis in stimulated single-cell brown adipocytes.* Sci Rep, 2017. **7**(1): p. 1383.
41. Jimenez, V., et al., *In vivo adeno-associated viral vector-mediated genetic engineering of white and brown adipose tissue in adult mice.* Diabetes, 2013. **62**(12): p. 4012-22.
42. Kozak, U.C., et al., *An upstream enhancer regulating brown-fat-specific expression of the mitochondrial uncoupling protein gene.* Mol Cell Biol, 1994. **14**(1): p. 59-67.
43. Inokuma, K., et al., *Uncoupling protein 1 is necessary for norepinephrine-induced glucose utilization in brown adipose tissue.* Diabetes, 2005. **54**(5): p. 1385-91.
44. von Essen, G., et al., *Adaptive facultative diet-induced thermogenesis in wild-type but not in UCP1-ablated mice.* Am J Physiol Endocrinol Metab, 2017. **313**(5): p. E515-e527.
45. Mei, J., et al., *The p53-inducible apoptotic protein AMID is not required for normal development and tumor suppression.* Oncogene, 2006. **25**(6): p. 849-56.
46. Wu, M., et al., *AMID is a p53-inducible gene downregulated in tumors.* Oncogene, 2004. **23**(40): p. 6815-9.
47. Yu, X.X., et al., *Cold elicits the simultaneous induction of fatty acid synthesis and beta-oxidation in murine brown adipose tissue: prediction from differential gene expression and confirmation in vivo.* FASEB J, 2002. **16**(2): p. 155-68.
48. Barquissau, V., et al., *White-to-brite conversion in human adipocytes promotes metabolic reprogramming towards fatty acid anabolic and catabolic pathways.* Mol Metab, 2016. **5**(5): p. 352-365.
49. Cannon, B. and J. Nedergaard, *The physiological role of pyruvate carboxylation in hamster brown adipose tissue.* Eur J Biochem, 1979. **94**(2): p. 419-26.

50. Luttik, M.A.H., et al., *The Saccharomyces cerevisiae NDE1 andNDE2 Genes Encode Separate Mitochondrial NADH Dehydrogenases Catalyzing the Oxidation of Cytosolic NADH.* Journal of Biological Chemistry, 1998. **273**(38): p. 24529-24534.
51. Wong, H.S., et al., *Production of superoxide and hydrogen peroxide from specific mitochondrial sites under different bioenergetic conditions.* J Biol Chem, 2017. **292**(41): p. 16804-16809.
52. Brand, M.D., *Mitochondrial generation of superoxide and hydrogen peroxide as the source of mitochondrial redox signaling.* Free Radic Biol Med, 2016. **100**: p. 14-31.
53. Aguirre, E. and S. Cadenas, *GDP and carboxyatractylate inhibit 4-hydroxynonenal-activated proton conductance to differing degrees in mitochondria from skeletal muscle and heart.* Biochim Biophys Acta, 2010. **1797**(10): p. 1716-26.
54. Echtay, K.S., et al., *A signalling role for 4-hydroxy-2-nonenal in regulation of mitochondrial uncoupling.* Embo j, 2003. **22**(16): p. 4103-10.
55. Chouchani, E.T., et al., *Mitochondrial ROS regulate thermogenic energy expenditure and sulfenylation of UCP1.* Nature, 2016. **532**(7597): p. 112-6.

Chapter 4:
Conclusion

White adipose tissue (WAT) plays a critical role by serving as the major energy storage site and by secreting adipokines that control various biological processes, such as appetite, metabolism and insulin sensitivity. In modern society, excess WAT leading to obesity has become an epidemic and is closely associated with metabolic diseases, such as type 2 diabetes. However, WAT deficiency, such as lipodystrophy, also manifests as insulin resistance (IR) with ectopic lipid accumulation in other tissues, such as liver, underscoring the importance of maintaining the proper WAT mass [1, 2]. WAT can expand not only through increased adipocyte volume but also by adipogenesis [3]. Understanding how adipogenesis is regulated may help in developing therapeutic strategies against obesity/lipodystrophy.

Pref-1 (Preadipocyte factor-1, also called Dlk1) is a widely used preadipocyte marker that we originally cloned and identified. By lineage tracing, Pref-1 has been shown to mark adipose precursors that are required for white adipose tissue (WAT) development and expansion. However, Pref-1 must be downregulated before undergoing adipocyte differentiation. Pref-1 is synthesized as a plasma membrane glycoprotein and have 6 EGF-repeats in the extracellular domain. Pref-1 ectodomain is cleaved to be released as the biologically active soluble Pref-1. Inhibition of adipogenesis by Pref-1 has been demonstrated via gain- and loss-of function studies in cultured cells as well as in mice *in vivo*. Thus, Pref-1 ablation increases adipose tissue mass in mice, whereas Pref-1 overexpression causes partial lipodystrophy with ectopic fat storage. Pref-1 activates MEK/ERK to induce Sox9, which in turn suppresses C/EBPβ and C/EBPδ, to inhibit adipocyte differentiation. However, the plasma membrane receptor for Pref-1, the most proximal and critical component of Pref-1 signaling, has not been known. By using recently developed diazirine photo-reactive linker combined with robust NHS-ester chemistry in live cells, we now have detected ST2 (also called IL1RL1) which is the known IL-33 receptor, as putative Pref-1 receptor. Our study clearly showed that ST2 is required for Pref-1 inhibitory effect on adipogenesis.

Pref-1 activates ERK, but not NF-κB. Thus, we do not predict Pref-1 affects other $ST2^+$ cells, such as immune cell types that respond to affect inflammation. In this regard, in immune cell types, IL-33-ST2-NF-κB pathway has been reported to increase Treg and LC2 cell population for maintenance of M2 macrophages, preventing HFD-induced WAT inflammation in mice [4, 5]. In our studies we are using 6-8 wk-old mice on chow diet to test the role of ST2 for Pref-1 induced partial lipodystrophy. Thus, Pref-1 effect we observe does not involve HFD-induced obesity or related WAT inflammation. we propose to study whether ST2 is required for Pref-1 mediated changes in adipose precursor populations in SVF. However, it is possible that $ST2^+$ immune cells may be affected by Pref-1. Although not a focus of our research, we will sort and examine Lin^+ cells using Treg markers, such as Foxp3 and CD4 [6-8]. Pref-1 administration could increase Treg and LC2 cells in WT and ST2-PreASKO mice. However, global ST2-KO mice would not respond to Pref-1 due to absence of ST2 in all cell types. If indeed, Pref-1 affects immune cell subpopulations, we will determine cytokine levels known to be secreted by immune cells, such as IL-2, -5 and -11. We will also examine macrophage marker F4/80, as well as M1 dendritic marker, CD11c, and the M2 marker, MGL1, to examine M1/M2 polarization. Other M1 and M2 polarization-related parameters of pro-/anti-inflammation will be documented also [9, 10].

While white adipose tissue is the primary energy storage organ, brown adipose tissue (BAT) dissipates energy through non-shivering thermogenesis. Discovery of the presence of BAT/BAT-like tissues in human adults has generated a considerable interest in BAT biology to design strategies against obesity and insulin resistance. Recently, we have identified Aifm2 as a lipid droplet (LD) associated protein that is expressed at a high level only in BAT, but not in other tissues, and is cold inducible. Aifm2 has 20% identify and 40% similarity in aa sequence to AIF (Apoptosis Inducing Factor) which is widely expressed in various tissues, including BAT. Although Aifm2 is BAT-specific and cold inducible, the function of Aifm2 in BAT is not known.

Aifm2 is a flavoprotein containing a NADH oxidase domain and we found Aifm2 to localize to mitochondria during thermogenesis. We found Aifm2 to increase cytosolic NAD/NADH, correlating with higher glycolytic rate leading to higher oxygen consumption/uncoupled respiration and heat production in BAT cells. We have generated Aifm2 knockout mice and these mice were cold-sensitive due to impaired thermogenesis and, with decreased energy expenditure, they exhibited a higher adiposity. Conversely, our transgenic mice overexpressing Aifm2 in $UCP1^{+}$ cells had a higher thermogenic capacity to better maintain body temperature upon cold exposure, increasing energy expenditure with decreasing adiposity. With these data, we concluded that Aifm2 promotes thermogenesis by generating NAD to maintain optimal glycolytic rate and mitochondrial oxidative metabolism, especially in the fed state.
Our overall prediction is that overexpression of Aifm2 in brown adipocytes will cause increase in the cytosolic NAD level and glycolysis, correlating with membrane depolarization, higher oxygen consumption and uncoupled respiration, resulting in higher heat production. Because thermogenic tissues, BAT and iWAT upon cold exposure, express high UCP1 but lower ATP synthase levels, we argue that the effect of Aifm2 on OCR would represent mainly from changes in uncoupled OCR.

GWAS database search revealed multiple SNPs of Aifm2 to be related to waist-hip ratio, body mass index and fasting glucose level-related insulin resistance, suggesting potential role of Aifm2 in human obesity and type 2 diabetes [11]. Interestingly, Aifm2 human mutation is located in the myristoylation site which is required for Aifm2 association with mitochondria. It would be critical to examine the underlining mechanism which Aifm2 translocates to the mitochondria and more importantly, how Aifm2 affect BAT function in human. Moreover, we also predict that, with its NADH oxidase activity, Aifm2 localized to the mitochondria facing intermembrane space has a potential key role in maintaining NAD in the cytoplasm for optimal glycolysis in aerobic condition, while providing electrons to mitochondrial ETC in tissue such as muscles during high intensity activity when oxygen availability limits aerobic respiration. In fact, we have found that Aifm2 mRNA indeed does increase significantly in high-intensity exercised muscle in mice. In addition, using GEO database, we found that Aifm2 increased in muscles We are currently examining Aifm2 function in muscles during high-intensity activity.

References

1. Melvin, A., S. O'Rahilly, and D.B. Savage, *Genetic syndromes of severe insulin resistance.* Curr Opin Genet Dev, 2018. **50**: p. 60-67.
2. Araujo-Vilar, D. and F. Santini, *Diagnosis and treatment of lipodystrophy: a step-by-step approach.* J Endocrinol Invest, 2018.
3. Jo, J., et al., *Hypertrophy and/or Hyperplasia: Dynamics of Adipose Tissue Growth.* PLoS Comput Biol, 2009. **5**(3): p. e1000324.
4. Molofsky, A.B., A.K. Savage, and R.M. Locksley, *Interleukin-33 in Tissue Homeostasis, Injury, and Inflammation.* Immunity, 2015. **42**(6): p. 1005-19.
5. Feuerer, M., et al., *Lean, but not obese, fat is enriched for a unique population of regulatory T cells that affect metabolic parameters.* Nat Med, 2009. **15**(8): p. 930-9.
6. Cipolletta, D., et al., *Appearance and disappearance of the mRNA signature characteristic of Treg cells in visceral adipose tissue: age, diet, and PPARgamma effects.* Proc Natl Acad Sci U S A, 2015. **112**(2): p. 482-7.
7. Cipolletta, D., et al., *PPAR-gamma is a major driver of the accumulation and phenotype of adipose tissue Treg cells.* Nature, 2012. **486**(7404): p. 549-53.

8. Li, C., et al., *TCR Transgenic Mice Reveal Stepwise, Multi-site Acquisition of the Distinctive Fat-Treg Phenotype.* Cell, 2018. **174**(2): p. 285-299 e12.
9. Hill, A.A., W. Reid Bolus, and A.H. Hasty, *A decade of progress in adipose tissue macrophage biology.* Immunol Rev, 2014. **262**(1): p. 134-52.
10. Morris, D.L., K. Singer, and C.N. Lumeng, *Adipose tissue macrophages: phenotypic plasticity and diversity in lean and obese states.* Curr Opin Clin Nutr Metab Care, 2011. **14**(4): p. 341-6.
11. Mei, J., et al., *The p53-inducible apoptotic protein AMID is not required for normal development and tumor suppression.* Oncogene, 2006. **25**(6): p. 849-56.